U. S. DEPARTMENT OF THE INTERIOR

U. S. GEOLOGICAL SURVEY

SEISMIC HAZARDS AT KILAUEA AND MAUNA LOA VOLCANOES, HAWAII

4/22/94 version

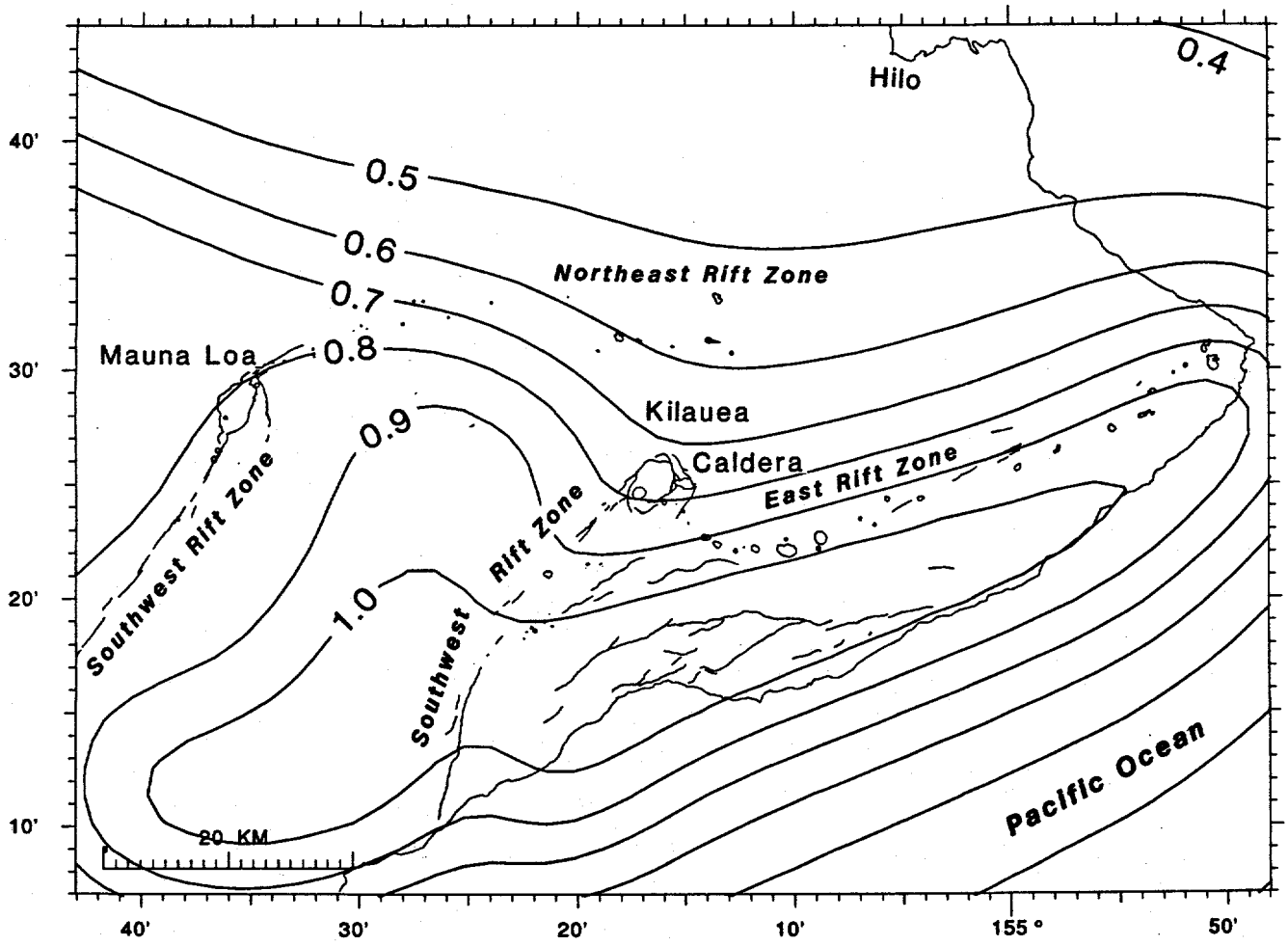

Peak ground accelerations (in g) for a 50 year exposure time with a 90% probability of not being exceeded.

by
Fred W. Klein [1]

Open File Report 94-216

This report is preliminary and has not been reviewed for conformity with U.S. Geological Survey editorial standards or with the North American Stratigraphic Code. Any use of trade, product, or firm names is for descriptive purposes only and does not imply endorsement by the U.S. Government.

[1] *MS977, 345 Middlefield Road, Menlo Park, CA 94025*

DISCLAIMER

DISCLAIMER

Portions of this document may be illegible in electronic image products. Images are produced from the best available original document.

ABSTRACT

A significant seismic hazard exists in south Hawaii from large tectonic earthquakes that can reach magnitude 8 and intensity XII. This paper quantifies the hazard by estimating the horizontal peak ground acceleration (PGA) in south Hawaii which occurs with a 90% probability of not being exceeded during exposure times from 10 to 250 years. The largest earthquakes occur beneath active, unbuttressed and mobile flanks of volcanos in their shield building stage. The flanks are compressed and pushed laterally by rift zone intrusions. The largest earthquakes are thus not directly caused by volcanic activity. Historic earthquakes (since 1823) and the best Hawaiian Volcano Observatory catalog (since 1970) under the south side of the island define linear frequency-magnitude distributions that imply average recurrence intervals for M>5.5 earthquakes of 3.4-5 years, for M>7 events of 29-44 years, and for M 8 earthquakes of 120-190 years. These estimated recurrences are compatable with the 107 year interval between the two major April 2, 1868 (M~7.9) and November 29, 1975 (M=7.2) earthquakes. Frequency-magnitude distributions define the activity levels of 19 different seismic source zones for probabilistic ground motion estimations. The available measurements of PGA (33 from 7 moderate earthquakes) are insufficient to define a new attenuation curve. We use the Boore et al. (1993) curve shifted upward by a factor of 1.2 to fit Hawaiian data. Amplification of sites on volcanic ash or unconsolidated soil are about two times those of hard lava sites. On a map for a 50 year exposure time with a 90% probability of not being exceeded, the peak ground accelerations are 1.0 g on Kilauea's and Mauna Loa's mobile south flanks and 0.9 g in the Kaoiki seismic zone. This hazard from strong ground shaking is comparable to that near the San Andreas Fault in California or the subduction zone in the Gulf of Alaska. Earthquake hazards observed in Hawaii in addition to ground shaking include submarine landslides, vibrational settling of subsurface materials, ground ruptures, earthquake induced landslides, cliff collapse and triggered volcanic eruptions. Catastrophic submarine landslides also follow a linear frequency-magnitude distribution where magnitude is calculated from estimated subsidence energy. Magnitude 8 landslides appear to be 2 or 3 orders of magnitude less frequent than magnitude 8 earthquakes. Great flank earthquakes may often trigger small submarine landslides or slumps, but great submarine landslides are relatively infrequent.

INTRODUCTION

Several damaging earthquakes have struck the island of Hawaii during the appoximately 170 years of written history. The largest known earthquake occurred on April 2, 1868 in the Kau district (Hitchcock, 1912; Wood, 1914). The estimated magnitude is 7.9 and the largest intensity was XII (Wyss and Koyanagi, 1992). Intensity XII on the Modified Mercalli scale is the level of ground shaking perceived by humans which means "damage nearly total. Large rock masses displaced. Lines of sight and level distorted. Objects thrown into the air". Extensive damage from ground shaking and from an accompanying tsunami was island wide. Nearly every house in the epicentral area was knocked from its foundation (Hitchcock, 1912). Five damaging earthquakes larger than magnitude 6

occurred during the period (1962-1993) of coverage by the seismic network operated by the Hawaiian Volcano Observatory (Koyanagi et al., 1966; Unger and Ward, 1979; Tilling et al., 1976; Buchanan-Banks, 1987; Bryan, 1992). This earthquake activity occurs in an area comparable in size to the San Francisco Bay region or the Los Angeles basin. Wyss and Koyanagi (1992) provide a very useful catalog of locations and magnitudes of damaging historic earthquakes. Since the early 1970's, at least one strong motion accelerogram was triggered for every M>6 earthquake. Clearly a seismic hazard exists and there is enough historic and instrumental data to begin to quantitatively assess the seismic hazard and the probable levels of ground motion in Hawaii.

Other studies of seismic hazard in Hawaii have recognized the hazard but have not localized or quantitatively estimated the probable ground shaking. Heliker (1990) published a popular booklet that discusses earthquake hazards but does not include a seismic hazard map. Johnson and Koyanagi (1987 and 1988) made an excellent case for several seismic hazards from various seismic source zones. Wyss and Koyanagi (1992b) argue on tectonic grounds that the flanks of active volcanoes that have not experienced recorded earthquakes are seismic gaps and are an unrecognized seismic hazard. Algermissen et al. (1990) and FEMA (1985) estimate that the horizontal peak ground acceleration (PGA) that has a 90% chance of not being exceeded within 50 years is between 0.2 and 0.4 g on Hawaii island. PGA is the maximum excursion in units of earth's gravity read from any directional component of an accelerogram, and is a physical measurement of strong ground motion. The PGA often occurs during the S wave and usually on one of the horizontal components. Algermissen's PGA estimate is made from sparse data on a small regional map scale. This paper calculates much higher expected PGAs using more extensive earthquake data on a more sharply focused map of south Hawaii.

The tectonic framework of Kilauea has been developed by several authors (eg. Eaton and Murata, 1960; Swanson et al., 1976; Ando, 1979; Furumoto and Kovach, 1979; Nakamura, 1980; Wyss et al., 1981; Crosson and Endo, 1982; Lipman et al., 1985; Dvorak et al., 1986; Eissler and Kanamori, 1987; Dieterich, 1988; Thurber and Gripp, 1988; Wyss, 1988; Klein and Koyanagi, 1989; Bryan and Johnson, 1991; Bryan, 1992; Tilling and Dvorak, 1993). The driving force behind growth and deformation of Hawaii volcanoes is the ascent of magma from sources below 60 km depth to shallow storage reservoirs under the calderas, and both intrusion and extrusion of lava from the calderas and their radiating rift zones. The intrusion and widening of dikes under the rift zones laterally compresses the adjacent flanks which then release the accumulated strain in large earthquakes. The largest earthquakes in Hawaii are of this flank type.

Most of the slip of the volcano flanks occurs near the base of the volcanic pile and above the pre-volcanic oceanic crust. Kilauea's south flank (fig. 1b) episodically slips seaward in events like the 1975 M=7.2 Kalapana earthquake: slip was on a near horizontal plane at 9-10 km depth which coincides with the oceanic sediment layer under the volcano. This decollement surface marks the boundary between a mobile flank above and a more stable block below. The decollement dips roughly 4 degrees to the NW because of the downward flexing of the lithosphere under the island's weight. Kilauea's south flank is buttressed to the north by Mauna Loa and is mobile toward its unbuttressed, seaward side. The flank slips laterally and subsides by the release of lateral compressive stress and gravitational slumping along normal faults. The rate of slip of the south flank may be 6-12 cm/yr (Dieterich, 1988) or 15-25 cm/yr (Owen et al., 1993), which is several times larger than the 2-3 cm/yr slip of the San Andreas Fault system in California (eg. Working group, 1990).

Modeling the seismic hazards of Hawaiian earthquakes can't be done by mapping fault zones because the primary slip does not occur on large faults that reach the surface. The primary earthquake hazards are from active but hidden faults within and at the base of volcano flanks.

The catalogs of historic and instrumentally located earthquakes can be used to quantitatively estimate the seismic hazard at Kilauea Volcano. A basic presentation of hazard is a map of the average recurrence interval between earthquakes of a certain magnitude in an earthquake source zone. This

paper uses average recurrence interval to mean the reciprocal of the rate of earthquakes per year expected from the frequency-magnitude distribution. The rates for large earthquakes are estimated from a linear fit to the distribution: the rates of large events are low and they are sparsely represented in the catalog. The average recurrence interval for large earthquakes has generally not been observed from repeated earthquakes. The estimation of an average recurrence interval should not be taken to mean there is a constant recurrence mechanism such as from a constant driving force like steady state plate tectonics.

We also demonstrate the seismic hazard with maps of the probable PGA from local earthquakes. This paper uses horizontal PGA values because they are generally higher and more structurally useful than the vertical component. We first estimate the rates of earthquakes in different magnitude ranges and the maximum magnitude for 19 different seismic source zones from a 23 year HVO earthquake catalog. Where possible, rates are modified from the historical catalog of large earthquakes. Estimating probable PGA also requires knowledge of the attenuation curve which depends on magnitude and distance. Unfortunately, only 33 PGA values have been measured from 7 moderate earthquakes in Hawaii. This does not permit derivation of an assumption-free Hawaiian curve, but we use the available data to select from existing published curves.

For each evaluation site we calculate the occurrence rate of each level of PGA. The calculations use the frequency of earthquakes in different magnitude intervals at each point within the source zone, and the expected PGA at the evaluation site from an earthquake at each magnitude. The PGA rates are summed for points within each seismic source zone which gives the probability distribution of PGAs for the evaluation site. Both the cumulative probability of PGAs greater than some value and the PGA with a given level of probability of non-exceedance can be calculated and generalized to different exposure times by assuming the earthquake rate does not vary in time. Then we calculate and map the level of PGA that has the same (90%) probability of not being exceeded during exposure times from 10 to 250 years. The 50 year exposure time is a typical period of human interest and is the period chosen for the PGA hazard map of the U.S. (Algermissen et al., 1990). A 50 year exposure time at 90% non-exceedence probability corresponds to an average return period of 474 years. Within the average return period, the probability of exceeding the PGA is 63% (Algermissen et al., 1982).

The maps of probable PGAs in this paper are for solid rock sites. More realistic maps should include the local site effects of unconsolidated ash or soil, which can amplify ground motion by two or more times. This paper addresses seismic hazard from estimates of strong ground motion, and does not estimate the seismic risk to structures.

SEISMICITY OF HAWAII 1970-92

The seismic network operated by the U.S. Geological Survey's Hawaiian Volcano Observatory (HVO) expanded and increased its sensitivity during the 1960's (Klein and Koyanagi, 1980). We therefore used the HVO earthquake catalog from 1970 through 1992 to portray the seismic zones of Hawaii. Earthquakes, analysis procedures and results of the HVO seismic network are described in a series of annual bulletins (eg. Hawaiian Volcano Observatory, 1969-1987; Nakata et al., 1991; Tomori et al., 1991). Figure 1 is a plot of earthquakes from this catalog. Table 1 and the large square symbols represent events with local magnitude larger than 5.0.

Earthquakes at the active volcanoes of Hawaii can be broadly classed into three types which are caused by different processes in the structural deformation of the volcano (eg., Klein et al., 1987). The first type are volcanic earthquakes under the active calderas and rift zones of Kilauea and Mauna Loa volcanoes. These generally accompany movement of magma along the conduit from the deep Hawaiian hot spot up to the summit magma reservoir, inflation of the reservoir and extension of the caldera above it, and growth of dikes under the caldera or rift zones by rapid intrusion of magma. These dike-related

volcanic earthquakes generally occur in swarms accompanying eruptions or intrusions and are located close to the causative conduit or dike. Their depths at Kilauea are mostly between 2 and 4 km. The swarms have not produced earthquakes larger than about magnitude 3.5 because the stress producing them is concentrated near the conduit and the stress is insufficient to rupture a large fault area. The ground shaking caused by these volcanic earthquakes is confined to the active rifts and is overshadowed by the hazard from surface rifting and lava flows from eruptive fissures. The small, volcanic earthquakes under Kilauea's caldera and rifts are not plotted in figure 1 and will not be considered a significant earthquake source in the probabilistic ground shaking calculations.

The second type are the tectonic earthquakes. They occur in the volcano flanks 2-20 km from the rift zones and mostly in the lower part of the crust. The most active flank areas are Kilauea's south flank, the Kaoiki seismic zone and the Hilea seismic zone (figs 1b and 3b). The active flank areas are adjacent to the volcanically active rift zones. Depths of small earthquakes are generally between 5 and 10 km under the south flank and 5 to 13 km in the Kaoiki (Crosson and Endo, 1982; Klein et al., 1987), though the largest earthquakes and most of the slip is at the base of these seismic zones (table 1). Both shallow volcanic earthquake swarms and deeper tectonic flank earthquakes occur in and near Kilauea's Lower East Rift Zone (Koyanagi, 1981).

The flank earthquakes release stress imposed as lateral compression by the growth of rift zone dikes (eg., Swanson et al., 1976; Ando, 1979; Furumoto and Kovach, 1979; Crosson and Endo, 1982; Dvorak et al., 1986; Bryan and Johnson, 1991; Wyss et al., 1992; Dvorak, 1994). Under the south flank, motion is largely southward slip of the flank block on near-horizontal planes. The Kaoiki and Hilea seismic zones show both right lateral slip on NW striking, near vertical fault planes and SE directed decollement slip on near-horizontal planes. Slip thus results from a compression axis joining the summits of Kilauea and Mauna Loa (Endo, 1985; Bryan and Johnson, 1991; Jackson et al., 1992). The largest earthquakes in Hawaii such as the 1868 Kau earthquake and the 1975 Kalapana earthquake are south of Mauna Loa's rift zones and are of this flank type. The maximum earthquake size under a flank undergoing basal slip is limited by the length and width of the flank.

The larger flank earthquakes are best represented by their rupture areas inferred from their aftershock zones (figure 2). The 1983 earthquake shows that most of the Kaoiki seismic zone can break in a single event, just as the 1975 Kalapana earthquake ruptured most of the south flank.

Earthquakes caused by active rifts and flanks can be seen at other Hawaiian volcanoes less seismically active than Kilauea (figure 1a). Earthquake swarms under Mauna Loa's Northeast Rift Zone and under the west flank that are 4-14 km from the summit caldera were caused by magma movement preceding and during Mauna Loa's 1975 and 1983 eruptions (figure 1b; Decker et al., 1983; Endo et al., 1988). The NNW trending seismicity on Mauna Loa's west flank exhibits the same type of seaward basal slip exhibited on the south side of Kilauea (Bryan and Johnson, 1991; Gillard et al., 1992). The M=6.9, August 21, 1951, Kona earthquake was probably of this type. Loihi submarine volcano produces earthquake swarms (Macdonald, 1952). The swarms at its summit and larger subsequent mainshocks on its flanks are much like the pattern seen at Kilauea Volcano (Klein, 1982b). Earthquakes occur NW of the dormant Hualalai Volcano along the extension of its NW rift zone, but the causative mechanism of these events has not been studied.

Earthquakes outline Kilauea's vertical magma conduit under the caldera. The earthquakes show that it widens with depth and plunges to the south and SW to merge with scattered earthquakes extending to 60 km depth. This earthquake cloud is a source of deep harmonic tremor, is centrally located between the active volcanoes Kilauea, Mauna Loa and Loihi. The deep earthquake zone appears to mark the Hawaiian hot spot (Aki and Koyanagi, 1981; Klein, 1982a). The most productive deep earthquake cluster is in the mantle between 25 and 35 km depth under Kilauea Caldera. The stresses driving these earthquakes may result from lithospheric bending and traction from the sliding flank block above which is concentrated around a weak magma conduit (Klein et al., 1987b).

The third class of earthquakes do not appear to be caused by an active rift or flank, but occur in diffuse zones under Mauna Kea, Kohala and in the mantle underneath the entire island (figures 1a and 1c). The causative stress for these diffuse earthquakes is probably unrelaxed stress from the subsidence of the island and flexure of the lithosphere under the gravitational load of the island (e.g. Elliot Endo, written communication, 1977; Klein and Koyanagi, 1989).

The relationship of the three classes of earthquakes to magmatic pressure affects their temporal occurrence and their maximum size. This is because the three classes of earthquakes are successively more distant from the pressure within magmatic conduits. The earthquake swarms under the summit caldera and rifts fluctuate on the scale of minutes to days in response to magmatic stresses. The response of the flanks to accumulated dike intrusion in the adjacent rift zone may last for several years or decades. The upper mantle earthquakes that result from lithospheric bending under the volcanic load probably continue for hundreds of thousands of years after the shield building phase stops, as they do under Kohala Volcano and older volcanoes in the chain. The probabilistic hazard calculations assume that earthquakes have a Poissonian distribution with a rate that does not change with time. Fluctuations in rate because of stress variations in a seismic cycle (Wyss, 1986) or variable intrusive activity in an adjacent rift zone (Dvorak et al., 1986; Dieterich, 1988) are not well known and will not be modeled.

EARTHQUAKE RATES IN HAWAII

Seismic hazard depends on the expected rates of different magnitude earthquakes in each seismic source zone. The complete sampling of small earthquakes helps estimate large earthquake rates. We use the HVO earthquake catalog from 1970 to 1992 to estimate rates because the expansion of the network and an improved analysis procedure during the 1960's made a more complete and accurate catalog after 1969. Because this 23 year period does not reflect the higher levels of pre-1970 historic seismicity in Kona, Hualalai and Hilea, the rate estimates for those areas are from the history of moderate to large earthquakes since the mid 1800's.

Figure 3 shows 11 shallow (0-20 km depth) and 8 deep seismic source zones in Hawaii. Earthquakes from the 1970-1992 catalog determined the basic rates for each region. Each region is assumed to behave as a tectonic unit; for the hazard calculations, each is assumed to have an earthquake rate that is temporally and spatially uniform but is magnitude-dependent. The regions do not necessarily correspond to the rupture area of the largest earthquake within them, however. Region 1 (figure 3b) approximately corresponds to the rupture area of the 1975 Kalapana earthquake as delimited by its aftershocks (figure 2). The Kalapana earthquake was not a uniform rupture of region 1 because the radiation was strongest from asperities within the rupture area (Wyss et al., 1981; Harvey and Wyss, 1986), and because the mainshock rupture extended perhaps 10-20 km offshore and outside the area of aftershocks (Ando, 1979; Eissler and Kanamori, 1987). Region 2 approximately corresponds to the rupture area of the 1983 Kaoiki earthquake (Koyanagi et al., 1984; Jackson et al., 1992). None of the other source zones have been filled by an earthquake which ruptured the entire zone during the period of intrumentally-located earthquakes. A large earthquake can rupture several adjacent zones, however: the source area of the M~7.9 great Kau earthquake of 1868 probably ruptured regions 1, 2, 3, 4 and part of regions 5 and 7 (Wyss, 1988).

The most recent 23 years of the HVO earthquake catalog are used to estimate the basic rates for each region. Figure 4 shows the log of the number of earthquakes versus magnitude for each of the 19 regions. The log of the cumulative number of earthquakes N of magnitude larger than M is generally linear within some magnitude range:

$$\log(N) = a - bM, \quad M_{min} < M < M_{max}$$

Figure 4 shows the linear fit of this Gutenburg-Richter law determined by the maximum likelihood method (Aki, 1965). We use local magnitude M_L determined by two Wood-Anderson and one other optical seismograph for most earthquakes, and either surface wave magnitude M_S or coda duration magnitude M_D when M_L is not available (eg. Nakata et al., 1991). The catalog is not complete below a minimum magnitude that varies with each source zone. The distribution for an individual zone for this short 1970-92 period rarely contains enough events close to the maximum size to show reliable departure from a linear relationship.

Aftershocks of the 1975 and 1983 earthquakes were not removed from the data sample. Aftershocks are generally too small to influence the frequency-magnitude distribution above M5.5 which principally controls the seismic hazard. Aftershocks are also part of the seismic hazard and have a similar spatial distribution to the continual seismicity. This study calculates the average hazard from all earthquakes as if seismicity were Poissonian with a probability constant in time.

The b-values of each region are a measure of the relative numbers of large and small events, and are tabulated in table 2 along with a-values and other parameters for each region. The a-value measures the number of magnitude 0 and larger earthquakes, but is not a measure of the rate of large earthquakes or total seismic energy. The b-value may be higher in areas of high stress concentration, i.e., areas close to volcanic vents (Mogi, 1962; Scholz, 1968). The b-value in most areas is close to the typical tectonic earthquake value of about 1.0. Region 4 is the vertical magma conduit under Kilauea caldera and has a high "volcanic" b-value of 1.70 +/- 0.04. This area experiences swarms of often long-period earthquakes, which are probably related to magma flow and perhaps emplacement of new vertical channels. Regions D2 and D3 also have high b values and magma conduits inferred from earthquake swarms. Region D1 has a "tectonic" b-value of 0.92 but also contains vertical magma conduits. This suggests that earthquakes in region D1 are driven by regional stresses, perhaps caused by lithospheric flexure, rather than magma pressure within the conduits (Klein, 1987b).

It is important to verify or supplement the rates of large earthquakes estimated from the 1970-1992 catalog. The largest events in each of the three most active regions (figure 4a, 4b and 4c) appear to occur more frequently than predicted by the linear fit to the distribution of smaller magnitudes. Figure 5 combines the earthquakes from regions 1-4 on the south side of the island. There is an excess of M>5.5 events, but it is difficult to fit a new linear frequency-magnitude distribution to only 4 large earthquakes. This excess of large earthquakes above the extrapolated distribution is seen elsewhere in the world and may result from characteristic earthquakes that rupture an entire zone without frequent moderate earthquakes to rupture parts of the zone (eg. Singh et al., 1983; Schwartz and Coppersmith, 1984; Papadopoulos et al., 1993). It is thus possible that a different tectonic process with a lower b value produces the largest flank earthquakes. It is also possible that different seismographs or different periods of the maximum signal produce slightly different magnitude scales above and below M 5.5.

The best comparison of the rates of M>5.5 earthquakes is with the catalog compiled by Wyss and Koyanagi (1992). Figure 6 shows the annualized frequency-magnitude distribution of earthquakes from south Hawaii for both the HVO, and Wyss and Koyanagi catalogs. We included 19 earthquakes for which Wyss and Koyanagi (1992) listed magnitudes and 13 earthquakes from 1823 to 1908 whose magnitudes were estimated from their largest intensity (their table 2 and figure 20). The distribution of the 1823-1992 catalog (x symbols, solid line) is linear above magnitude 5.5. This linearity and the fact that M>5.5 earthquakes are felt island wide means the catalog is probably complete above magnitude 5.5. The distribution of the Wyss and Koyanagi catalog has a slope of 0.63 and fits the slope for the 1970-1992 catalog above M=5.2. The a, b and other parameters for the 1823-1992 and adjusted 1970-1992 rates are listed in table 3. The adjusted distributions for regions 1 and 2 are plotted in figures 4a and 4b. The rate from the 1970-1992 HVO catalog is about 1.5 times that of the historic catalog for M>5.5. It does not seem likely that the historic earthquake catalog is systematically incomplete or that it underestimates magnitudes compared to the HVO catalog because modern magnitudes were used for its calibration (Wyss and Koyanagi, 1992).

The rates of seismicity have changed in the different seismic source zones during the last 150 years. The Hilea seismic zone (region 3) has declined in activity. It produced a magnitude 7 earthquake on March 28, 1868, the great M~8 Kau earthquake of April 2, 1868 and its aftershocks, and a M6.1 event on September 14, 1919 (Wyss and Koyanagi, 1992). The historic activity in Kona and west Mauna Loa (region 7) and Hualalai (region 8) is also higher than the 1970-1992 seismicity. Kona produced a M6.9 earthquake on August 21, 1951 and three other magnitude 6 events during 1950-52. A series of earthquakes at Hualalai in September and October 1929 culminated with a M6.5 event on October 5. The seismicity observed during 1970-1992 does not reflect this higher historic activity. The apparent decrease of seismicity under Mauna Loa's west and south flanks may have accompanied the decreasing frequency of eruptions at Mauna Loa and increasing frequency at Kilauea that occurred after 1950 (eg. Klein, 1982b).

I estimate the seismic hazard from earthquakes in Hilea, Kona and Hualalai (regions 3, 7 and 8) from frequency-magnitude distributions of historic seismicity (Wyss and Koyanagi, 1992). When earthquake magnitudes were not determined, the estimated magnitudes were scaled from the maximum intensity using Wyss and Koyanagi's relationship. Wyss and Koyanagi listed only two events from regions 7 and 8 prior to 1914, thus I used 1914-1992 as the period for estimating average earthquake rates in those regions. Most aftershocks of the 1868 Kau earthquake could not be located from isoseismal maps (Wyss and Koyanagi, 1992) but the Lyman diary kept in Hilo demonstrated that aftershocks continued above the background level of felt earthquakes for about 6 years (Wyss, 1988). I therefore assigned all earthquakes with maximum intensity of V or greater during the first two years of aftershocks to region 3. The number of historic Hilea earthquakes is thus a minimum estimate. The resulting numbers of earthquakes of maximum intensity V or greater (M>5.6 approximately) and the a- and b-values of the frequency-magnitude distribution are listed in table 3 for regions 3, 7 and 8. The historic distributions are shown with x symbols in figures 4c, 4g and 4h after scaling to a 23 yr observation period.

The completeness and magnitudes in the historic earthquake record are uncertain, but we seek only an estimate of earthquake rates expressed by the two parameters a and b in the Gutenberg-Richter frequency-magnitude distribution. We will use earthquake rates derived from the a and b values listed in the bottom of table 3 for magnitude 5.2 and larger in the calculation of expected PGA. For regions 1 and 2, the parameters in table 3 reflect adjustments to the 1970-1992 distribution for the higher occurrence of M>5.5 earthquakes. For regions 3, 7 and 8, the a and b values are derived from the historic record: these are used in place of the un-adjusted parameters in table 2 derived from smaller 1970-1992 earthquakes. PGAs calculated from the un-adjusted 1970-1992 rates (table 2) are shown for comparison in appendix 1.

The estimated recurrence intervals of large earthquakes in south Hawaii based on the 1970-1992 earthquake catalog are comparable with the interval between the two historic magnitude 7 earthquakes. Table 3 shows the average recurrence interval of south Hawaii earthquakes for several magnitudes. These recurrence intervals are estimated from the frequency-magnitude distribution and are not based on intervals between observed events. The recurrence intervals of M>6.5 events from tables 2 and 3 are also shown in map view in figure 7. The Wyss and Koyanagi (1992) and HVO catalogs imply that the recurrence interval of M>7 earthquakes is 29-44 years, and that of M 8 earthquakes is 124-185 years. This recurrence is compatable with the 107 year interval between the 1868 M=7.9 and 1975 M=7.2 events. Wyss (1988) suggests a very tentative recurrence of great M~8 events like the 1868 Kau earthquake of 80-160 years based on geodetic arguments. This interval agrees with that implied by the frequency-magnitude distributions.

The estimates of earthquake rates and thus the probable hazard in regions without large historic earthquakes are probably too low. The distributions of regions 1, 2, 3, 7 and 8 based on the 1970-1992 seismicity were adjusted upward because of historic earthquakes or a non-linear distribution. A similar adjustment might be made for other regions if there was more data. The average recurrence intervals for other regions in table 2 and figure 7 based on extrapolating the low-magnitude distribution are thus

likely to be overestimates.

PEAK GROUND ACCELERATION ATTENUATION CURVES FOR HAWAII

We will model peak ground accelerations (PGAs) by choosing a published attenuation curve because the existing PGA measurements (33 values from 7 moderate earthquakes) are not sufficient to derive a Hawaiian attenuation curve. The earthquake with the most PGA measurements is the M6.6 Kaoiki earthquake of 1983. Figure 8 plots observed PGAs for the Kaoiki earthquake (Buchanan-Banks, 1987) and several published attenuation curves for a M6.6 earthquake. We use a PGA which is the maximum chosen from the two horizontal components, and the distance is measured to the closest point of the surface projection of the aftershock zone. We seek a curve to fit Kilauea and Mauna Loa earthquakes as recorded on lava or rock sites (solid symbols in figures 8 and 9). The Campbell (1989) and Boore et al. (1993) curves look most promising because their distance decline approximates that of the intensity decay of the Kaoiki earthquake (figure 8; Wyss and Koyanagi, 1992, their figures 48B and 50) scaled to PGA using their relationship.

The attenuation relation should have the same distance decay and same mean value as Hawaiian PGAs. To choose between the curves, we plot the residual (ratio of observed to calculated) PGA values for each curve (figure 9). We can not use the Seed and Idriss (1983) curve because there is no magnitude scaling term.

The Boore et al. (1993) attenuation relationship best approximates the distance dependence of the sparse Hawaiian PGA data (figure 9a). The predicted PGAs from other curves fall off too rapidly with distance resulting in an overestimate of near PGAs and/or an underestimate of far PGAs (figures 9b-f). We use the Boore et al. relationship for site class B which is essentially a rock site. The coefficient of the distance term of the Boore et al. (1993) attenuation curve is the smallest of the curves considered (table 4). To approximate the PGAs at Hawaiian rock or lava sites, the Boore et al. (1993) curve must be shifted upward by a factor of 1.20 because the mean of the natural logs of the ratios of the observed to calculated PGAs is 0.18 +/- 0.45. The Campbell (1989) relationship also approximates the Hawaiian PGAs (figure 9e), but it was only derived from magnitudes up to 5.0 and distances out to 30 km (table 5). Figure 9g shows the residuals of the Boore et al. relationship versus magnitude: although the curve is not excluded by the data, there are not enough earthquakes to judge the adequacy of its magnitude dependence. We will use the Boore et al. (1993) relationship, modified by a small upward shift (table 4) in the expected PGA calculations.

Sites underlain by more than 0.5 m of ash or soil experience systematically higher PGAs (open symbols in figures 8 and 9; Buchanan-Banks, 1987). The limited data suggest that ash typically gives a site amplification of about 2.0 (figure 9a). Spectra of accelerograms recorded on ash often show a resonance peak caused by local site amplification. For example, the accelerogram from the 1983 Kaoiki earthquake recorded at the Fish and Wildlife Service Headquarters in Hilo on 3 m of ash has a peak at 3 hz which is 4-5 times higher than neighboring frequencies. Intensities may be influenced by site effects such as an ash layer. The intensity curve for the 1983 Kaoiki earthquake after scaling to PGA (figure 8) gives a better fit to the ash sites than the lava or rock sites. One must therefore increase the PGAs calculated in this paper upward to compare with ash covered sites or with maximum intensity in areas with ash or soil cover.

Modeling probabable PGAs in Hawaii also requires an attenuation curve for upper mantle earthquakes at a depth of 30-40 km. Unfortunately, the only PGA measured for a sub-crustal earthquake is from the M6.1 Honomu earthquake in 1973 (Nielsen et al., 1977; Wyss and Koyanagi, 1992). Krinitzsky et al. (1988) present an attenuation relation for sub-crustal earthquakes deeper than 20 km derived from subduction events in Japan. We also consider their attenuation curve for crustal earthquakes, but calculated using a mantle source depth. The two Krinitzsky et al. curves and the Boore et al. (1993)

curve for a crustal source are plotted in figure 10 with the observed PGA value for the 1973 M=6.1 Honomu earthquake. Of the three curves plotted, the average slope of the Krinitzsky et al. (1988) sub-crustal curve in the distance range 20-100 km best approximates the intensity decay curve of Wyss and Koyanagi (1992) for this earthquake. The intensity curve is scaled to PGA with the Hawaiian peak ground acceleration vs. intensity relation of Wyss and Koyanagi (1992; their figure 50). We will use the Krinitzsky et al. subcrustal curve because its distance decay rate is similar to that of intensity and it approximates the curve for a crustal source (dashed line, figure 10) at distances greater than about a focal depth. We do not have enough data to confidently choose a deep source attenuation curve, but the relative rate of deep earthquakes is low and they produce a probable PGA (figure A1c) much smaller than the crustal earthquakes. Krinitzsky et al.'s (1988) sub-crustal relation is

$$\log(PGA) = -0.91 + 0.35M - \log((d^2 + 100^2)^{1/2}) - 0.00255d$$

where PGA is in g, M is local magnitude and d is epicentral distance.

Maps of PGA calculated from the preferred attenuation curve can be compared with the observations in figure 11. Sources of seismic radiation for the crustal earthquakes are assumed uniform over the area of the aftershock zone. This assumption may overestimate the radiation coming from the eastern and western 15 km of the Kalapana rupture zone (figure 11a). Horizontal and vertical displacement (Ando, 1979; Lipman et al., 1985), concentration of aftershocks (Crosson and Endo, 1982; figure 1b) and location of hard asperities producing pulses in the accelerogram records (Harvey and Wyss, 1986) were largest in the central 40 km of the rupture. The overestimation of the PGA expected at the Punaluu recording site on Hawaii's south coast (figure 11a) is partly explained by assuming strong radiation from the western rupture zone.

The calculated areas of largest PGA (figure 11) do not exactly correspond to the isoseismal maps of intensity (figure 12). Site effects including amplification by surface ash layers and source complexity could account for the different shapes of calculated PGA and intensity contours for the 1975 Kalapana earthquake. The intensity VII contours correspond to larger calculated PGAs (0.4-0.5 g) for the south flank earthquakes than for the Kaoiki and deep 1951 earthquakes (~0.2 g). As in other parts of the world, PGA does not precisely correlate with intensity (Trifunac and Brady, 1975; Murphy and O'Brien, 1977; McGuire, 1984; Krinitzsky and Chang, 1988; Wyss and Koyanagi, 1992).

PROBABLE PEAK GROUND ACCELERATIONS FOR SOUTH HAWAII

The ingredients are now assembled to calculate the probabalistic peak ground accelerations (PGAs) for Kilauea Volcano: we have defined several seismic source zones with earthquake rates at each magnitude interval, and attenuation curves for PGA as a function of magnitude and distance. We use the SeisriskIII computer program to calculate the probable PGAs (Bender et al., 1982 and 1987). The theory of the seisriskIII probability calculations was developed by Cornell (1968) and used by Algermissen et al. (1982; 1990) to calculate the seismic hazard map of the United States. For each evaluation site and point within an seismic source zone, SeisriskIII uses the frequency of earthquakes at each magnitude and calculates the expected PGA from an earthquake at that magnitude and distance. The frequencies of occurrence of PGAs are summed for points within each source zone which gives the probability distribution of PGAs for the evaluation site. SeisriskIII then calculates the PGA with a specified probability of not being exceeded during a certain exposure time from the distribution. SeisriskIII assumes a log-normal distribution of PGAs about the values predicted by the attenuation relationship. The calculations can be generalized to different exposure times by assuming the earthquake rate does not vary in time and that earthquake probability follows the Poisson distribution.

Figure 13 maps the horizontal PGA that has a 90% probability of not being exceeded (10% probability of being exceeded at least once) during an exposure time of 50 years. This map could be used by an engineer to estimate the horizontal PGA a structure must withstand to survive for 50 years with a 10% risk of exceeding the design PGA. Fifty years is a typical period of human interest and is the period used for the seismic hazard map of the U.S. (Algermissen et al., 1990). The active south flanks of Kilauea and Mauna Loa can possibly expect (with a 10% probability) an occurrence of PGA of 1.0 g within 50 years. The probabilistic PGAs (0.4-1.0 g) are considerably higher but much better resolved than the 0.3 g value for Hawaii in Algermissen et al.'s (1990) map. The 1 g PGA in south Hawaii for a 50 year exposure time is comparable with the values for the San Andreas Fault in California and the subduction zone in the Gulf of Alaska, which exceed 0.8 g (Algermissen et al., 1990). Values of vertical PGA exceeding 1 g have historically occurred in Hawaii because rocks were thrown up over undisturbed turf (Brigham, 1909) and people were "bounced around like balls" (Wyss and Koyanagi, 1992) during the great Kau earthquake of 1868. Because the horizontal PGA is generally larger than the vertical component, it is probable that the horizontal PGA in 1868 significantly exceeded 1 g.

Several other assumptions were made in calculating the PGAs of figure 13. The effects of changing some of the assumptions are treated in appendix 1. The 1970-1992 earthquake catalog was used to calculate the seismicity rate parameters (tables 2 and 3). In the Hilea, Kona and Hualalai zones, however, the longer historic catalog was used (table 3). The maximum magnitudes of earthquakes allowed to occur in the PGA calculation are given in table 2 for each region. The PGAs from all events larger than M7.7 were limited to those of a M7.7 earthquake (table 2). A source smoothing of 4 km was used to soften the boundary between a high and low seismicity region. The Boore et al (1993) relation for PGA given distance and magnitude does not consider non-linearity or saturation of strong ground motion at high accelerations. Only 33 observations from 7 moderate earthquakes are available to choose an attenuation curve. Thus the predicted PGAs from M>7.2 earthquakes and those exceeding 0.7 g have not been tested by instrumental measurement.

A random variation in the observed PGAs (excluding ash sites) is assumed and included in the probabilistic PGA calculations: PGAs larger than the value calculated from the attenuation curve will occur when random variations are considered. This is because the PGAs are assumed to be log-normally distributed about the best fitting attenuation curve. The standard deviation of the log-ratio of observed PGAs to those calculated from the Boore et al. (1993) relationship is 0.45 (natural log), i.e. 57% (figure 9a). The probable PGAs on Kilauea's south flank are raised by about 0.2-0.3 g when the effect of the observed variation is considered (see also appendix 1). The standard deviation seen for Hawaiian PGAs is similar to that found by Boore et al. (1993) and within the range of those from other studies (table 4).

The contours of probable PGA on Kilauea (figure 13) follow the shapes of the seismic source zones of figure 3b. The PGA contours also mimic the source zones of the 1975 Kalapana and 1983 Kaoiki earthquakes (figures 2 and 11) because the ruptures and aftershocks of these earthquakes helped determine the choice of the source zones. The expected PGA values (figure 13) are similar to those calculated for the 1975 and 1983 earthquakes (figure 11) when increased by about 50% to allow for random variation. This similarity indicates that events of their size are probable during the next 50 years. The likelihood of earthquakes similar to those in 1975 and 1983 within 50 years is also seen from the magnitudes of events with a 50 year average recurrence time in regions 1 and 2 (table 2).

The level of PGA with a 90% probability of not being exceeded can be calculated by the SeisriskIII program for a variety of exposure times (figure 14). Some aspects of the probable PGA maps for times longer than 50 years may not be realistic. The high PGA levels in the south flanks result from the high probabilities that earthquakes of the maximum size (and their large PGAs) will occur during the exposure time: the PGA that has only a 10% chance of being exceeded must then be raised to perhaps unrealistic levels. The high seismicity, the variation of PGAs about those given by the attenuation curve, and long exposure times where the occurrence rates of high PGAs become important,

together produce PGAs greatly exceeding 1 g in a range beyond instrumental observations. The fact that the area for which some level of PGA, say 1.0 g, enlarges with longer exposure times is an important result, however. Seismicity will shift over time and the PGA contours will change shape when the volcanoes shift magmatic activity to different parts of the rift zones. The probability of this shift increases with longer exposure times. For these reasons the PGA maps for 100 and 250 year exposure times should be interpreted with caution, and maps for longer exposure times are not realistic.

The probabalistic PGAs for exposure times other than those mapped in figures 13 and 14 can be inferred from the seismic hazard curves of figure 15. The four sites range from the highest hazard at Wood Valley, which is representative of the Hilea and Kilauea south flank seismic zones, to the least hazard at Kohala at the northern tip of the island. For an exposure time of 50 years and a 90% probability of not being exceeded, the entire island of Hawaii can expect a PGA of greater than 0.3 g.

The historic earthquakes since 1823 emphasize the south flanks of Mauna Loa and Kilauea as major hazard zones. The historic epicenters of larger events for which isoseismal maps are available (figure 16a; Wyss and Koyanagi, 1992) extend through the south flanks of Kilauea and Mauna Loa. The map of maximum historic intensity (figure 16b) is largely controlled by the intensities of the M=7.9 great Kau earthquake of April 2, 1868. The area of intensity IX shaking approximates the inferred rupture zone of the 1868 earthquake (Wyss, 1988). The maximum intensity X contour (figure 16b) covers both south flanks and approximates the 0.9 g contour of the 50 year PGA map (figure 13). Thus historic intensities and the calculated PGA map both show the mobile south flanks of Kilauea and Mauna Loa are the areas of greatest seismic hazard in Hawaii.

EARTHQUAKE HAZARDS IN ADDITION TO GROUND SHAKING

Submarine landslides and tsunamis. Submarine landslides surround each of the Hawaiian islands, sometimes up to 200 km long and 5000 km^3 in volume (Moore, 1964; Lipman et al., 1988; Moore et al., 1989; Moore et al., 1994). Several of the older Hawaiian shields appear to have lost at least 30% of their volume to submarine landsliding (Holcomb and Searle, 1991). Catastrophic submarine landslides might be triggered by a nearby earthquake, or themselves might trigger earthquake slip. Submarine landslides and fast moving debris avalanches pose a hazard from the strong shaking they can produce and the possibility of slumping of large blocks of volcano flanks into the sea.

Tsunamis from local earthquakes in Hawaii have historically generated waves tens of meters high. The tsunami from the 1868 Kau earthquake destroyed more than 100 houses in the epicentral area and killed 46 people (Hitchcock, 1912). The 1868 tsunami may have been 18 m high because it overran palm trees (Wood, 1914) but is reported by Tilling et al. (1976) to have reached 13.7 m at Keahou landing. The tsunami from the 1975 Kalapana earthquake killed two people with a 14.6 m wave at Halape on the south coast (Tilling et al., 1976). Tsunamis from catastrophic submarine landslides may be several hundred meters high locally. A tsunami from a submarine landslide may have locally produced 100,000 yr old deposits of coral and boulder fragments at an elevation of 375 m on the island of Lanai that can't be attributed to sedimentation by worldwide high stands of the ocean (Moore and Moore, 1984 and 1988).

Large flank earthquakes like the 1975 Kalapana event can be related to submarine landslides. The 1975 Kalapana earthquake generated long period surface waves that can be better modeled by a single force which is generated by a large-scale slump of the south flank than the double force typical of a continental earthquake (Eissler and Kanamori, 1987). The Kalapana earthquake can thus be viewed as a landslide that traveled only a few meters. The submarine Hilina slump south of the Hilina Pali fault scarps on Kilauea's south flank coincides with the largest rupture and seaward displacement from the 1975 Kalapana earthquake (Moore and Peck, 1965; Lipman et al., 1985; Moore et al., 1989). The Hilina slump is a creeping mass on a flank oversteepened by lava flows and seaward movement of

Kilauea's south flank block. A 20-30 km by 40 km rupture surface slipped in the 1975 Kalapana earthquake which pushed the south flank up to 8 m seaward at the coast and uplifted the submerged flank to produce a tsunami with a compressional first motion (Hatori, 1975; Ando, 1979; Lipman et al., 1985). It is likely that this submarine tectonic movement also triggered some submarine landslide movement.

An approximate calculation (appendix 2) estimates that large submarine landslides visible around Hawaii are catastrophic events with "magnitudes" of 7.5 to 8.8. These are rare events, however: a magnitude 8 landslide is about 2 to 3 orders of magnitude less likely than a magnitude 8 earthquake (appendix 2). Submarine landslides thus pose a real hazard, but with annual probabilities of large ground shaking small compared to earthquakes.

Site amplification. Site amplification of ground motion in Hawaii results from the thickness of volcanic ash or soil under the site. The ash is usually severely weathered volcanic glass with a high clay and often a high water content (Buchanan-Banks, 1987). The map of ash deposits on Hawaii (Buchanan-Banks, 1987) shows significant deposits on Mauna Kea, the Hilea area near Pahala and Wood Valley, and the Puna district north of Kilauea's East Rift Zone. Observed peak ground accelerations (PGA) (figure 9a) are on average two times higher than the PGAs calculated for a lava site. Nielsen et al. (1977) found the velocity response of ash sites to be 5-10 times that of rock sites for aftershocks of the 1973 Honomu earthquake. Structural damage in the Honomu earthquake was greatest on the 25 m thick ash deposits in the Pueo area just north of Hilo (Nielsen et al., 1977). Buchanan-Banks (1987) noted that damage and recorded PGAs from the 1983 Kaoiki earthquake were worse on sites with more than 0.5 m of ash. For example, the accelerograph at the Fish and Wildlife Service in Hilo on 3 m of ash recorded PGAs 5 times higher than the University of Hawaii at Hilo which is on lava. Site amplification of ash sites in Hawaii may depend on the response of the recording instrument and thus on the frequencies produced by the earthquake, however: Rojan and Morrill (1977) found that the University of Hawaii at Hilo seismoscope showed the same amplitude as another seismoscope on ash at the same epicentral distance. Observations are few, but a site on ash can expect 1-5 times the shaking of a lava or rock site.

Liquefaction and vibrational settling. Cases of true liquefaction, i.e. the transformation of saturated soil into a fluid mass with no shear resistance, have not been reported in Hawaii. Vibrational settling of ash and materials used as fill under roads and in cracks and fissures occurred, however, during the 1975 Kalapana and 1983 Kaoiki earthquakes (Tilling et al., 1976; Buchanan-Banks, 1987). Most of the observations of settling were in circum-caldera and rift zone cracks near Kilauea Caldera. Nielsen et al. (1977) noted that volcanic ash liquefied after several passes of heavy equipment during road construction, and considered liquefaction possible under heavy earthquake shaking of long duration.

Ground ruptures. Each of the larger (M>6) recent earthquakes in Hawaii produced ground ruptures or surface faulting. Most of the surface faulting appears to be secondary because the primary decollement slip surfaces of events like the 1868 Kau and 1975 Kalapana earthquakes are near-horizontal at the base of the volcanic pile. Rupture is at a depth of 9-13 km and does not reach the surface. An exception is the Kaoiki seismic zone, where strike-slip faulting came within 1-2 km of the surface and produced significant en echelon tension cracks where the inferred fault plane intersects the surface (Jackson et al., 1992). Normal faults such as the Hilina Pali on Kilauea's south flank and the Kealakekua Fault in Kona are either secondary slump block faults, or the surface expressions of listric faults that do not extend to the surface, are concave upward, and may flatten to near horizontal with depth (Swanson et al., 1976; Lipman et al., 1985). These normal faults often slip in large earthquakes but may not be the primary fault.

Ground ruptures are a common occurrence during large Hawaiian earthquakes. The great 1868 Kau earthquake opened numerous faults and fissures in and southwest of Kilauea's Southwest Rift Zone (Hitchcock, 1912). The Kaoiki earthquakes of November 20, 1974 and November 16, 1983 produced

left stepping extension cracks along a northeast trend (Jackson et al., 1992). Cracks in Kilauea's Southwest Rift Zone experienced extensional and compressional deformation in the 1983 Kaoiki earthquake (Buchanan-Banks, 1987). The 1868 Kau earthquake (Hitchcock, 1912) and 1975 Kalapana earthquake (Tilling et al., 1976; Lipman et al., 1985) reactivated normal faulting along Kilauea's Hilina fault system. The Kalapana earthquake produced nearly continuous ground breakage for 25 km with downward slip of the south block of up to 1.5 m. The Kalapana earthquake also opened extensional cracks with separation of up to 1 m along the north and east rims of Kilauea Caldera, near pit craters of the East Rift Zone, and in the Koae Fault Zone a few km south of Kilauea Caldera.

Cracks, non-eruptive fissures and graben faulting within active rift zones also pose a hazard. This ground breakage occurs above the emplacement of a dike during an intrusion or eruption. Earthquakes with magnitudes less than 3 often accompany intrusions and dike emplacement (e.g. Klein et al., 1987) and can shake the region close to the fissure, but do not cause damage. Sites in the rift zones are exposed to volcanic hazards such as lava flows that are in addition to the seismic hazard.

Earthquake induced landslides and cliff collapse. Slope failures and rockfalls from steep cliffs frequently accompany large earthquakes in Hawaii. Most of these are slopes and cliffs dislodged by ground shaking rather than caused by slip on the primary earthquake fault. The April 2, 1868 Kau earthquake triggered a landslide 1-2 miles wide, 3 miles long and 30 feet thick that carried trees, animals and men with it and killed 31 people (Hitchcock, 1912; Wood, 1914). Extensive damage was done to roads, trails and cliffs at Kilauea Caldera by the 1975 Kalapana and 1983 Kaoiki earthquakes (Tilling et al., 1976; Lipman et al., 1985; Buchanan-Banks, 1987). The 1983 earthquake caused more than 200 rock slides, some as large as 3000 m^3. The PGA at the nearby Hawaiian Volcano Observatory was 0.67 g. There were several rock slides in steep roadcuts that caused road closures north of Hilo after the 1973 Honomu (Nielsen, 1977), 1975 and 1983 earthquakes. The 1983 Kaoiki earthquake caused collapse of the roofs of several lava tubes in the epicentral area, and rock slides on the Kealakekua Fault 50 km from the epicenter in Kona (Buchanan-Banks, 1987). The 1983 event produced no major but several minor 15 m^3 slope failures of ash deposits in the Hilo area.

Triggered volcanic eruptions. Large flank earthquakes on the south side of Hawaii can trigger volcanic eruptions. Triggering could result from either shaking and weakening of the rock surrounding the volcanic plumbing system, or from local changes in magma pressure as stress is redistributed. A small, 250,000 m^3 eruption in Kilauea Caldera commenced 45 minutes after the 1975 Kalapana earthquake (Tilling et al., 1977). A new dike apparently started working its way to the surface during the strong earthquake shaking. The 1983 Kaoiki earthquake did not trigger an eruption because Kilauea's East Rift Zone was erupting at the time.

The great Kau earthquake of April 2, 1868 did not independently trigger volcanic activity: an increase in the Kilauea eruption, a new Mauna Loa eruption, and numerous foreshocks preceeded the earthquake (eg. Wood, 1914). Increased Kilauea volcanism followed the strong shaking and a Mauna Loa eruption occurred immediately after the aftershock on April 5, 1868. Earthquakes and eruptions in March and April 1868 were probably related, but apparently did not occur in a clear cause-and-effect relationship.

The large flank earthquakes in Hawaii act to relieve the horizontal compressive stress built up by repeated rift zone intrusions. This stress release also acts to regionally relieve pressure within the magma system. The 1975 Kalapana earthquake apparently released confining stress near Kilauea's East Rift Zone because the rift switched from a mode of frequent eruptions to frequent intrusions where magma did not have enough pressure to reach the surface (Klein, 1982b). After the Kalapana earthquake, Kilauea Caldera was unable to sustain high levels of inflation of its summit magma reservoir (Lipman et al., 1985). Similarly, Mauna Loa's volume rate of eruption declined to half its pre-earthquake level after the 1868 Kau earthquake and the subsequent period of sustained summit activity (Lockwood and Lipman, 1987). It thus seems that large flank earthquakes can trigger small eruptions

but are unlikely to initiate large, sustained eruptions.

CONCLUSIONS

1. A significant seismic hazard exists in south Hawaii from large tectonic earthquakes that can reach magnitude 8 and intensity XII. This hazard is greatest on the southern flanks of Kilauea and Mauna Loa volcanoes in an area comparable in size with the San Francisco Bay region or the Los Angeles basin. The largest earthquakes are under active and mobile volcano flanks, and not directly caused by volcanic activity.

2. The largest earthquakes, such as the 1868 Kau and 1975 Kalapana earthquakes, can rupture an entire volcano flank by decollement slip. These unbuttressed flanks are stressed by successive intrusions in adjacent rift zones.

3. The earthquake catalog gathered by the Hawaiian Volcano Observatory from 1970-1992 includes small magnitudes and yields earthquake rates as a function of magnitude for several seismic source zones. The historic (1823-1992) catalog of earthquakes must be used to supplement earthquake rates, especially in the Hilea, Kona and Hualalai regions where the 1970-1992 seismicity was relatively low.

4. The log-frequency versus magnitude distributions are nearly linear for the 19 regions into which the seismicity was divided. The linear fit thus gives an estimate of the rate of large magnitude earthquakes. In the three most active regions of south Hawaii (using 1970-1992 earthquakes) and in the Kona and Hualalai regions (using historic earthquakes), rates of M>5.5 earthquakes are higher than those extrapolated from the frequency-magnitude distribution of small 1970-1992 earthquakes. Thus, bi-linear distributions are used where appropriate. The rates for M>5.5 earthquakes have the greatest effect on the probable strong ground motion calculations.

5. The estimated recurrence intervals in south Hawaii are about 3.4-5 years for M>5.5 earthquakes, 29-44 years for M>7 earthquakes, and 120-180 years for M 8 earthquakes. These rates are compatable with the 107 year interval between the M~7.9 1868 and M=7.2 1975 events. The 1823-1992 earthquake catalog for south Hawaii of Wyss and Koyanagi (1992) appears complete above M=5.5, but yields a rate of M>5.5 events which is 67% of the 1970-1992 HVO catalog rate. Both catalogs yield higher rates of M>5.5 earthquakes than the rate extrapolated from smaller magnitudes in the HVO catalog. This suggests a different process controls M>5.5 earthquakes such as rupture of regions by characteristic earthquakes.

6. The slope of the linear part of the log-frequency versus magnitude distribution (b-value) is between 0.9 and 1.3 for most seismic source zones. b-values of 1.3-1.7 characterize three of the four regions under Kilauea Caldera through which magma ascends from the mantle. Historic M>5.5 earthquakes under south Hawaii have a b-value of about 0.63.

7. The Boore et al. (1993) attenuation curve includes both distance and magnitude scaling and is found to best fit the peak ground accelerations from Hawaii crustal earthquakes after it is scaled upward by a factor of 1.2.

8. The Boore et al. (1993) curve is appropriate for lava or rock sites. Sites underlain by more than 0.5 m of ash or soil experience systematically higher peak ground accelerations which average about 2.0 times and range from 1.0 to 5.0 times that of lava or rock sites. Facilities constructed on thick ash or soils are more likely to be damaged during an earthquake than facilities constructed on lava or rock.

9. For mantle earthquake sources, this paper uses the attenuation curve of Krinitzsky et al. (1988) derived from subduction zone earthquakes. There is only one useful accelerogram from a mantle earthquake and the choice of this curve is primarily constrained by its similarity to the decay of intensity

from mantle earthquakes.

10. The active south flanks of Kilauea and Mauna Loa can reasonably expect (90% probability of not being exceeded) a peak ground acceleration of 1.0 g within an exposure time of 50 years. This acceleration is comparable with the values for the San Andreas Fault in California and the subduction zone in the Gulf of Alaska, which exceed 0.8 g (Algermissen et al., 1990). The probable PGA in the Kaoiki seismic zone is 0.9 g and the western Kona flank of Mauna Loa might exceed 0.7 g. These PGAs are higher than the earlier estimate of 0.3 g from Algermissen et al.'s (1990) map of the U.S. For an exposure time of 50 years and a 90% probability of not being exceeded, the entire island of Hawaii can expect a PGA of greater than 0.3 g.

11. Earthquake hazards in addition to the calculated ground shaking include submarine landslides which may trigger or be triggered by flank earthquakes, tsunamis generated by local earthquakes, site amplifications at sites underlain by thick ash or soil, vibrational settling of subsurface materials, ground ruptures, earthquake induced landslides, cliff or lava tube collapse and triggered volcanic eruptions. Risk can be reduced by avoiding construction near cliffs, on unstable slopes, over lava tubes, within tsunami inundation zones, or on thick ash or soil.

12. Catastrophic submarine landslides also follow a linear log-frequency versyus magnitude distribution where magnitude is calculated from estimated subsidence energy. Magnitude 8 landslides appear to be 2 or 3 orders of magnitude less frequent than magnitude 8 earthquakes. Great flank earthquakes may often trigger small submarine landslides or slumps, but great submarine landslides are relatively infrequent.

ACKNOWLEDGEMENTS

This study would not have been possible without the hard work and care that the present and past staff of the Hawaiian Volcano Observatory put into the seismic network and earthquake catalog. The consistency and completeness of the catalog through the years are largely due to the efforts of Robert Koyanagi. Some of the many HVO seismology staff members whose efforts made this work possible include Jennifer Nakata, Paul Okubo, Alvin Tomori, Wilfred Tanigawa and Jon Tokuuke. I appreciate the guidance from Bill Joyner and the useful suggestions made by Dave Boore and Paul Okubo. This work was funded by the U.S. Department of Energy in support of the Hawaii Geothermal Project environmental impact analysis.

REFERENCES

Algermissen, S.T., D.M. Perkins and P.C. Thenhaus, 1982, Probabilistic estimates of maximum acceleration and velocity in rock in the contiguous United States, U.S. Geological Survey Open-File Report 82-1033, 99 pp.

Algermissen, S.T., D.M. Perkins and P.C. Thenhaus, S.L. Hanson and B.L. Bender, 1990, Probabilistic earthquake acceleration and velocity maps for the United States and Puerto Rico, U.S. Geological Survey miscellaneous field studies map MF-2120, two oversize sheets.

Aki, K., 1965, Maximum liklihood estimate of b in the formula log N = a -bM and its confidence limits, Bull. Earthquake Res. Inst. Tokyo Univ., v. 43, p. 237-239.

Aki, K. and R.Y. Koyanagi, 1981, Deep volcanic tremor and magma ascent mechanism under Kilauea, Hawaii, Jour. Geophysical Res., v.86, p. 7095-7109.

Ando, M., 1979, The Hawaii earthquake of November 29, 1975: low dip angle faulting due to forceful injection of magma, J. Geoph. Res. v. 84, pp. 7616-7626.

Bender, B., and D.M. Perkins, 1982, SEISRISK II: A computer program for seismic hazard estimation, U.S. Geological Survey Open-File Report 82-293, 103 pp.

Bender, B., and D.M. Perkins, 1987, SEISRISK III: A computer program for seismic hazard estimation, U.S. Geological Survey Bulletin 1772, 48 pp.

Brigham, W.T., 1909, The volcanoes of Kilauea and Mauna Loa on the island of Hawaii: Bernice Pauahi Bishop Museum, Memoir 2 no. 4, pp. 478-497.

Bryan, C.J., 1992, A possible triggering mechanism for large Hawaiian earthquakes derived from analysis of the 26 June 1989 Kilauea south flank sequence, Bulletin of the Seismological Society of America, v. 82, pp. 2368-2390.

Bryan, C.J. and C.E. Johnson, 1991, Block tectonics of the island of Hawaii from a focal mechanism analysis of basal slip, Bulletin of the Seismological Society of America, v. 81, pp. 491-507.

Buchanan-Banks, J.M., 1987, Structural damage and ground failures from the November 16, 1983 Kaoiki earthquake, Island of Hawaii, U.S. Geological Survey professional paper 1350 chapter 44, pp. 1187-1220.

Campbell, K.W, 1989, The dependence of peak horizontal acceleration on magnitude, distance and site effects for small-magnitude earthquakes in California and eastern North America, Bulletin of the Seismological Society of America, v. 79, pp. 1311-1346.

Clague, D.A. and G.B. Dalrymple, 1987, The Hawaiian-Emperor volcanic chain, part 1, geologic evolution, in Volcanism of Hawaii, R.W. Decker, T.L. Wright and P.H. Stauffer, eds., U.S. Geological Survey Professional Paper 1350, pp. 5-54.

Cornell, C.A., 1968, Engineering seismic risk analysis, Bulletin of the Seismological Society of America, v.58, pp. 1583-1606.

Crosson, R.S. and E.T. Endo, 1982, Focal mechanisms and locations of earthquakes in the vicinity of the 1975 Kalapana earthquake aftershock zone 1970-1979: implications for tectonics of the south flank of Kilauea Volcano, Island of Hawaii, Tectonics, v. 1, pp. 495-542.

Decker, R.W., R.Y. Koyanagi, J.J. Dvorak, J.P. Lockwood, A.T. Okamura, K.M. Yamashita, W.R. Tanigawa, 1983, Seismicity and surface deformation of Mauna Loa Volcano, Hawaii, EOS Transactions of the America Geophysical Union, v. 64, p. 545-547.

Dieterich, J.R., 1988, Growth and persistence of Hawaiian Volcanic rift zones, Jour. Geophysical Res., v. 93, p. 4258-4270.

Dvorak, J.J., A.T. Okamura, T.T. English, R.Y. Koyanagi, J.S. Nakata, M.K. Sato, W.T. Tanigawa and K.M. Yamashita, 1986, Mechanical response of the south flank of Kilauea Volcano, Hawaii, to intrusive events along the rift systems, Tectonophysics, v. 124, pp. 193-209.

Dvorak, J.J., 1994, An earthquake cycle along the south flank of Kilauea Volcano, Hawaii, Jour. Geophysical Res., in press.

Eaton, J.P. and K.J. Murata, 1960, How volcanoes grow, Science, v. 132, p. 925.

Eissler, H.K. and H. Kanamori, 1987, A single-force model for the 1975 Kalapana, Hawaii, earthquake, Jour. Geophysical Res., v.92, p. 4827-4836.

Endo, E.T., 1985, Seismotectonic framework for the southeast flank of Mauna Loa Volcano, Hawaii, [Ph.D. thesis]: Seattle, University of Washington, 349 pp.

Endo, E.T., R.Y. Koyanagi, J.S. Nakata and A.H. Tomori, 1988, A catalog of earthquake focal mechanisms for Mauna Loa, Hawaii: September 1983 to January 1984, U.S. Geological Survey Open File Report 88-XXX, 39 pp.

Federal Emergency Management Agency, 1985, National Earthquake Hazards Reduction Program recommended provisions for the development of seismic regulations for new buildings, 1985 edition, part 2, commentary: Earthquake hazards reduction series 18, Building seismic safety council, 200 pp.

Furumoto, A.S. and R.L. Kovach, 1979, The Kalapana earthquake of November 29, 1975: an intraplate earthquake and its relation to geothermal processes, Physics of the Earth and Planet. Int., v. 18, pp. 197-208.

Gillard, D., M. Wyss and J.S. Nakata, 1992, A seismotectonic model for western Hawaii based on stress tensor inversion from fault plane solutions, Jour. Geophysical Res., v. 97, pp. 6629-6641.

Harvey, D. and M. Wyss, 1986, Comparison of a complex rupture model with the precursor asperities of the 1975 Hawaii Ms=7.2 earthquake, J. of Pure and Applied Geophysics, v. 124, pp. 957-973.

Hatori, T., 1976, Wave source of the Hawaii tsunami in 1975 and the tsunami behavior in Japan, Zishin, v. 2(29), pp. 355-363.

Hawaiian Volcano Observatory, 1969-1987, Summaries 49-72 (1968 through 1973, issued quarterly) and Summaries 74-85 (1974 through 1985, issued annually), published by the Hawaiian Volcano Observatory.

Heliker, C., 1990, Volcanic and seismic hazards on the island of Hawaii, U.S. Geological Survey general interest publication available from the USGS, 48 pp.

Hitchcock, C.H., 1912, The Hawaiian earthquakes of 1868, Bulletin of the Seismological Society of America, v. 2, pp. 181-192.

Holcomb, R.T. and R.C. Searle, 1991, Large landslides from oceanic volcanoes, Marine Geotechnology, v. 10. pp. 19-32.

Jackson, M.D., E.T. Endo, P.L. Delaney, T. Arnadottir and A.M. Rubin, 1992, Ground ruptures of the 1974 and 1983 Kaoiki earthquakes, Mauna Loa Volcano, Hawaii, Jour. Geophysical Res., v. 97, pp. 8775-8796.

Johnson, C.E. and R.Y. Koyanagi, 1987, Earthquake hazards of Hawaii: evaluation, monitoring, and risk assessment (abstract), Abstracts with programs, Cordilleran section, Geological Society of America, v. 19, p. 392.

Johnson, C.E. and R.Y. Koyanagi, 1988, A Monte-Carlo approach applied to the estimation of seismic hazard for the state of Hawaii (abstract), Seismological Res. Lett., v. 59, no. 1, p. 18.

Joyner, W.B. and D.M. Boore, 1981, Peak horizontal acceleration and velocity from strong-motion records including records from the 1979 Imperial Valley, California, earthquake, Bulletin of the Seismological Society of America, v.71, pp. 2011-2038.

Klein, F.W., 1982a, Earthquakes at Loihi submarine volcano and the Hawaiian hotspot, Jour. Geophysical Res., v. 87, pp. 7719-7726.

Klein, F.W., 1982b, Patterns of historical eruptions at Hawaiian volcanoes, Jour. Volc. and Geothermal Res., v. 12, pp. 1-35.

Klein, F.W. and R.Y. Koyanagi, 1980, Hawaiian Volcano Observatory seismic network history 1950-79, U.S. Geological Survey Open File Report 80-302, 84 pp.

Klein, F.W., R.Y. Koyanagi, J.S. Nakata and W.R. Tanigawa, 1987, The seismicity of Kilauea's magma system, in Volcanism of Hawaii, R.W. Decker, T.L. Wright and P.H. Stauffer, eds., U.S. Geological Survey Professional Paper 1350 chapter 43, pp. 1019-1186.

Klein, F.W., R.Y. Koyanagi, W.R. Tanigawa and J.S. Nakata, 1987b, Earthquakes near Kilauea's vertical magma conduit between 7 and 36 km depth, Hawaii symposium on how volcanoes work, Hilo, Hawaii, January 1987.

Klein, F.W., and R.Y. Koyanagi, 1989, The seismicity and tectonics of Hawaii, in The Eastern Pacific Ocean and Hawaii, volume N of the Decade of North American Geology, J. Winterer, D. Hussong and R. Decker eds., Geological Society of America, pp. 238-252.

Koyanagi, R.Y., H.L. Krivoy and A.T. Okamura, 1966, The 1962 Kaoiki, Hawaii, earthquake and its aftershocks, Bull. Seismol. Soc. Am., v. 56, pp. 1317-1335.

Koyanagi, R.Y., 1981, Seismicity of the Lower East Rift Zone of Kilauea Volcano, Hawaii, 1960 to 1980, U.S. Geological Survey Open-File Report 81-984, 26 pp.

Koyanagi, R.Y., E.T. Endo, W.R. Tanigawa, J.S. Nakata, A.H. Tomori and P.N. Tomura, 1984, Kaoiki, Hawaii earthquake of November 16, 1983: a preliminary compilation of seismographic data at the Hawaiian Volcano Observatory, U.S. Geological Survey Open-File Report 84-798, 36 pp.

Krinitzsky, E.L., F.K. Chang and O.W. Nuttli, 1988, Magnitude-related earthquake ground motions, Bulletin of the Association of Engineering Geologists, v.25, pp. 399-423.

Krinitzsky, E.L. and F.K. Chang, 1988, Intensity-related earthquake ground motions, Bulletin of the Association of Engineering Geologists, v.25, pp. 425-435.

Lipman, P.W., J.P. Lockwood, R.T. Okamura, D.A. Swanson and K.M. Yamashita, 1985, Ground deformation associated with the 1975 Magnitude-7.2 earthquake and resulting changes in activity of Kilauea Volcano, Hawaii, U.S. Geological Survey professional paper 1276, 45 pp.

Lipman, P.W., W.R. Normark, J.G. Moore, J.B. Wilson and C.E. Gutmacher, 1988, The giant submarine Alika debris slide, Mauna Loa, Hawaii, Jour. Geophysical Res., v. 93, pp. 4279-4299.

Lockwood, J.P. and P.W. Lipman, 1987, Holocene eruptive history of Mauna Loa Volcano, in Volcanism of Hawaii v. 2, R.W. Decker, T.L. Wright and P.H. Stauffer, eds., U.S. Geological Survey Professional Paper 1350, pp. 509-536.

Macdonald, G.A., Hawaiian volcanoes during 1952, U.S. Geological Survey Bulletin 1021-B, 108 pp. plus 14 plates.

McGuire, R.K., 1984, Ground motion estimation in regions with few data, Proceedings of the 8th World Conference on Earthquake Engineering, v. 2, pp. 327-334.

Mogi, K., 1962, Study of the elastic shocks caused by the fracture of heterogeneous materials and its relation to earthquake phenomena, Bull. Earthquake Res. Inst. Tokyo Univ., v. 40, p. 125-175.

Moore, J.G., 1964, Giant submarine landslides on the Hawaiian Ridge, U.S. Geological Survey Professional Paper 501-D, D95-D98.

Moore, J.G. and D.L. Peck, 1965, Bathymetric, topographic, and structural map of the south-central flank of Kilauea volcano, Hawaii, U.S. Geol. Survey map I-456.

Moore, J.G. and G.W. Moore, 1984, Deposit from a giant wave on the island of Lanai, Hawaii, Science, v. 226, pp. 1312-1315.

Moore, G.W. and J.G. Moore, 1988, Large-scale bedforms in boulder gravel produced by giant waves in Hawaii, Geol. Soc. Am. Special Paper 229, pp. 101-110.

Moore, J.G., D.A. Clague, R.T. Holcomb, P.W. Lipman, W.R. Normark and M.E. Torresan, 1989, Prodigious submarine landslides on the Hawaiian Ridge, Jour. Geophysical Res., v. 94, pp. 17,465-17,484.

Moore, J.G., W.R. Normark and R.T. Holcomb, 1994, Giant Hawaiian underwater landslides, Science, v.264, pp. 46-47.

Murphy, J.R. and L.J. O'Brien, 1977, The correlation of peak ground acceleration amplitude with seismic intensity and other physical parameters, Bulletin of the Seismological Society of America, v.67, pp. 877-915.

Nakamura, K., 1980, Why do long rift zones develop in Hawaiian volcanoes: a possible role of thick oceanic sediments (in Japanese with English abstract), Bull. Volcanol. Soc. Japan, v. 25, pp. 255-269.

Nakata, J.S., R.Y. Koyanagi, W.R. Tanigawa, A.H. Tomori and P.G. Okubo, 1991, Hawaiian Volcano Observatory summary 89 part 1, seismic data, January to December 1989, U.S. Geological Survey Open-File Report 91-564, 102 pp.

Nielsen, N.N., A.S. Furumoto, W. Lum and B.J. Morrill, 1977, The Honomu, Hawaii, earthquake, report of inspection, National Academy of Science, Washington D.C., 79 pp.

Owen, S., P. Segall, T. Arnadottir, J. Freymueller and A. Miklius, 1993, Rapid displacement of the south flank of Kilauea volcano determined by GPS (abstract), Trans. Am. Geophys. Union, v. 74, p. 106.

Papadopoulos, G.A., H.G. Skafida and I.T. Vassiliou, 1993, Nonlinearity of the magnitude-frequency relation in the Hellenic Arc-trench system and the characteristic earthquake model, Jour. Geophysical Res., v. 98, pp. 17,737-17,744.

Rojahn, C. and B.J. Morrill, 1977, The island of Hawaii earthquakes of November 29, 1975: strong motion data and damage reconnaissance report, Bull. Seismol. Soc. Am., v. 67, pp. 493-515.

Scholz, C.H., 1968, The frequency-magnitude relation of micro-fracturing in rock and its relation to earthquakes, Bull. Seismol. Soc. Am., v. 58, p. 399-415.

Schwartz, D.P. and K.J. Coppersmith, 1984, Fault behavior and characteristic earthquakes: examples from the Wasatch and San Andreas fault zones, Jour. Geophysical Res., v. 89, pp. 5681-5698.

Seed, H.B. and I.M. Idriss, 1983, Ground motions and soil liquifaction during earthquakes: Monograph series v. 5, Earthquake Engineering Research Institute, Berkeley CA, 133 p.

Singh, S.K., M. Rodriguez, and L. Esteva, 1983, Statistics of small earthquakes and frequency of occurrence of large earthquakes along the Mexican subduction zone, Bull. Seismol. Soc. Am., v. 73, pp. 1779-1796.

Swanson, D.A., W.A. Duffield and R.S. Fiske, 1976, Displacement of the south flank of Kilauea Volcano: the result of forceful intrusion of magma into the rift zones, U.S. Geological Survey Professional Paper 963, 39 p.

Switzer, J.C. and R.L. Porcella, 1988, Catalog of U.S. Geological Survey strong-motion records, 1988, U.S. Geological Survey Circular 1057, 28 pp.

Switzer, J.C. and R.L. Porcella, 1990, Catalog of U.S. Geological Survey strong-motion records, 1990, U.S. Geological Survey Circular 1093, 24 pp.

Thurber, C.H. and A.E. Gripp, 1988, Flexure and seismicity beneath the south flank of Kilauea Volcano and tectonic implications, Jour. Geophysical Res., v. 93, pp. 4271-4278.

Tilling, R.I., R.Y. Koyanagi, P.W. Lipman, J.P. Lockwood, J.G. Moore and D.A. Swanson, 1976, Earthquake and related catastrophic events, Island of Hawaii, November 29, 1975: a preliminary report, U.S. Geological Survey circular 740, 33 pp.

Tilling, R.I. and J.J. Dvorak, 1993, Anatomy of a basaltic volcano, Nature, v. 363, pp. 125-133.

Tomori, A.H., J.S. Nakata, P.G. Okubo, W.R. Tanigawa and J.P. Tokuuke, 1991, Hawaiian Volcano Observatory summary 90 part 1, seismic data, January to December 1990, U.S. Geological Survey Open-File Report 91-578, 79 pp.

Trifunac, M.D. and A.G. Brady, 1975, On the correlation of seismic intensity scales with the peaks of recorded strong ground motion, Bulletin of the Seismological Society of America, v.65, pp. 139-162.

Unger, J.R. and P.W. Ward, 1979, A large, deep Hawaiian earthquake - The Honomu event of April 26, 1973, Bulletin of the Seismological Society of America, v. 69, pp. 1771-1781.

Wood, H.O., 1914, On the earthquakes of 1868 in Hawaii, Bulletin of the Seismological Society of America, v.4, pp. 169-203.

Working group on California earthquake probabilities, 1990, Probabilities of large earthquakes in the San Francisco Bay region, California, U.S. Geological Survey circular 1053, 51 pp.

Wyss, M., 1986, Regular intervals between Hawaiian earthquakes: implications for predicting the next event, Science, v. 234, pp. 726-728.

Wyss, M., 1988, A proposed source model for the great Kau, Hawaii earthquake of 1868, Bulletin of the Seismological Society of America, v. 78, pp. 1450-1462.

Wyss, M., F.W. Klein and A.C. Johnston, 1981, Precursors to the Kalapana M=7.2 earthquake, Jour. Geophysical Res., v. 86, pp. 3881-3900.

Wyss, M., A.C. Johnston and F.W. Klein, 1981, Multiple asperity model for earthquake prediction, Nature, v. 289, pp. 231-234.

Wyss, M., D. Gillard and B. Liang, 1992, An estimate of the absolute stress tensor in Kaoiki, Hawaii, Jour. Geophysical Res., v. 97, pp. 4763-4768.

Wyss, M., and R.Y. Koyanagi, 1992, Isoseismal maps, macroseismic epicenters and estimated magnitudes of historic earthquakes in the Hawaiian Islands, U.S. Geological Survey Bulletin 2006, 93 pp.

Wyss, M., and R.Y. Koyanagi, 1992b, Seismic gaps in Hawaii, Bulletin of the Seismological Society of America, v. 82, pp. 1373-1387.

APPENDIX 1 - GROUND MOTION UNDER DIFFERENT ASSUMPTIONS

The estimation of probabilistic peak ground acceleration (PGA) requires making several assumptions and choices. Figure 13 shows the PGAs with a 90% probability of not being exceeded in a 50 year exposure time from all 19 seismic source zones. I believe figure 13 uses the most reasonable assumptions and choices and it gives the preferred results. It is useful to see how sensitive these results are to changes made in the assumptions, however. Changing assumptions is accomplished by changing the input parameters to the SeisriskIII program used to calculate the probable PGAs. All of the figures in this appendix are PGA maps with a 90% probability of not being exceeded in a 50 year exposure time (474 year return period).

Figure A1 shows the contribution to the PGAs of figure 13 from different earthquake source zones. Figure A1a is the contribution from all crustal regions 1-11. Crustal sources account for nearly all of the shaking hazard because figures A1a and 13 are similar. The other maps in appendix 1 should be compared to figure A1a. Figure A1b uses only the regions 5-11, which contribute very little to the hazard on Kilauea. The deep regions D1-D8 (figure A1c) also contribute little to the Kilauea hazard.

We will now vary earthquake rates from different frequency-magnitude distributions and compare the PGAs to figure A1a. Lowering the rates of M>5.5 earthquakes in regions 1, 2 and 3 from those in the lower half of table 3 by the factor 0.67 to the rate from the 1823-1992 catalog reduces the maximum expected PGA on Kilauea's south flank by less than 0.1 g (figure A2). Using a rate of M>5.5 earthquakes extrapolated from M<5.5 events in all regions (table 2) lowers the probabilistic PGA on Kilauea by less than 0.2 g and at the Hilea source zone (figure 1b) by 0.5 g (figure A3). This last assumption ignores the major historic earthquakes in Hilea and Kona, and uses a line that does not fit the large earthquake distribution in figure 6. The discrepancy between figures A1a and A3 illustrates the errors one would make if one used a microearthquake catalog containing only a few years. Figure A4 shows PGAs from the M>5.5 rates in regions 1-2 (table 3) but uses the 1970-1992 rates in regions 3, 7 and 8 (table 3 line 4, and table 2 lines 7 and 8). Kilauea is still very hazardous even at the lower rates.

The variation of observed accelerations at individual sites produces a large effect on the probabilistic PGAs. The standard deviation of the natural log of the observed PGAs at lava sites in Hawaii is 0.45 (a factor of 57%) relative to the modified Boore at al. (1993) curve (figure 9a). A standard deviation of zero assumes all observations will fit the curve exactly and yields the PGAs of figure A5. Allowing for random lava site variability thus increases the probabilistic PGAs on Kilauea's south flank by about 0.3 g (compare figures A1a and A5). Note that sites underlain by more than 0.5 m of ash are excluded from this random variability calculation. The PGAs of ash sites will be higher than for lava sites. If we ignored the distinction between ash and lava sites and considered all PGA data together, the probabilistic PGAs would be considerably higher both because of the higher mean PGA (figure 9a) and the larger standard deviation.

The maximum PGA allowed in the probabilistic PGA calculations is that calculated for a M7.7 earthquake. M8.2 earthquakes are allowed to occur at a rate given by the frequency magnitude distribution (table 2) but their PGA is assumed saturated at the value for a M7.7 earthquake. Using the modified Boore at al. (1993) relation (table 4, last line), the calculated PGA from a M7.7 event at zero distance is 0.98 g. It is possible that PGAs close to the source may not be larger for a M8 event than a M7 earthquake, even though the duration of strong shaking would be longer. Figure A6 assumes the PGA from earthquakes saturates at the levels calculated for an M=7.2 earthquake (0.78 g at zero distance). This M7.2 saturation reduces the maximum probabilistic PGA by less than 0.1 g from the M7.7 saturation in figure A1a. Note that a high earthquake occurrence rate, random site variability and a 90%

Using a different attenuation curve can change both the shape and level of the probabilistic PGA contours. The Krinitzsky et al. (1988) curve (Figure A7) produces much higher PGAs than the Boore et al. curve at distances close to the source. The Campbell and Bozorgnia (1994) curve also produces higher near-source PGAs but with a faster decay with distance (figure A8).

The variations of calculated PGAs seen by altering the earthquake rates to different historical periods (figure A2), saturation (figure A6) and attenuation curve (figure A8) within reasonable bounds illustrates that probabilistic PGAs can vary by 0.1-0.2 g. The variation of individual sites (figure 9a), the lack of observations of M>7.5 earthquakes and the scarcity of accelerograms at distances less than 10 km are larger sources of unpredictability.

APPENDIX 2 - THE SIZE AND RATE OF SUBMARINE LANDSLIDES

Giant submarine landslides are a major catastrophe, but do they happen often enough to pose a significant hazard on a time scale of decades? It is important to guess the occurrence rate of submarine landslides in different size categories, and see whether great earthquakes often cause great landslides. Landslide size is important because small slides are probably more frequent and will sometimes be missed as a separate unit on the sea floor. Like earthquakes, we will estimate a "magnitude" for each landslide and plot a frequency-magnitude distribution. A landslide "magnitude" permits comparison with earthquakes of similar size.

I define the magnitude of a submarine landslide by the total potential energy it releases through subsidence. The energy released is the product of mass, the average change in elevation (dH), and the acceleration of gravity (g). Mass is the product of density (d), the area (a) and average thickness (t). I use Richter's (1958) relation between seismic energy Es in ergs and magnitude (M)

$$\log(Es) = 11.4 + 1.5M$$

The seismic energy Es is the total energy released times the seismic efficiency (s), which I assume is 0.01. I also assume the density (d) is 2 g/cm^3. Thus

$$M = 0.67 \log(d\ a\ t\ g\ dH\ s) - 7.6.$$

Landslide magnitude is not very sensitive to small changes in the assumed parameters because of the log function and 0.67 factor.

As a check whether this "landslide magnitude" is reasonable, I will crudely estimate the landslide magnitude of the 1975 Kalapana earthquake and compare it to the M=7.2 surface wave magnitude. This event can be viewed seismologically either as an earthquake or a slump (e.g. Ando, 1979; Eissler and Kanamori, 1987). For this calculation I estimate the potential energy lost to subsidence under gravity. I assume the south flank block lost potential energy by sliding laterally on a gently dipping decollment plane and by elastic relaxation and subsidence as it decompressed. Maximum subsidence of the surface of the south flank block during the earthquake was 3.5 m at the coastline with a 30 km by 5 km area of 1 m or larger on-shore subsidence (Lipman et al., 1985). The maximum subsidence was on the submarine flank because the center of the subsidence contours is offshore. I assume the subsidence averaged over the 25 km by 40 km area of major faulting (Ando, 1979) was 1.3 m which is compatible with the synthetic model of Ando (1979, his figure 12). The average change in height dH is approximately 1.3 m through the block of thickness 9 km. This yields a "landslide magnitude" of 7.3 for the Kalapana earthquake, which is surprisingly similar to the seismological magnitude. This ignores many sources of energy including elastic strain and unknown elevation change of the block's base. The assumptions seem justified because I am modeling the earthquake as a slump for comparison with submarine landslides and slumps.

Study of the population of submarine landslides has increased recently with exploration of the exclusive economic zone (e.g. Lipman et al., 1988; Moore et al., 1989). Landslides consist of debris avalanches which are thin but travel large distances at great speeds, and slumps which are thick, slow moving and move repeatedly. Moore et al. (1989) tabulate 17 major submarine landslides identifiable as separate units on the Hawaiian Ridge. While this is certainly not a complete catalog of all large landslides, it is interesting to see whether known landslides have a linear frequency-magnitude distribution.

For simplicity I assume that debris avalanches begin at sea level and distribute their mass evenly on the slope between sea level and the Hawaiian deep at approximately 4 km depth. Their average elevation change dH is thus 2 km. I assume an average thickness of 50 meters which is at the low end of the observed thickness range of 0.05-2 km of Hawaiian debris avalanches (Moore et al., 1989). Slumps can be up to 10 km thick and I assume they are 500 m thick on average. The average elevation change of a slump is unknown, but 200 m is believable and blocks of this size are common within landslides. These assumed dimensions are convenient because their product is 0.1 km^2 for both debris avalanches and slumps. Thus it is not neccesary to distinguish between different types of landslides because landslide magnitude will depend only on surface area. With these very simplified assumptions,

$$M = 0.67 \log(A) + 6.0$$

where A is the landslide area in km^2.

The largest submarine landslides in the state of Hawaii have a linear log-frequency-magnitude distribution with slope (b value) of about 1.85 (figure A9). The largest landslide is the M=8.8 Nuuanu debris avalanche which has an area of 23,000 km^2 (Moore et al., 1989). This slide represents the collapse of the entire northeast flank of the extinct Koolau volcano on Oahu. The landslides adjacent to the seismically active areas of south and southwest Hawaii are a smaller sample but appear to have a linear distribution with slope about 1.06. If the frequency-magnitude distribution of a large landslide population is linear, the table of landslides for the state of Hawaii is complete above M=8.3 (2700 km^2 area). The distribution levels off below this magnitude. The south and southwest Hawaii sample is complete above M=8.1 (1300 km^2 area). Smaller slides are missing from the population because they are reduced in "magnitude" by being partly covered by newer slides, because remobilized slumps are only counted once, or because they are indistinguishable from adjacent small slides that have identical morphology.

It is very difficult to estimate the rate of great submarine landslides. The Alika debris avalanche west of Mauna Loa Volcano is bracketed in age between a 13 thousand year old coral reef and the Ninole basalt roughly dated at a few hundred thousand years (Lipman et al., 1988). The slide may have caused a giant wave that washed 325 m high on Lanai at about 100 thousand years. For want of a better number, I assume that the population of submarine landslides near south and southwest Hawaii formed during the last 200 thousand years, twice the approximate age of the Alika debris slide.

It is interesting to compare the very approximate rate of great submarine landslides with the rate of south Hawaii earthquakes that occur at the head areas of the slides. Figure A10 shows the annualized frequency-magnitude distributions of south Hawaii earthquakes (from figure 6) and great landslides (from figure A9). It is clear that earthquakes and submarine landslides form two separate populations: landslide frequency is not just an extrapolation of the frequency of M>8 earthquakes. The chance of a M=8 landslide is 2 or 3 orders of magnitude less than a M=8 earthquake. In other words, there is less than a 1% chance that a great earthquake will trigger a great submarine landslide.

Smaller submarine landslides are probably closely linked to large flank earthquakes. The 1975 Kalapana and 1868 Kau earthquakes produced submarine subsidence and seaward displacement, and possible movement of the Hilina slump south of Hawaii (Moore et al., 1989). This suggests that remobilization of submarine landslides occurs much more frequently than formation of new ones which contribute to the population of landslides counted in figure A9. These smaller submarine landslides that accompany flank earthquakes may either form a separate population of events than the great landslide distribution on figure A10, or may be the unmapped continuation of the linear distribution to lower magnitudes. If the latter extrapolation is the case, one could speculate that the average recurrence of M5 landslides (0.03 km^2) is 50 years and coincides with the average recurrence of M 7.1-7.4 earthquakes (table 3).

The frequency-magnitude distribution of submarine landslides may represent the landslide rate for the state of Hawaii, but the distribution may not be useful to estimate the hazard in a particular region. Great earthquakes can recur in the same place when stress returns to its preseismic level. Unlike great earthquakes, great landslides and debris avalanches are catastrophic and the occurrence of another landslide in the same place may not be possible until the volcano builds enough material to slide again. Submarine slumps, however, can slip episodically and a frequency-magnitude distribution may estimate the hazard of their recurrence.

It is possible that each Hawaiian volcano experiences about one great landslide in its lifetime. In south Hawaii, extrapolation of the landslide curve in figure A10 implies that M8.8 landslides may recur every 200,000 to 300,000 years. This is the approximate interval that new volcanic centers form on the island of Hawaii (Clague and Dalrymple, 1987). The liklihood that a volcano will partly collapse in its lifetime agrees with the commonality of submarine landslides in the Hawaiian chain (Moore et al., 1994) and in the world (e.g. Holcomb and Searle, 1991).

Great M8 flank earthquakes can be considered either earthquakes or landslides. The conclusion to be drawn from this appendix is that they are at the high magnitude end of the earthquake population rather than the low energy end of the great submarine landslide population. Great flank earthquakes may often trigger a small submarine landslide or slump, but great submarine landslides are relatively infrequent compared to great earthquakes.

Table 1.

--ORIGIN TIME--				--	-LAT N--		--LON W--		DEPTH	N	N	RMS	ERH	ERZ		DUR	AZ	MIN	N	LOCAL
YR	MON	DA	HRMN	SEC	DEG	MIN	DEG	MIN	KM	RD	S	SEC	KM	KM	REMKS	MAG	GAP	DS	FM	MAG
72	SEP	5	131	33.85	19	19.84	155	12.37	10.47	23		.07	.6	.4	SF2F		143	5	20	M =5.0
72	DEC	23	904	52.74	19	35.35	155	55.57	14.93	25		.15	1.4	99.0	KON *		204	36	22	M =5.1
73	APR	26	1026	31.53	19	51.96	155	9.09	39.96	26		.11	2.5	4.0	KEA	6.2	213	18	22	M =6.2
74	NOV	30	354	23.82	19	26.52	155	24.96	7.91	27		.12	.5	1.4	KAO	5.6	69	7	27	M =5.4
74	DEC	31	1240	48.42	19	18.29	155	21.96	5.54	24		.15	.6	1.6	SWR		118	4	21	M =5.4
75	NOV	29	335	40.68	19	21.75	155	2.34	9.69	28		.07	.8	.4	SF5F	5.9	149	4	27	M =5.9
75	NOV	29	447	40.10	19	20.45	155	0.25	9.26	24		.08	1.1	.7	SF5F	7.3	204	5	23	M =7.2
76	FEB	20	1951	17.38	20	16.03	155	59.38	20.63	37	3	.13	1.5	3.3	KOHF	5.0	306	27	34	M =5.0
77	APR	20	1849	23.19	19	56.38	155	19.51	12.05	34	2	.11	1.3	.7	KEAF	4.5	247	6	24	M =5.0
77	JUN	5	2342	19.10	19	21.75	155	4.89	9.35	35		.10	.6	.4	SF5	4.7	80	5	35	M =5.1
79	SEP	21	2159	37.62	19	20.81	155	4.24	9.19	43		.11	.6	.4	SF5F	5.4	101	3	39	M =5.5
82	JAN	21	1152	41.17	19	13.91	155	35.53	10.32	41		.12	.9	.5	LSWF	5.6	218	3	40	M =5.4
82	JAN	21	1229	13.88	19	13.11	155	33.10	13.73	36	1	.12	.6	.5	DLSF	5.4	126	8	33	M =5.4
83	SEP	9	630	55.35	19	19.89	155	7.32	9.02	46	1	.10	.5	.4	SF4F	5.2	105	5	45	M =5.4
83	NOV	16	613	0.15	19	25.76	155	27.11	10.92	36		.12	.4	.9	KAO	6.7	56	4	36	M =6.6
87	FEB	3	1622	33.81	20	3.55	156	26.84	0.38	55	5	.13	1.5	.4	DISF	5.1	229	70	50	M =5.2--4
88	MAR	1	2241	56.36	19	19.70	155	12.49	10.37	56	8	.11	.4	.3	SF2F	4.6	81	5	49	M =5.2--3
88	MAR	24	1429	52.15	19	57.01	156	24.58	2.64	56	5	.11	1.2	.9	DISF	5.2	226	69	51	M =5.0--3
88	MAR	27	1733	41.59	19	56.57	156	24.70	2.79	56	10	.11	1.2	.8	DISF	5.6	227	69	47	M =5.2--3
88	JUL	3	1938	9.31	19	12.92	155	27.36	9.60	47		.14	.6	.5	LSWF	4.9	115	6	52	M =5.4--2
89	JUN	25	1727	3.91	19	21.69	155	5.01	9.27	53		.11	.5	.4	SF5	6.2	81	5	55	M =6.2--1
89	DEC	27	2313	17.11	19	19.68	155	12.38	9.58	46	1	.10	.4	.3	SF2F		83	5	49	M =5.3--2
91	MAY	8	821	11.98	19	20.56	156	12.98	31.38	50	3	.11	1.3	1.6	KONF		263	35	50	M =5.5--1
91	DEC	9	1314	30.48	18	50.11	155	50.94	46.42	50	3	.10	1.8	.6	DISF		299	25	48	M =5.2--2

Table 1. List of local magnitude 5.0 and larger earthquakes from the HVO 1970-1992 earthquake catalog. These events are plotted as large symbols in figures 1 and 3. Times and dates are in Hawaii standard time. NRD is the total number of P and S readings, NS is the total number of S readings, RMS is the root-mean-square travel time residual and is a measure of the location imprecision, ERH is the horizontal location error, ERZ is the vertical location error, REMKS is a geographic location code, DUR MAG is the magnitude derived from the coda duration of the high-gain standard network stations, AZ GAP is the maximum azimuthal gap between stations as seen at the epicenter, MIN DS is the distance in km to the closest station, N FM is the number of first motions and LOCAL MAG is the local magnitude derived from Wood-Anderson and other low-gain seismographs. Local magnitudes since 1986 show the number of observations used to compute the median magnitude.

Table 2.

Earthquake rate and maximum magnitude parameters											
seismic source zone	a	b	sd(b)	min. mag. (b)	n(b)	maximum magnitude catalog 1970-92	historic 1823-1992	occur-rence	accel-eration	M>6.5 average recurrence interval (yr)	magnitude of 50 year recurrence
1	4.538	0.942	0.01	2.1	8363	7.2	7.9(1)	8.2	7.7	15*	7.3
2	4.145	0.991	0.01	1.8	5295	6.6	7.9(1)	8.2	7.7	67*	6.3
3	3.934	1.038	0.04	2.3	809	5.4	7.9(1)	8.2	7.7	28-190*	6.8-5.6
4	5.565	1.703	0.04	2.1	2256	4.0	5.9(2)	6.5	6.5	<800-320,000	5.2-4.2
5	3.134	0.979	0.07	2.3	176	4.8	7.9(1)	8.2	7.7	<1700	4.9
6	4.322	1.152	0.05	2.5	638	4.4	-	8.2	7.7	<1460	5.2
7	4.959	1.301	0.04	2.6	864	5.1	6.9(3)	7.7	7.7	59-3200	6.4-5.1
8	5.105	1.610	0.17	2.8	91	4.1	6.5(4)	7.5	7.5	79-230,000	6.2-4.2
9	2.732	0.796	0.08	2.7	88	5.2	-	7.5	7.5	277	5.6
10	3.454	1.107	0.15	2.8	52	4.9	-	7.5	7.5	<5500	4.7
11	4.295	1.100	0.04	2.5	809	5.0	5.7(5)	8.2	7.7	<714	5.4
D1	3.494	0.926	0.04	2.2	660	4.8	6.3(6)	7.0	7.0	<330	5.6
D2	4.268	1.343	0.08	2.4	255	4.5	-	6.7	6.7	<29,000	4.4
D3	4.771	1.543	0.11	2.5	188	4.6	6.0(7)	6.7	6.7	<180,000	4.2
D4	2.666	0.940	0.12	2.4	59	4.3	-	6.7	6.7	<2800	4.6
D5	3.830	1.164	0.08	2.5	191	4.5	-	6.7	6.7	<5460	4.8
D6	3.727	0.993	0.07	2.8	203	5.5	-	6.7	6.7	<540	5.5
D7	3.542	0.942	0.05	2.5	355	6.2	6.2(8)	6.7	6.7	<380	5.6
D8	2.578	0.855	0.12	2.6	52	4.3	~6(9)	6.7	6.7	<960	5.0

* The frequency of M>5.2 earthquakes in regions 1, 2 and 3 is greater than is predicted by the extrapolated fit to lower magnitudes (figure 6), but the increase is not seperately resolvable into each region. Thus the average intervals of M>6.5 earthquakes and the earthquake magnitude corresponding to a 50 year recurrence listed for these regions are adjusted to reflect the higher frequency of large earthquakes in the historical record. The adjusted values of a and b are given in table 3.

(1) The M=7.9 earthquake on 4/2/1868 ruptured several regions
(2) The largest historic earthquake was M=5.9 on 1/2/1935
(3) The largest historic earthquake was M=6.9 on 8/21/1951
(4) The largest historic earthquake was M=6.5 on 10/5/1929
(5) The largest historic earthquake was M=5.7 on 6/28/1935
(6) The largest historic earthquake was M=6.3 on 4/22/1951
(7) The largest historic earthquake was M=6.0 on 8/14/1955
(8) The largest historic earthquake was M=6.2 on 4/26/1973
(9) The largest historic earthquake was M~6 on 3/20/1927

Table 2. Earthquake rate parameters for the 19 seismic source zones (figure 3). "a" and "b" are the unadjusted maximum liklihood estimates of the yearly frequency-magnitude distribution log(N) = a -bM where M is magnitude and N is the cumulative number per year of earthquakes larger than or equal to M. "a" and "b" are unadjusted estimates from the 1970-1992 HVO earthquake catalog. Sd(b) is the estimated standard deviation of b, and mag(b) is the minimum magnitude of the linear part of the distribution used to compute a and b. The catalog should be complete for earthquakes larger than mag(b). n(b) is the total number of earthquakes larger than or equal to mag(b).

The maximum magnitudes are: catalog, the largest event in the 1970-1992 catalog in that region; historic, the largest event in the 1823-1992 historical catalog; occurrence, the largest event allowed to occur in the estimated peak ground acceleration (PGA) calculation, i.e. the largest event the region is tectonically capable of producing either singly or together with neighboring regions; and acceleration, all events larger than this magnitude are saturated and produce PGAs limited to this magnitude. M>6.5 average interval in years is the expected average recurrence of M>6.5 earthquakes, i.e. the reciprocal of the annualized rate from the frequency-magnitude distribution. The average interval is thus not observed from repeated earthquakes.

Intervals are estimated from the 1970-1992 HVO catalog. If two numbers are given, the lower is from the historic earthquake catalog (table 3). All intervals derived from the 1970-1992 catalog are maximum estimates because large earthquakes can occur in areas that were only mildly active during 1970-1992, such as the historic earthquakes in regions 3, 4, 7 and 8. All intervals larger than 100 years are thus arbitrarily marked with a less than sign (<). The 800 yr interval for region 4 is crudely estimated from a linear frequency-magnitude distribution with slope -1.70 which produces one magnitude 5.9 event per 80 years, i.e. one January 2, 1935 size earthquake since the founding of the HVO in 1912. The magnitude of 50 year recurrence is read from the frequency-magnitude distribution at the rate of 0.02 earthquakes per year. If two magnitudes are given, the higher is determined from the historic frequency-magnitude distribution (table 3).

Table 3.

Historical earthquake rate parameters										
region or seismic zone	time period	a	b	min. mag. (b)	n(b)	average recurrence interval (yr) M> 5.5	M> 6.5	M> 7.0	M> 8.0	magnitude of 50 year recurrence
south side of island	1823-1992	2.749	0.627	5.5	32	5.0	21	44	185	7.1
1+2+3 (adjusted)	1970-1992	2.923	0.627	4.9	18	3.4	14	29	124	7.4
1+2+3 (un-adjusted)	1970-1992	4.891	1.002	2.0	17800	-	-	-	-	-
3 (Hilea)*	1970-1992	1.797	0.627	4.9	-	-	-	-	-	-
1 (south flank)	1970-1992	2.900	0.627	4.9	-	3.5	15	31	-	7.3
2 (Kaoiki)	1970-1992	2.252	0.627	4.9	-	16	67	137	-	6.3
3 (Hilea)	1823-1992	3.942	0.830	~5.6	54	4.2	28	74	-	6.8
7 (Kona & MLO)	1914-1992	6.606	1.290	~5.6	20	3.1	59	265	-	6.4
8 (Hualalai)	1914-1992	4.455	0.990	~5.6	6	10	79	300	-	6.2

* not used in hazard or expected acceleration calculations

Table 3. Alternate earthquake rate parameters for combined seismic source regions and for single regions using the historic earthquake catalog. The values for regions 1, 2, 3, 7 and 8 in the lower section of the table are used instead of those in table 2 in the expected peak ground acceleration calculations for M>5.2 earthquakes. The time period refers to the catalog used to tabulate earthquakes.

"a" and "b" are the maximum liklihood estimates of the yearly frequency-magnitude distribution log(N) = a -bM where M is magnitude and N is the cumulative number per year of earthquakes larger than or equal to M. The adjusted a and b values for regions 1, 2 and 3 reflect the higher rates for M>5.5 earthquakes seen in both the historic and HVO catalogs compared to rates extrapolated from the distribution of M<5 earthquakes (figure 6). The a and b values must be adjusted either because the log-frequency versus magnitude distribution is non-linear, or because the historic earthquake rate was higher than the 1970-92 rate. The adjusted a and b values are used to generate the probabilistic PGA values in figure 13. The adjusted values use b=0.627 derived from the 1823-1992 south Hawaii catalog and an "a" value such that the two magnitude distributions match at M=5.2.

Min-mag(b) is the minimum magnitude of the linear part of the frequency-magnitude distribution. The minimum magnitudes from the historic catalogs are approximate because magnitudes from many earthquakes were derived from maximum intensity. "n(b)" is the number of events greater than the minimum magnitude. The average recurrence interval in years is for earthquakes at four different magnitude levels derived from the frequency-magnitude distribution, not from observed repetition of earthquakes. The magnitude of 50 year recurrence is read from the frequency-magnitude distribution at the rate of 0.02 earthquakes per year.

Table 4.

Coefficients of terms in several attenuation curves									
Authors	A	B	C	D	E	F			
(site type)	constant	M	log(r)	log(u)	log(d+c)	r	c	h	sigma (ln)
Joyner & Boore (1981) (rock site)	-1.02	0.249	-1.0			0.00255		7.3	0.60
Campbell (1981) (empirical)	-1.747	0.377			-1.09		8.14 (for M=7)		0.372
Krinitzsky et al. (1988) (shallow source, hard site)	-1.76	0.385	-1.0			0.00255		source depth	0.75
Campbell (1989) (deep soil or rock)	-1.033	0.270			-1.0		7.28		0.506
Boore et al. (1993) (class B, rock site)	-1.176	0.216	-0.777					5.48	0.472
Campbell & Bozorgnia (1994) (soft rock)*	-1.037	0.372	-0.227	-1.328			13.80 (for M=7)	rupture depth	0.39 (PA>0.21)
this study (Boore et al. (1993) modified)	-1.057	0.216	-0.777					5.48	0.45

The general form of an attenuation curve is

$$\log(PA) = A + BM + C\log(r) + D\log(u) + E\log(d+c) + Fr$$

where

$$r^2 = d^2 + h^2$$
$$u^2 = d^2 + h^2 + c^2$$

where PA is peak acceleration (maximum of horizontals) in g; M is magnitude; d is epicentral distance to the surface projection of the rupture zone in km; and sigma (ln) is the standard deviation of the natural logarithm of the residual ratios. Campbell (1981) and Campbell and Bozorgnia (1994) allow c to be a function of magnitude.

* Assuming an average of strike-slip and thrust mechanisms.

Table 4. Coefficients of terms in the peak ground acceleration (PGA) attenuation relations for several published studies. The relation of Boore et al. (1993) best fits the distance dependence of Hawaiian observations when the curve is adjusted upward by a factor of 1.20 (last line of table). Sigma is the standard deviation of the natural logarithm of the ratios of PGA observations to the value predicted by each curve. The sigma values are taken from each paper but the value for this study is for Hawaiian data relative to the Boore et al. (1993) curve (figure 9a). The constants in the Campbell relations are adjusted for the maximum rather than the mean horizontal component.

Table 5.

Magnitude and distance ranges of several attenuation relationships		
Authors	magnitude range	maximum distance
Joyner & Boore (1981)	5.0 to 7.7	200
Campbell (1981)	5.0 to 7.7	50
Krinitzsky et al. (1988)	5.0 to 7.4	200
Campbell (1989)	2.5 to 5.0	30
Boore et al. (1993)	5.0 to 7.7	100
Campbell & Bozorgnia (1994)	4.7 to 7.6	60

Table 5. Ranges of magnitude and distance of observations used to derive the peak ground acceleration attenuation relations in table 4. The curves should be applied with caution outside these ranges.

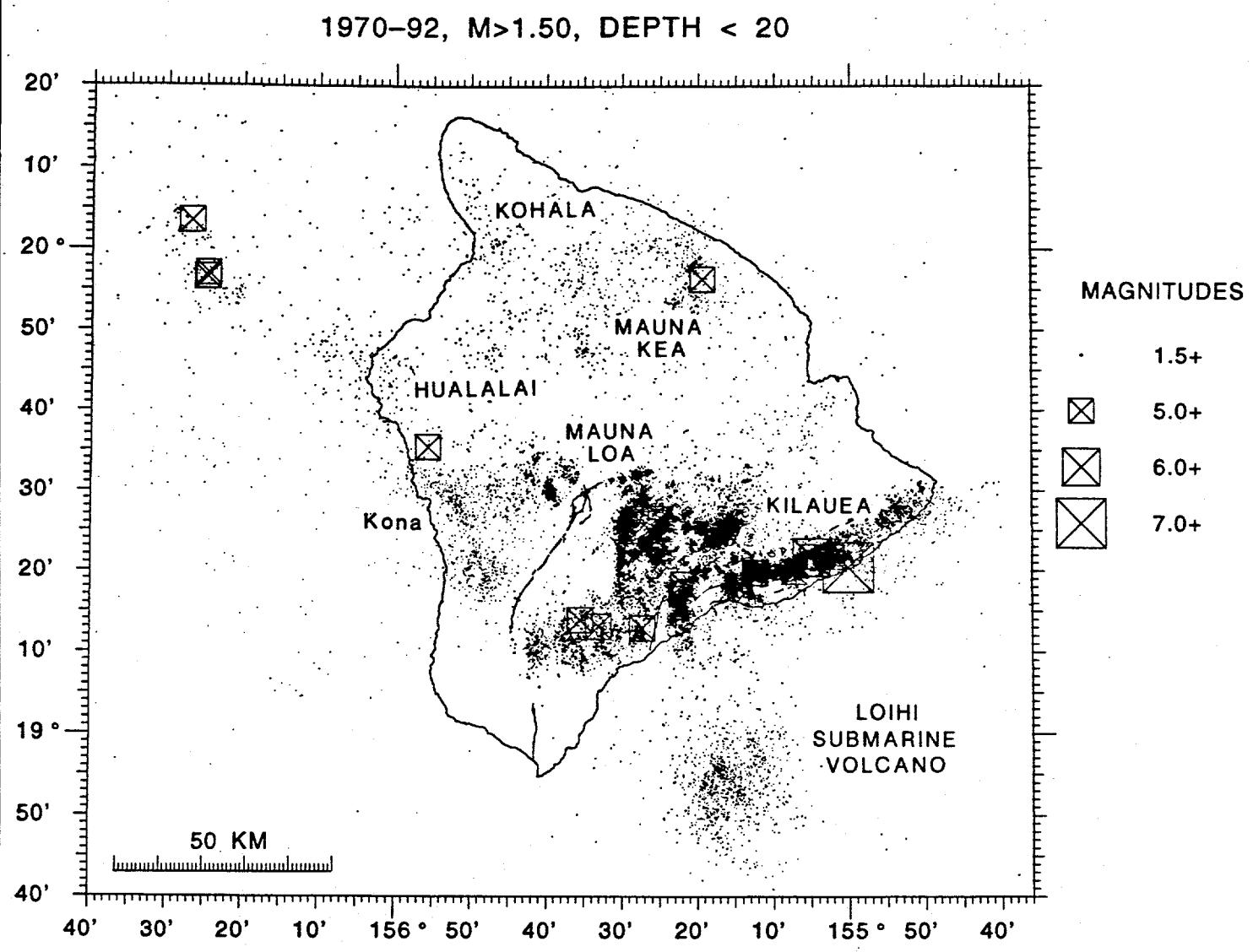

Figure 1a. Epicenter maps of the Hawaiian Volcano Observatory (HVO) earthquake catalog for the period of the best earthquake detection and location capability during 1970-1992. The map includes magnitudes 1.5 and larger. The magnitude threshold of completeness increases from about 1 near Kilauea Caldera to about 2.8 at a point 50 km off the west coast. Earthquakes with magnitudes 5.0 and larger are shown with large square symbols and are listed in table 1. Depths are shallower than 20 km. Hawaii has relatively few earthquakes with reliable depths between the Moho (13-19 km depth) and 21 km, thus the shallow maps show the seismicity typical of the crust and volcanic pile. Shallow (0-5 km depth) magma-related earthquakes from Kilauea's caldera and rift zones seldom exceed magnitude 3 and are omitted from the map.

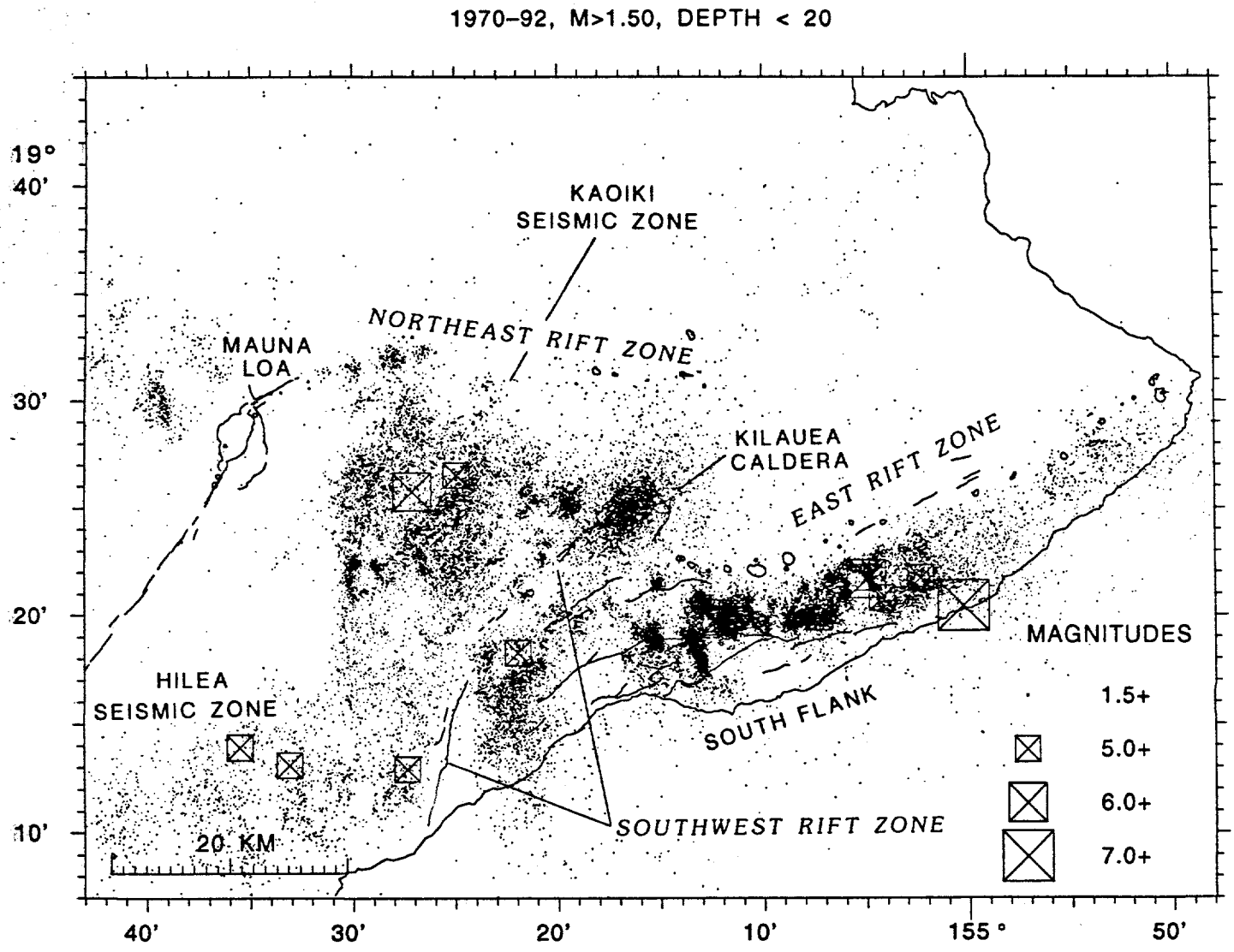

Figure 1b. Epicenter maps of the Hawaiian Volcano Observatory (HVO) earthquake catalog for the period of the best earthquake detection and location capability during 1970-1992. The map includes magnitudes 1.5 and larger. The magnitude threshold of completeness increases from about 1 near Kilauea Caldera to about 2.8 at a point 50 km off the west coast. Earthquakes with magnitudes 5.0 and larger are shown with large square symbols and are listed in table 1. Depths are shallower than 20 km. Hawaii has relatively few earthquakes with reliable depths between the Moho (13-19 km depth) and 21 km, thus the shallow maps show the seismicity typical of the crust and volcanic pile. Shallow (0-5 km depth) magma-related earthquakes from Kilauea's caldera and rift zones seldom exceed magnitude 3 and are omitted from the map.

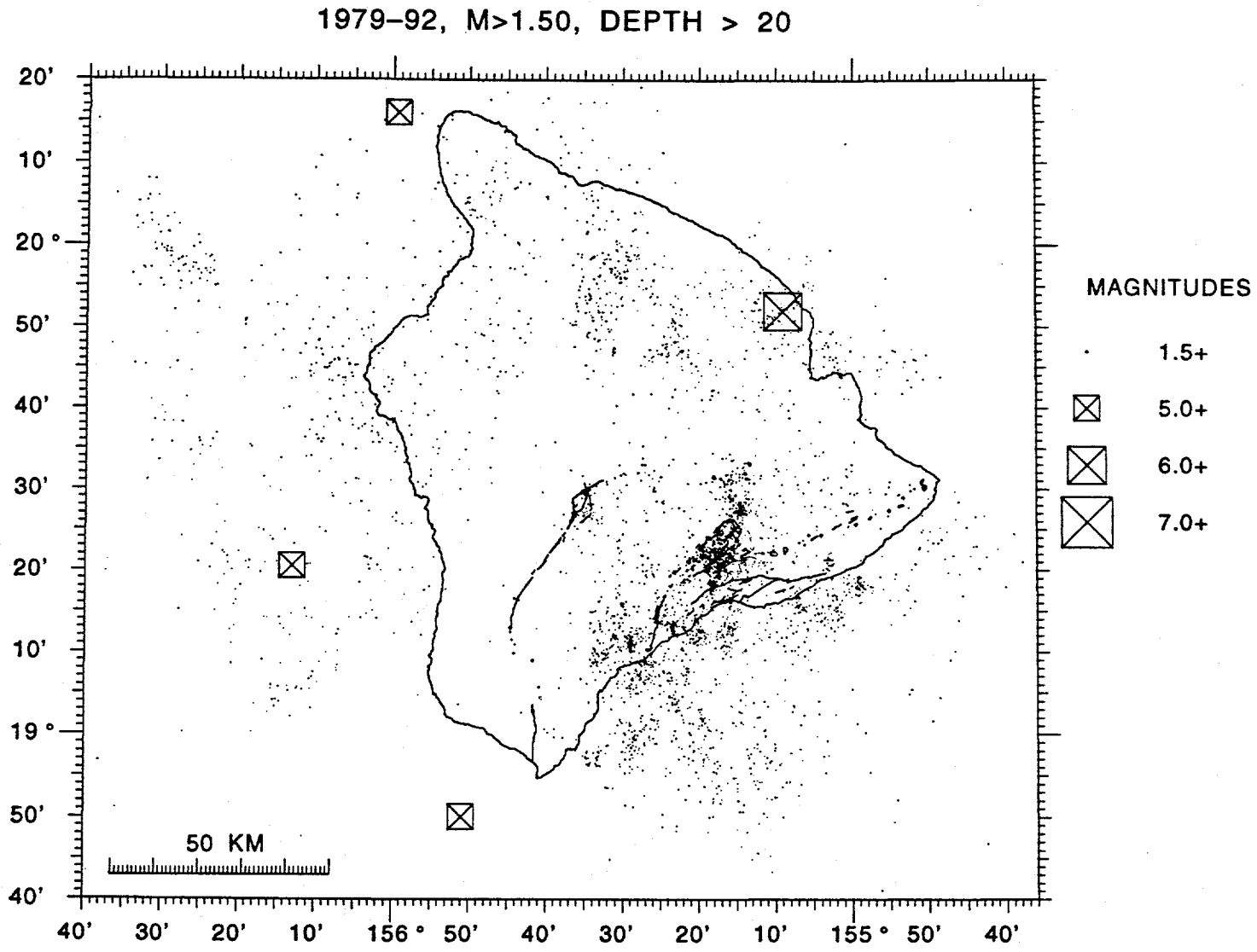

Figure 1c. Epicenter maps of the Hawaiian Volcano Observatory (HVO) earthquake catalog for the period of the best earthquake detection and location capability during 1970-1992. The map includes magnitudes 1.5 and larger. The magnitude threshold of completeness increases from about 1 near Kilauea Caldera to about 2.8 at a point 50 km off the west coast. Earthquakes with magnitudes 5.0 and larger are shown with large square symbols and are listed in table 1. Earthquakes are below 20 km depth. Hawaii has relatively few earthquakes with reliable depths between the Moho (13-19 km depth) and 21 km, thus the map shows activity in the upper mantle.

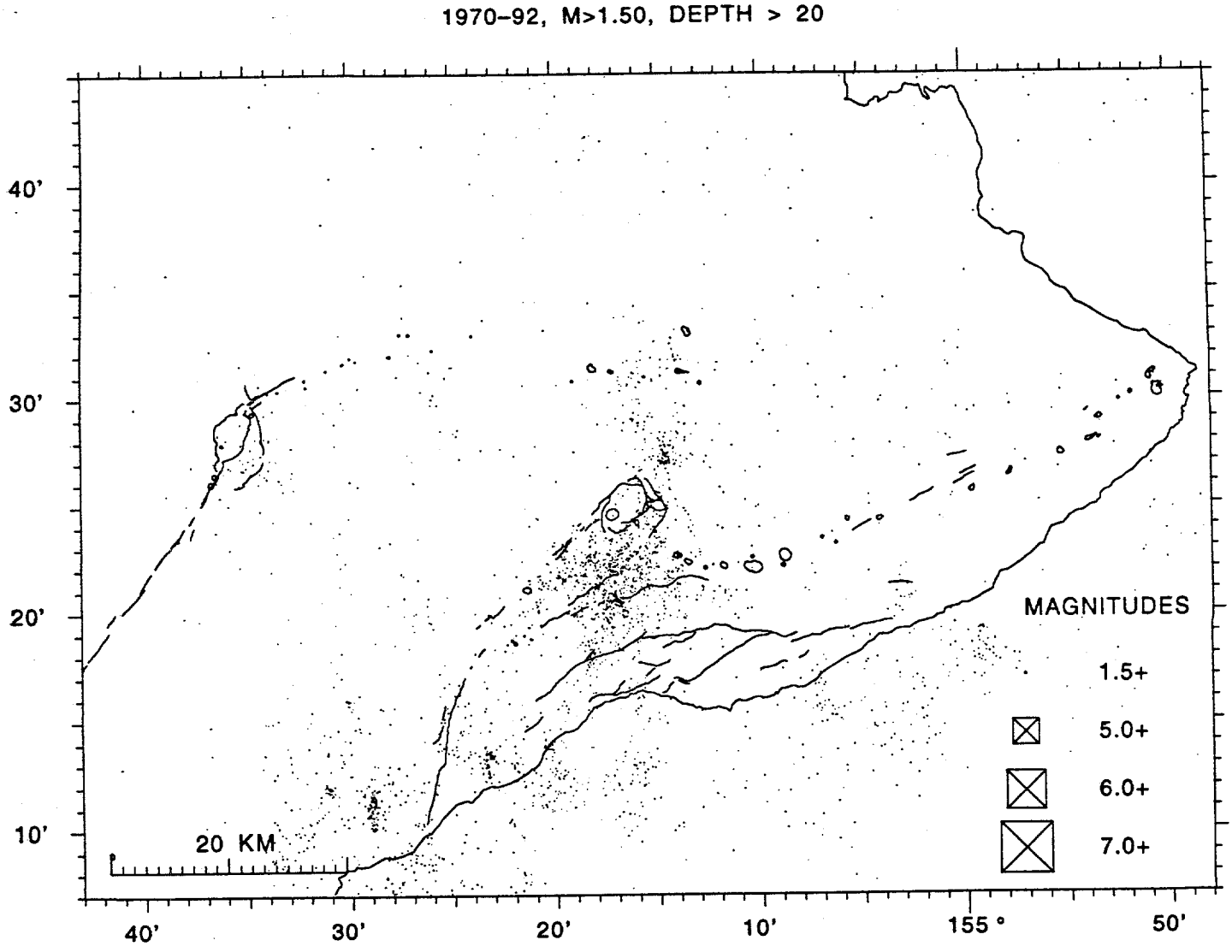

Figure 1d. Epicenter maps of the Hawaiian Volcano Observatory (HVO) earthquake catalog for the period of the best earthquake detection and location capability during 1970-1992. The map includes magnitudes 1.5 and larger. The magnitude threshold of completeness increases from about 1 near Kilauea Caldera to about 2.8 at a point 50 km off the west coast. Earthquakes with magnitudes 5.0 and larger are shown with large square symbols and are listed in table 1. Earthquakes are below 20 km depth. Hawaii has relatively few earthquakes with reliable depths between the Moho (13-19 km depth) and 21 km, thus the map shows activity in the upper mantle.

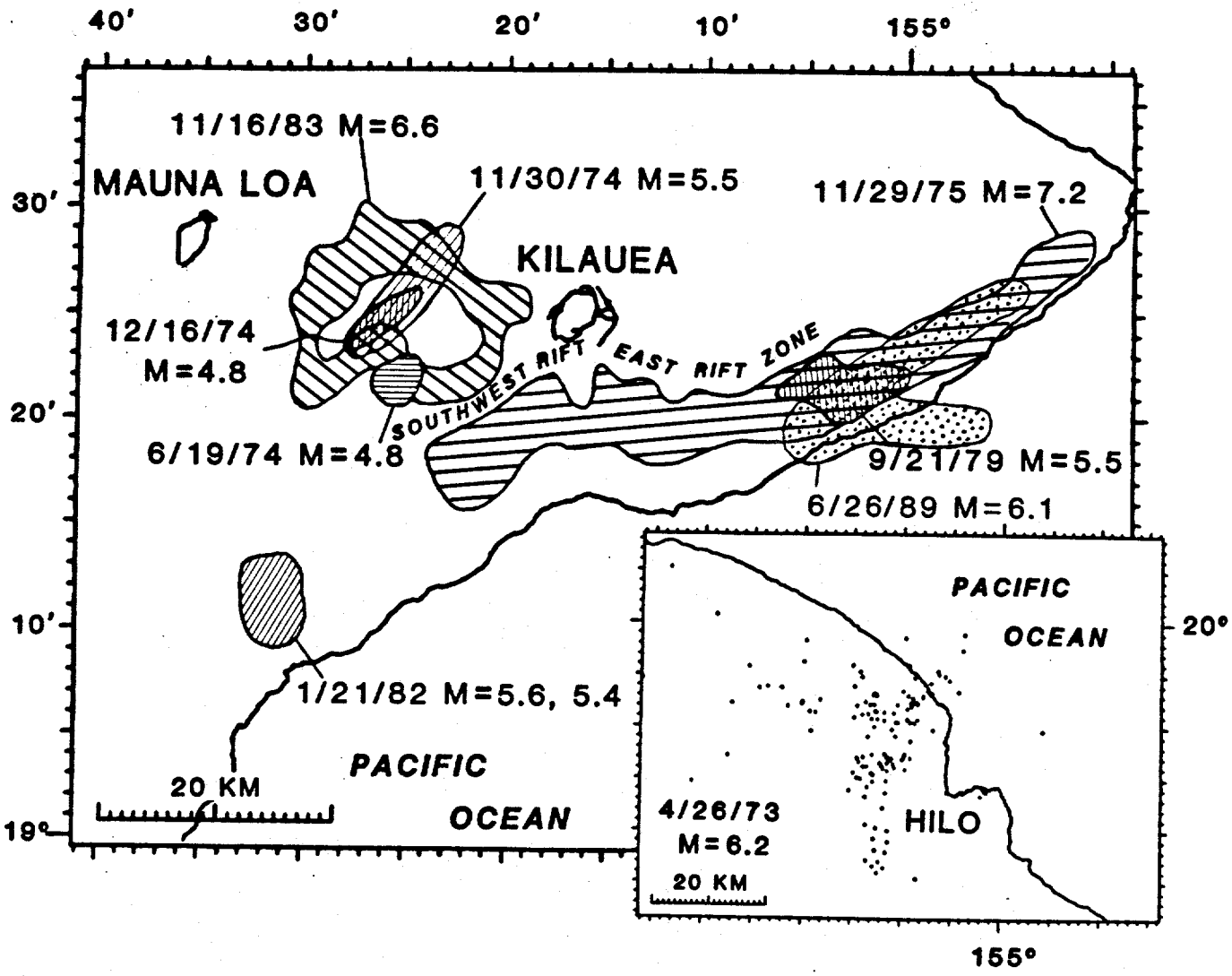

Figure 2. Outlines of aftershock zones (approximate rupture areas) of large earthquakes near Kilauea volcano after 1970.

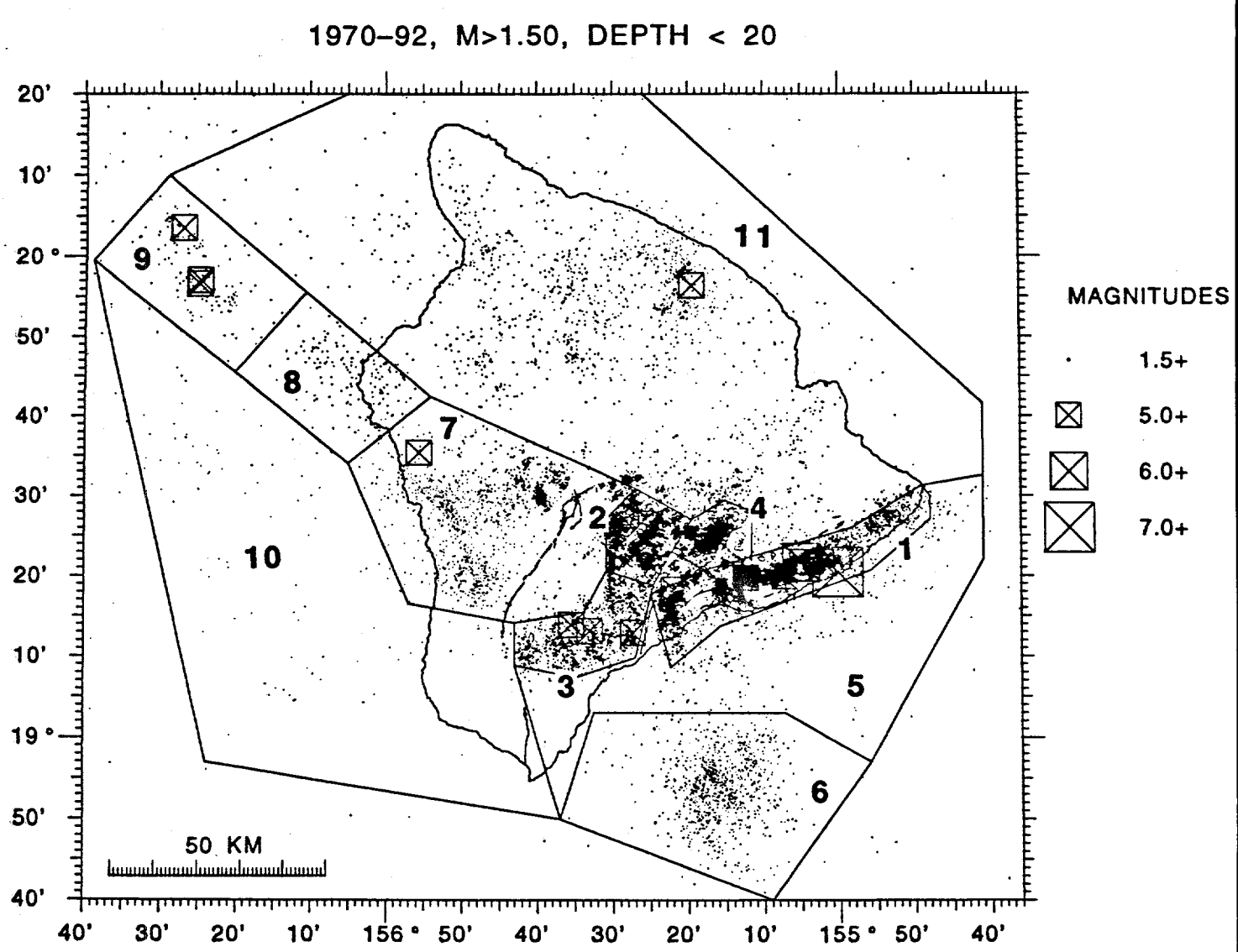

Figure 3a. The seismic source zones used for calculating earthquake rates superimposed on the epicenter maps of figure 1. The source zones are also used as areas of homogeneous seismicity for calculating the probable peak ground acceleration maps.

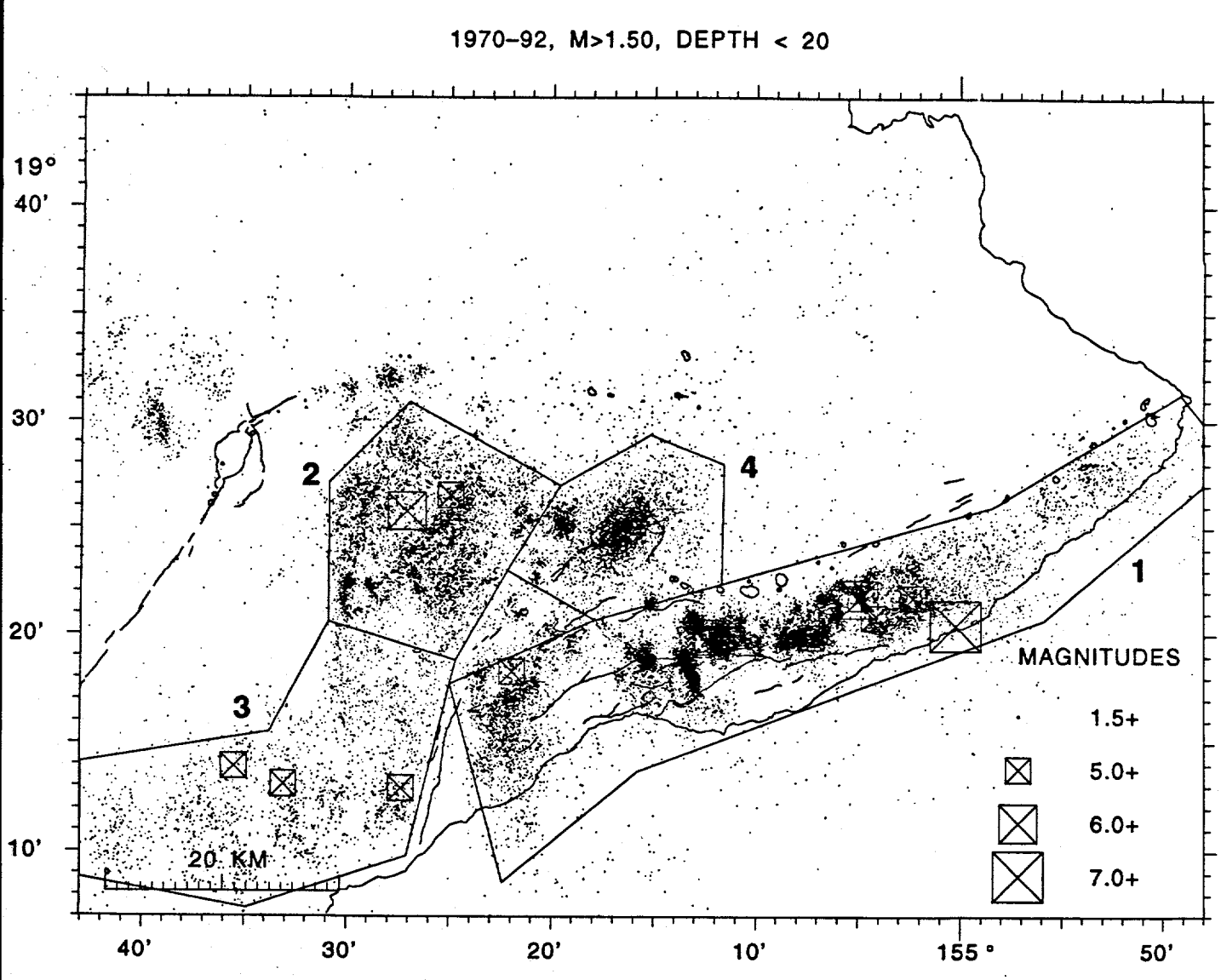

Figure 3b. The seismic source zones used for calculating earthquake rates superimposed on the epicenter maps of figure 1. The source zones are also used as areas of homogeneous seismicity for calculating the probable peak ground acceleration maps.

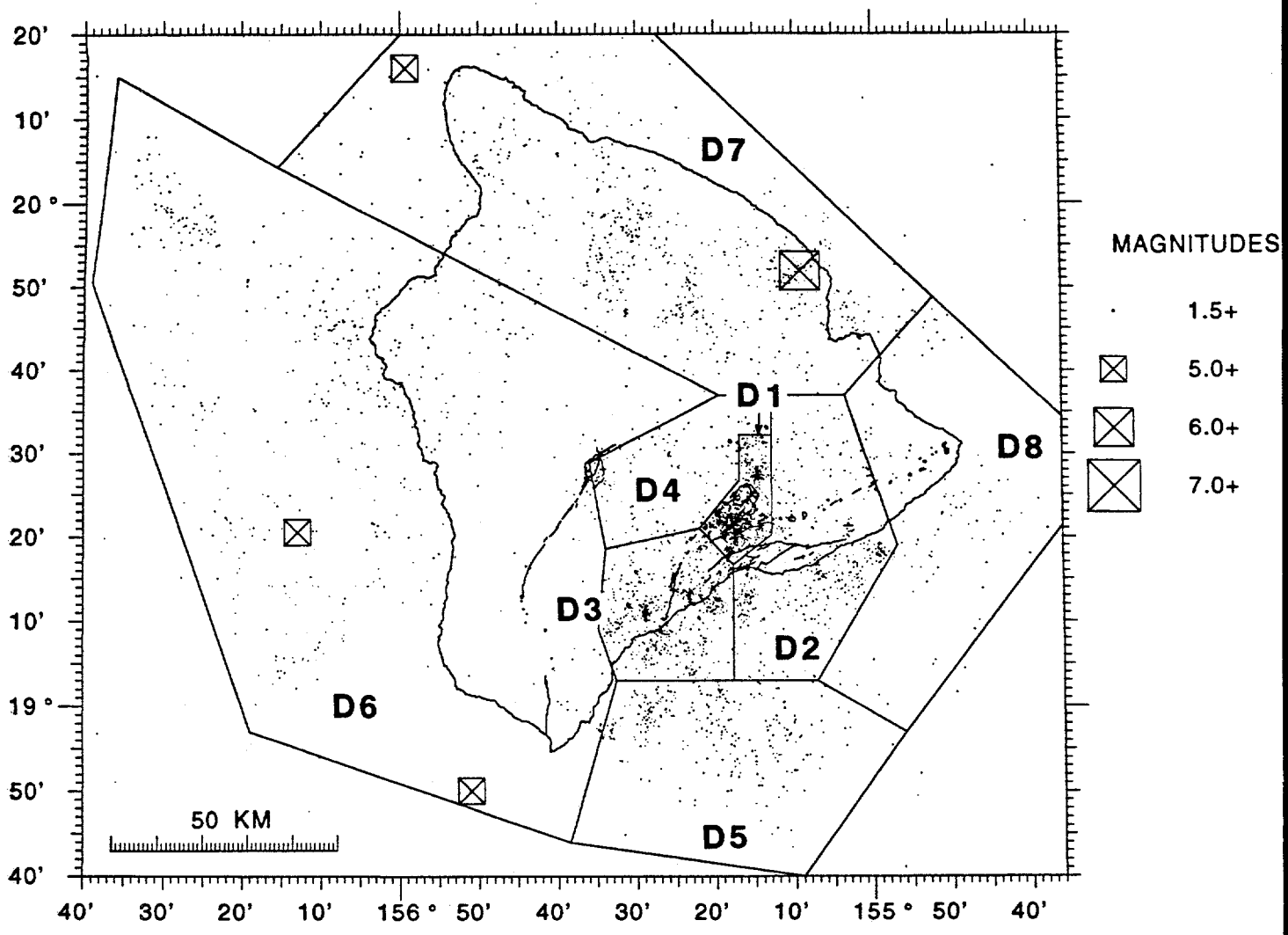

Figure 3c. The seismic source zones used for calculating earthquake rates superimposed on the epicenter maps of figure 1. The source zones are also used as areas of homogeneous seismicity for calculating the probable peak ground acceleration maps.

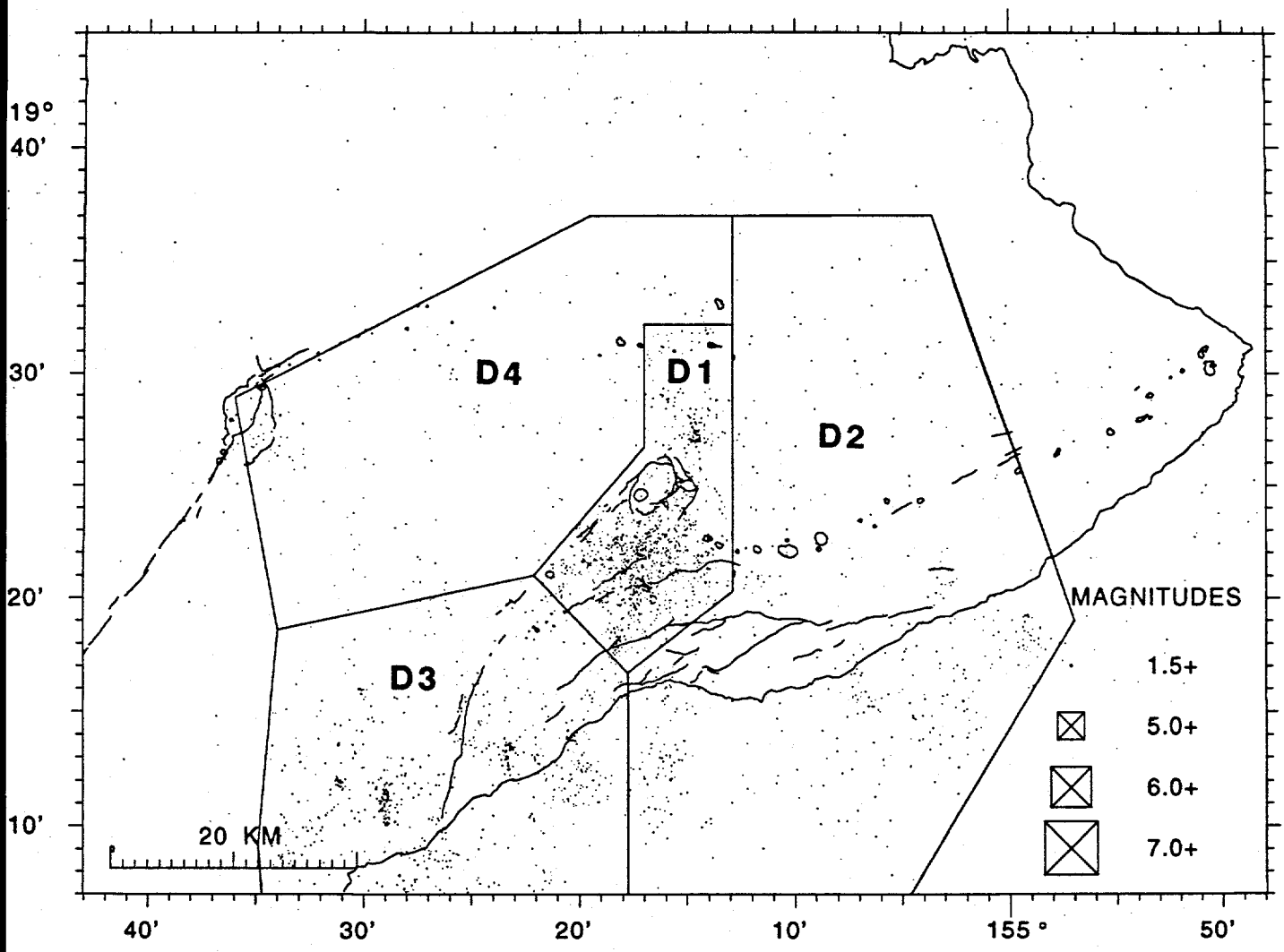

Figure 3d. The seismic source zones used for calculating earthquake rates superimposed on the epicenter maps of figure 1. The source zones are also used as areas of homogeneous seismicity for calculating the probable peak ground acceleration maps.

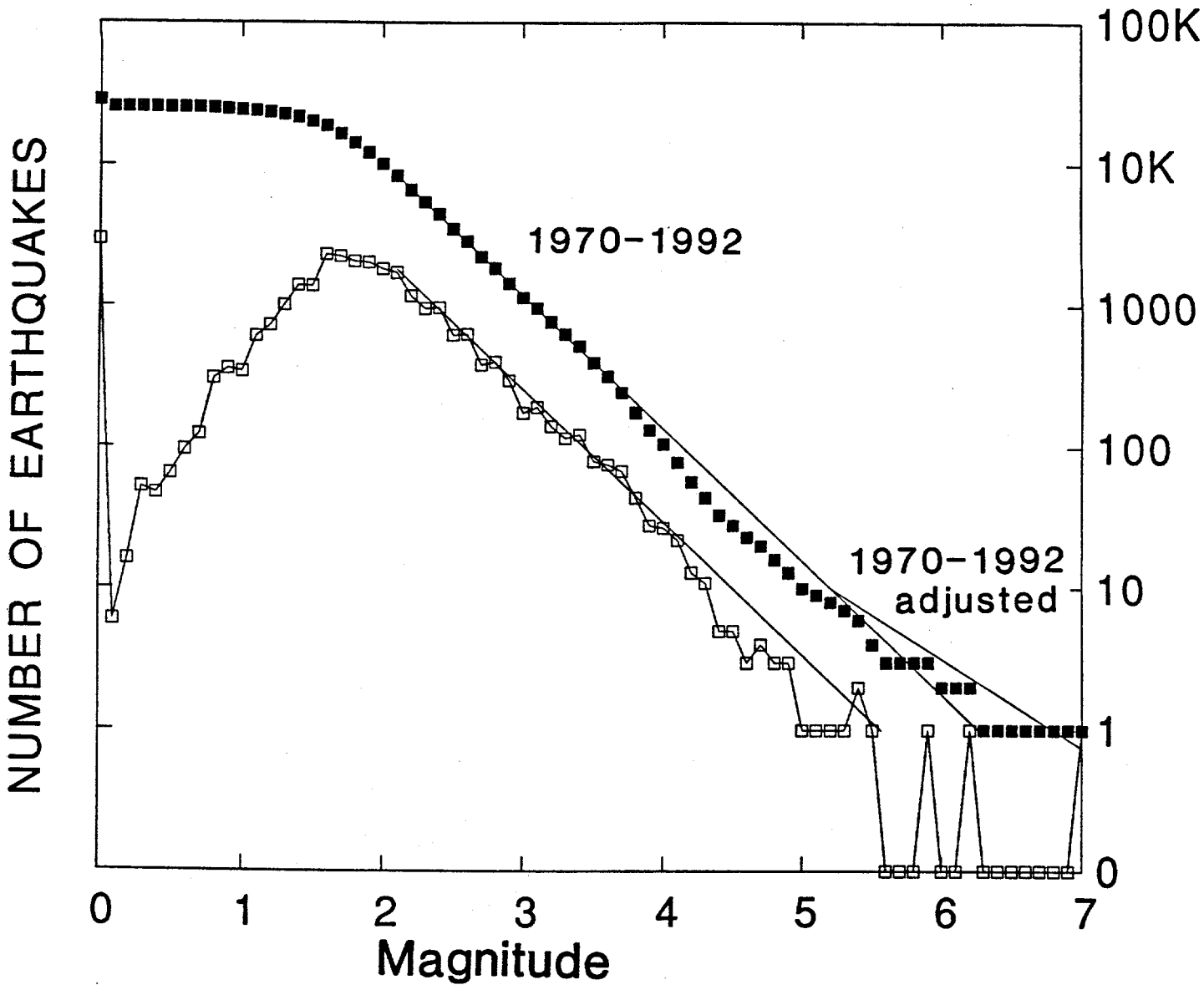

Figure 4a.

Figure 4. Log of earthquake frequency versus magnitude for the 19 seismic source zones (regions) of figure 3. The earthquakes are from the HVO catalog for 1970-1992. Open squares show the number of earthquakes per 0.1 magnitude interval and solid squares show the cumulative number of events larger than magnitude M. The straight lines are the maximum liklihood fit to the linear part of the distribution. If earthquakes obey the Gutenberg-Richter law, both the interval (open squares) and cumulative (solid squares) distributions are linear with the slope -b for earthquakes larger than the minimum magnitude for which the catalog is complete. The adjusted distributions for M>5.2 earthquakes based on their higher observed frequency during 1970-92 are plotted in (a) and (b). The historic distributions from the Wyss and Koyanagi catalog (1992) are shown with x symbols in figures (c), (f) and (g) after scaling to the number of earthquakes expected in 23 years.

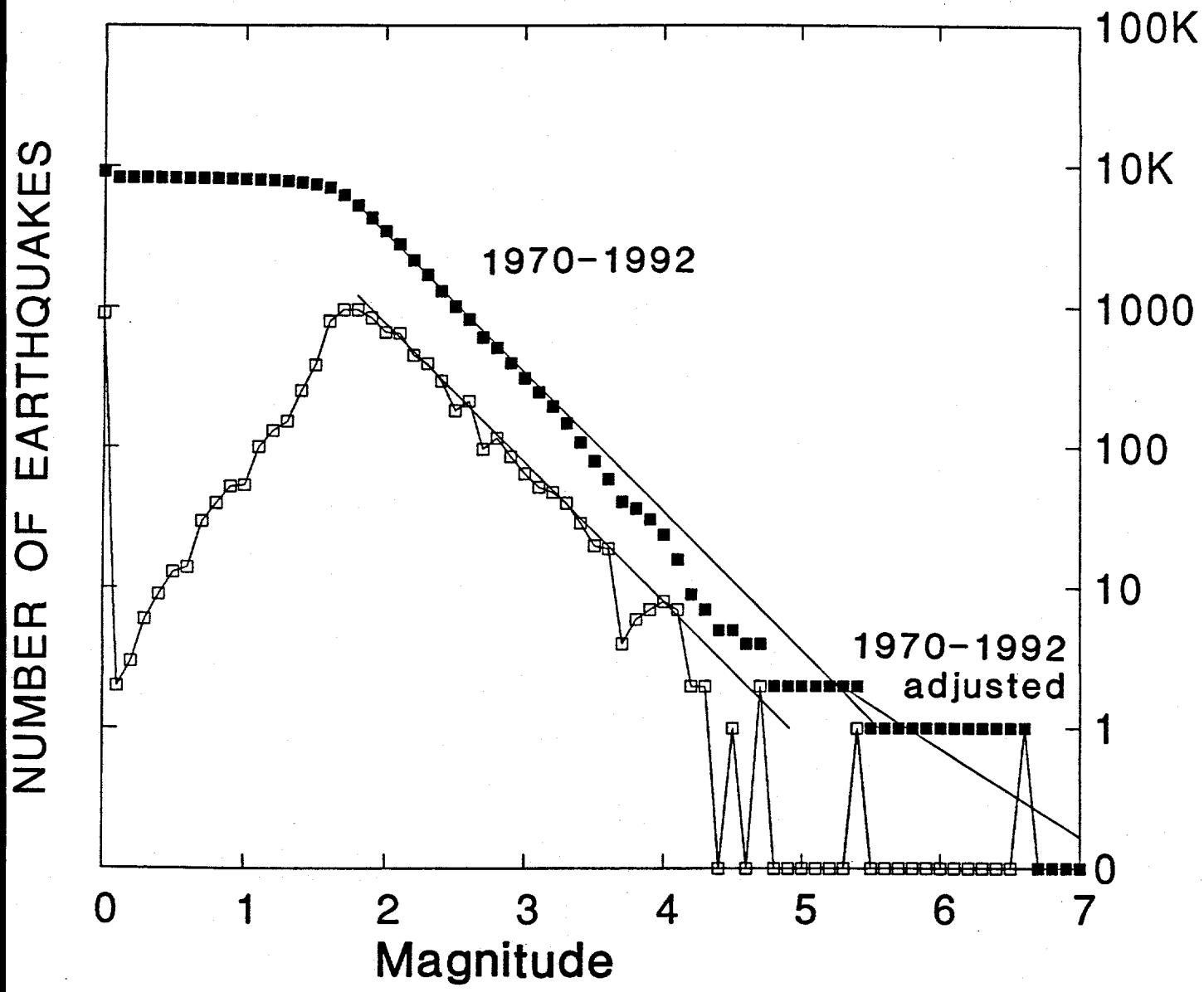
Region 2 (Kaoiki seismic zone)
B= 0.99 +/-0.01 USING 5295. EVENTS
NUMBER OF EARTHQUAKES
100K
10K
1000
100
10
1
0
1970-1992
1970-1992
adjusted
0
1
2
3
4
5
6
7
Magnitude

Figure 4b.

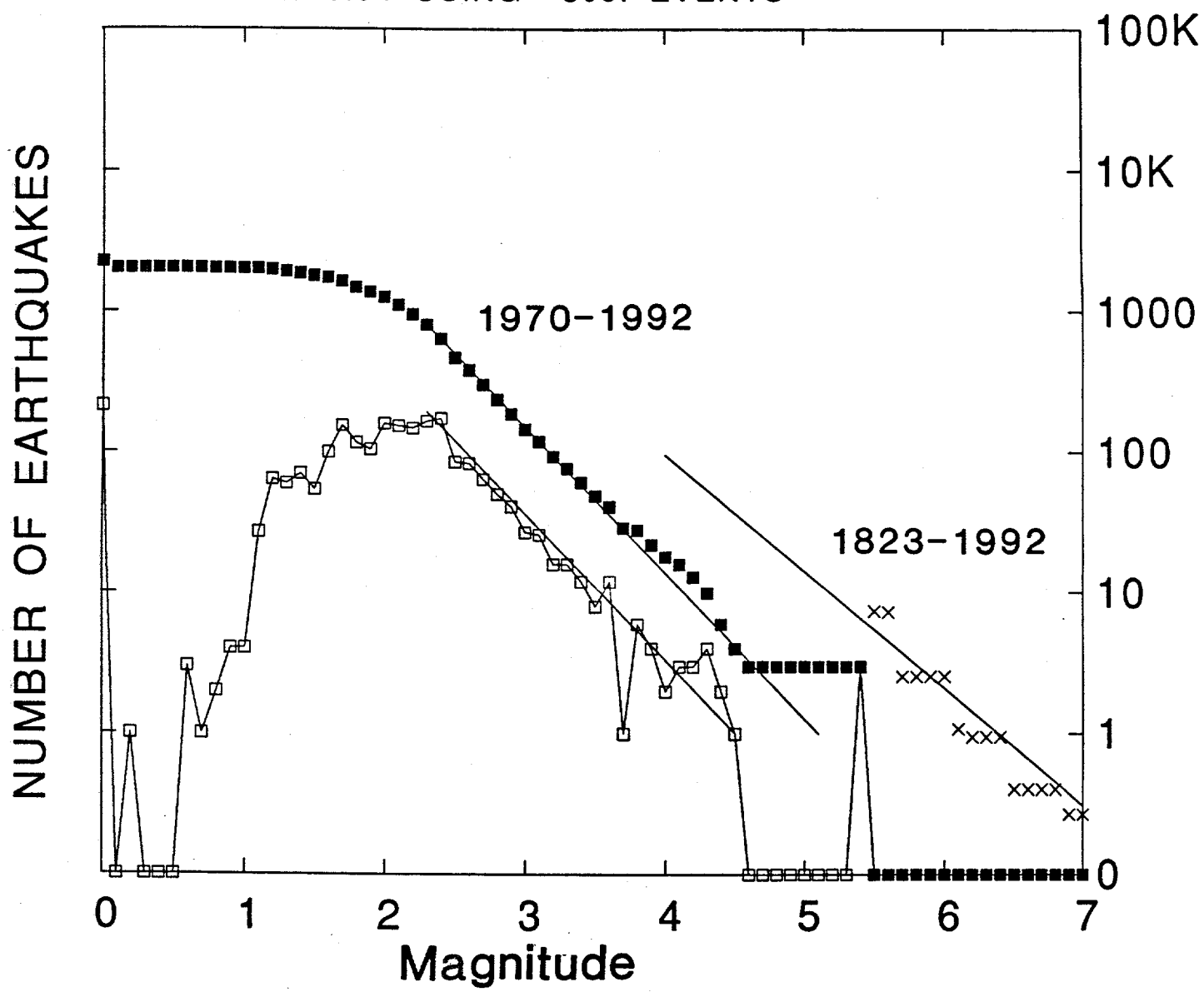
Region 3 (Hilea seismic zone)
B= 1.04 +/-0.04 USING 809. EVENTS
NUMBER OF EARTHQUAKES
100K
10K
1000
100
10
1
0
1970-1992
1823-1992
0
1
2
3
4
5
6
7
Magnitude

Figure 4c.

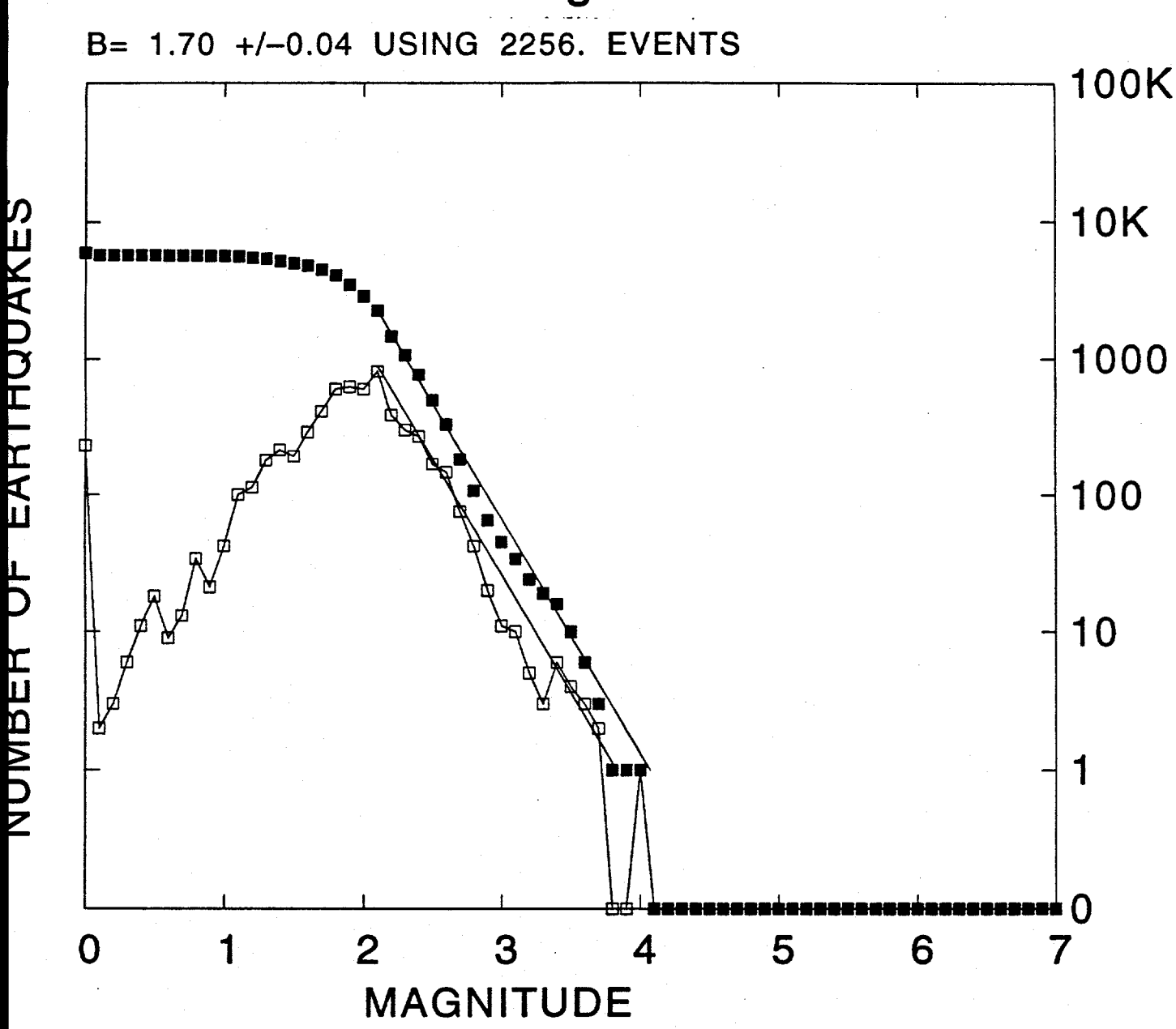
Region 4
B= 1.70 +/-0.04 USING 2256. EVENTS
NUMBER OF EARTHQUAKES
100K
10K
1000
100
10
1
0
0
1
2
3
4
5
6
7
MAGNITUDE

Figure 4d.

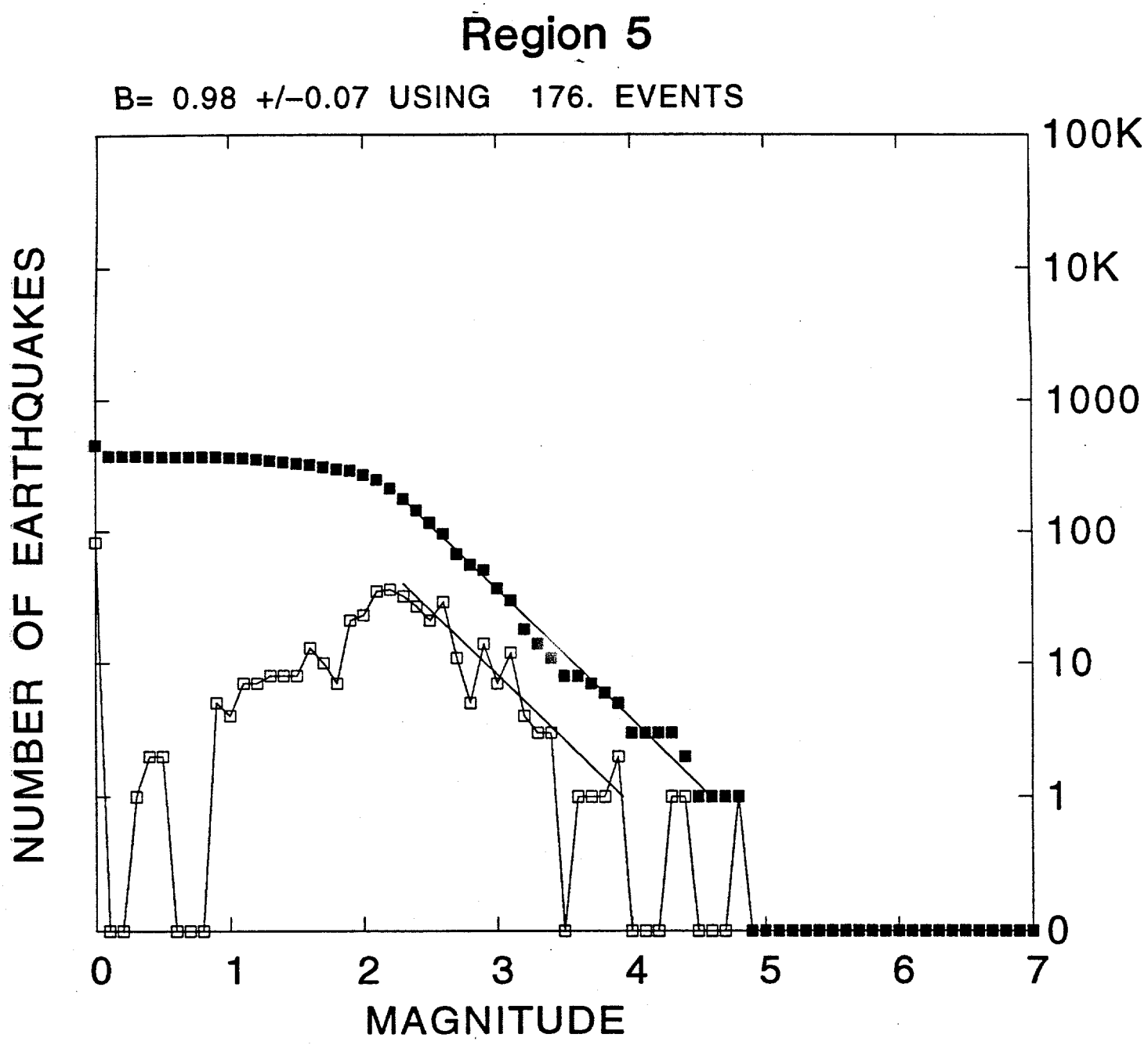
Region 5
B= 0.98 +/-0.07 USING 176. EVENTS
NUMBER OF EARTHQUAKES
100K
10K
1000
100
10
1
0
0
1
2
3
4
5
6
7
MAGNITUDE

Figure 4e.

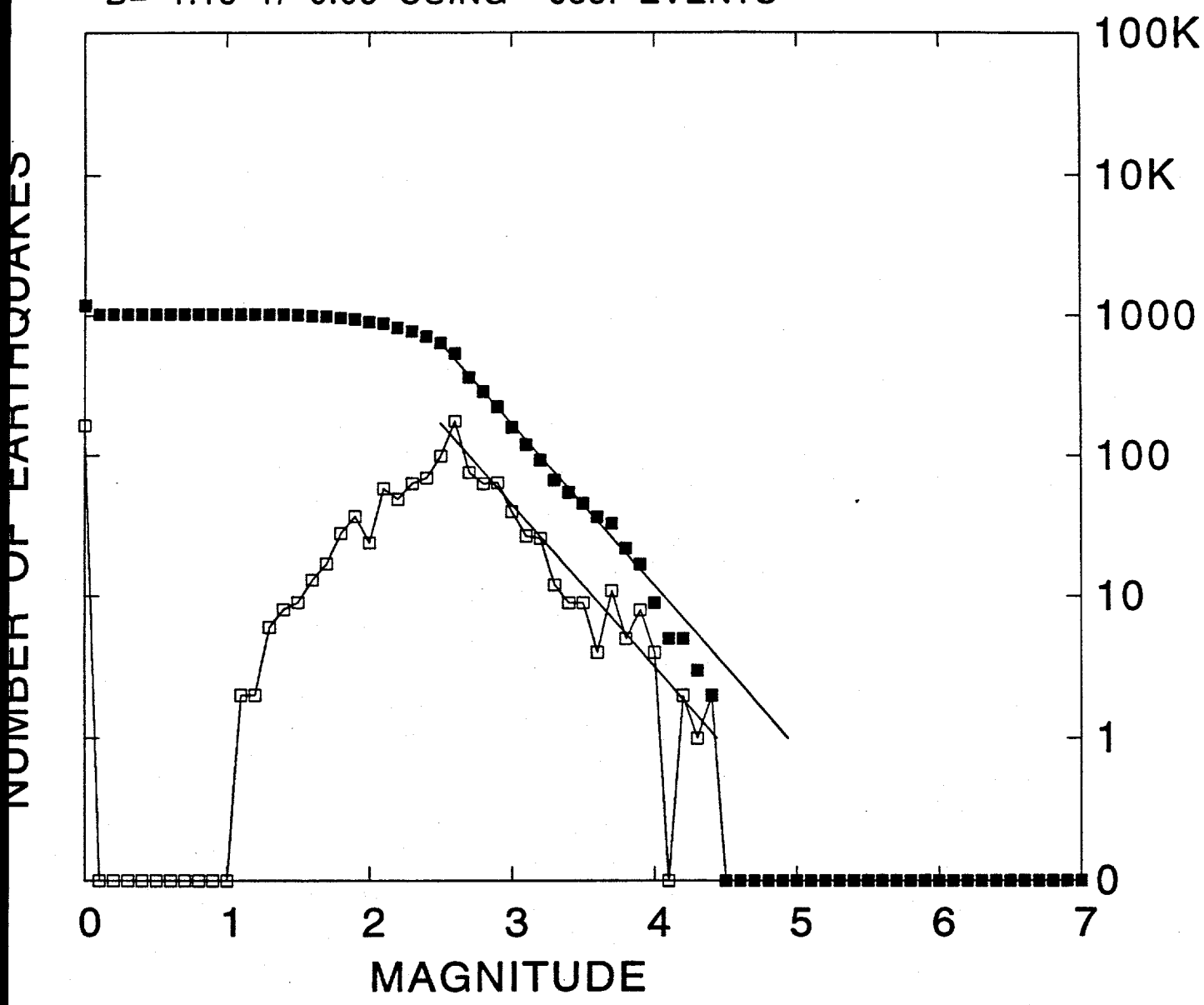
Region 6
B= 1.15 +/-0.05 USING 638. EVENTS
NUMBER OF EARTHQUAKES
100K
10K
1000
100
10
1
0
0
1
2
3
4
5
6
7
MAGNITUDE

Figure 4f.

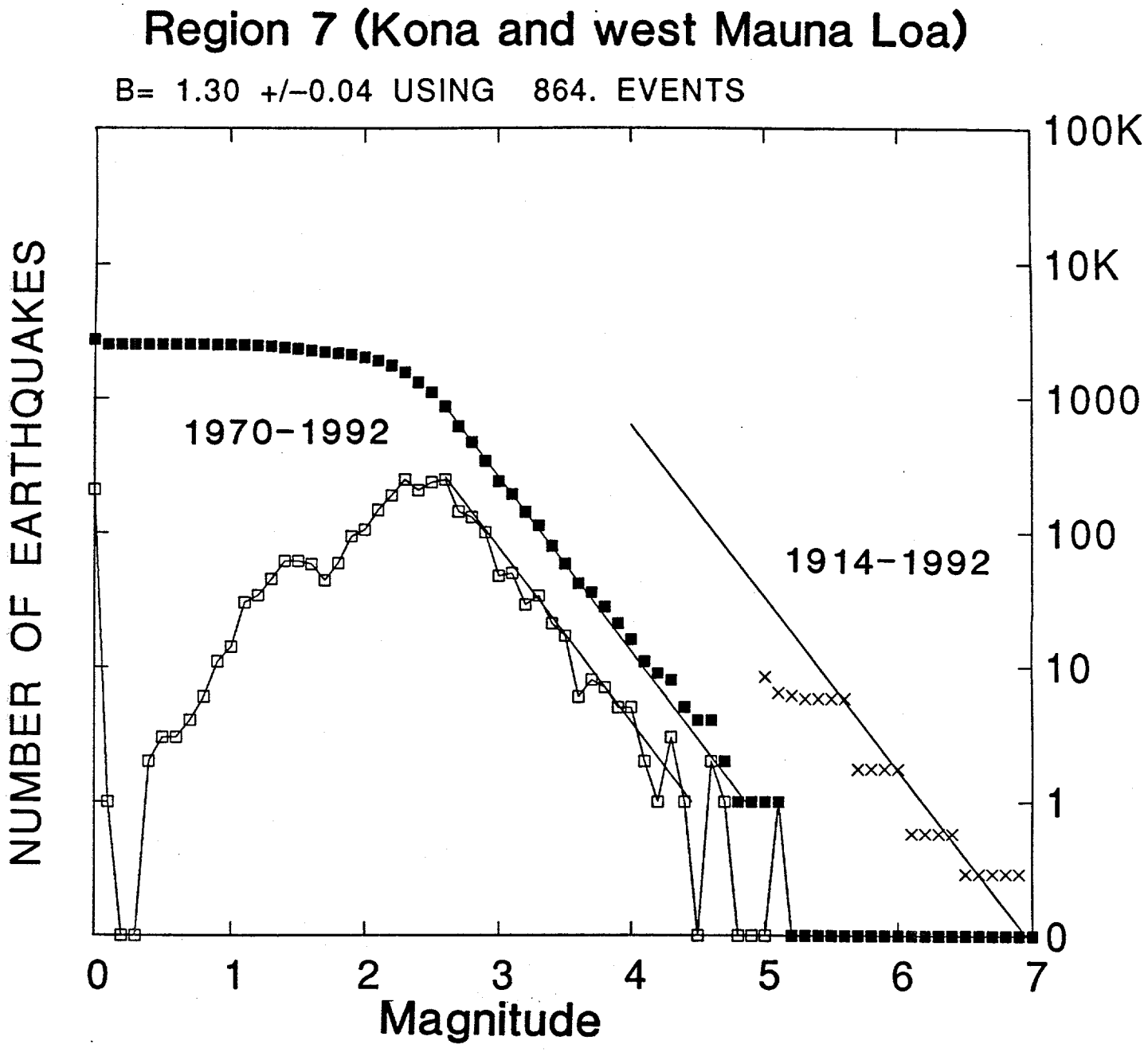
Region 7 (Kona and west Mauna Loa)
B= 1.30 +/-0.04 USING 864. EVENTS
NUMBER OF EARTHQUAKES
100K
10K
1000
100
10
1
0
1970-1992
1914-1992
0
1
2
3
4
5
6
7
Magnitude

Figure 4g.

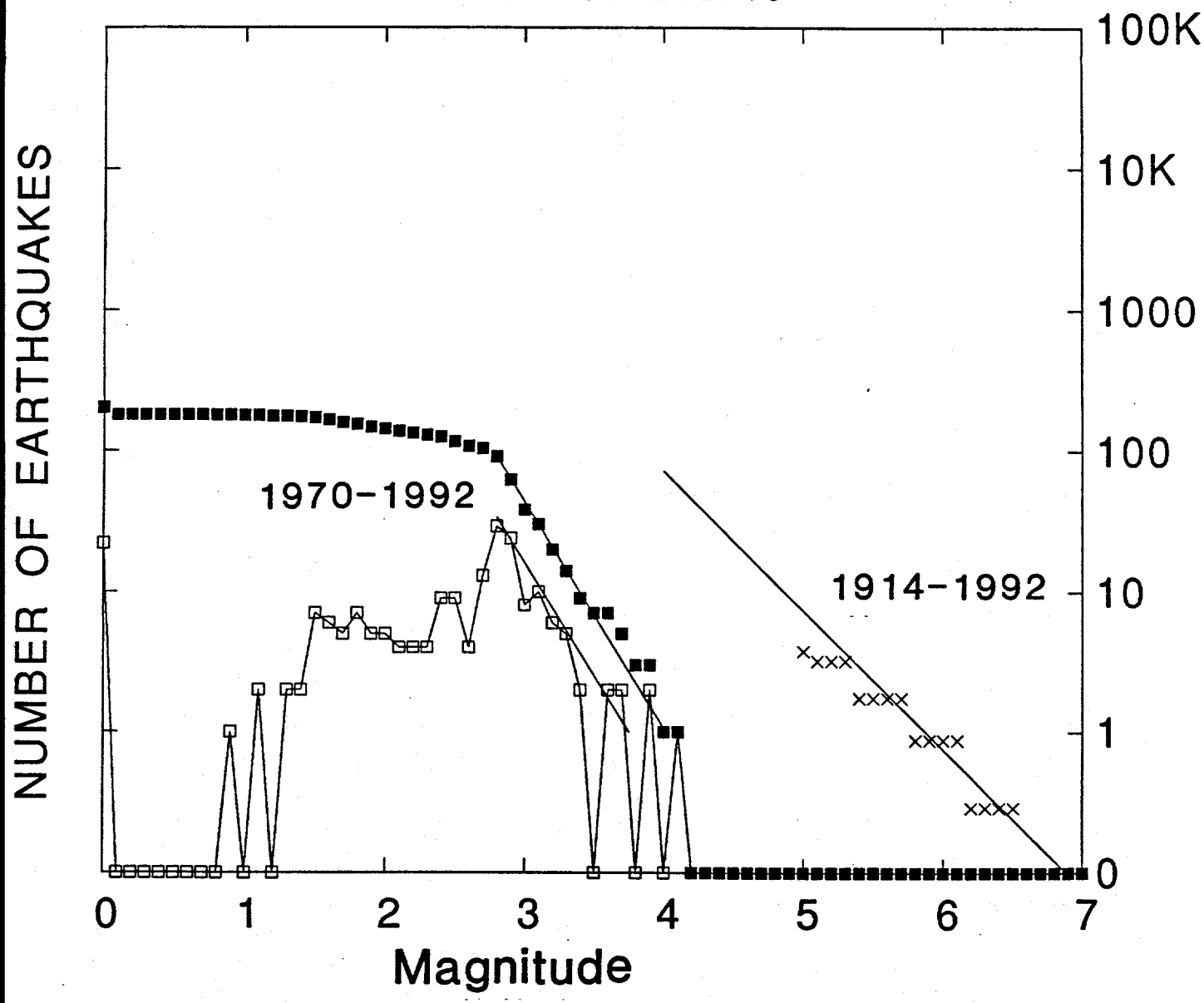
Region 8 (Hualalai)
B= 1.61 +/-0.17 USING 91. EVENTS
NUMBER OF EARTHQUAKES
100K
10K
1000
100
10
1
0
1970-1992
1914-1992
0
1
2
3
4
5
6
7
Magnitude

Figure 4h.

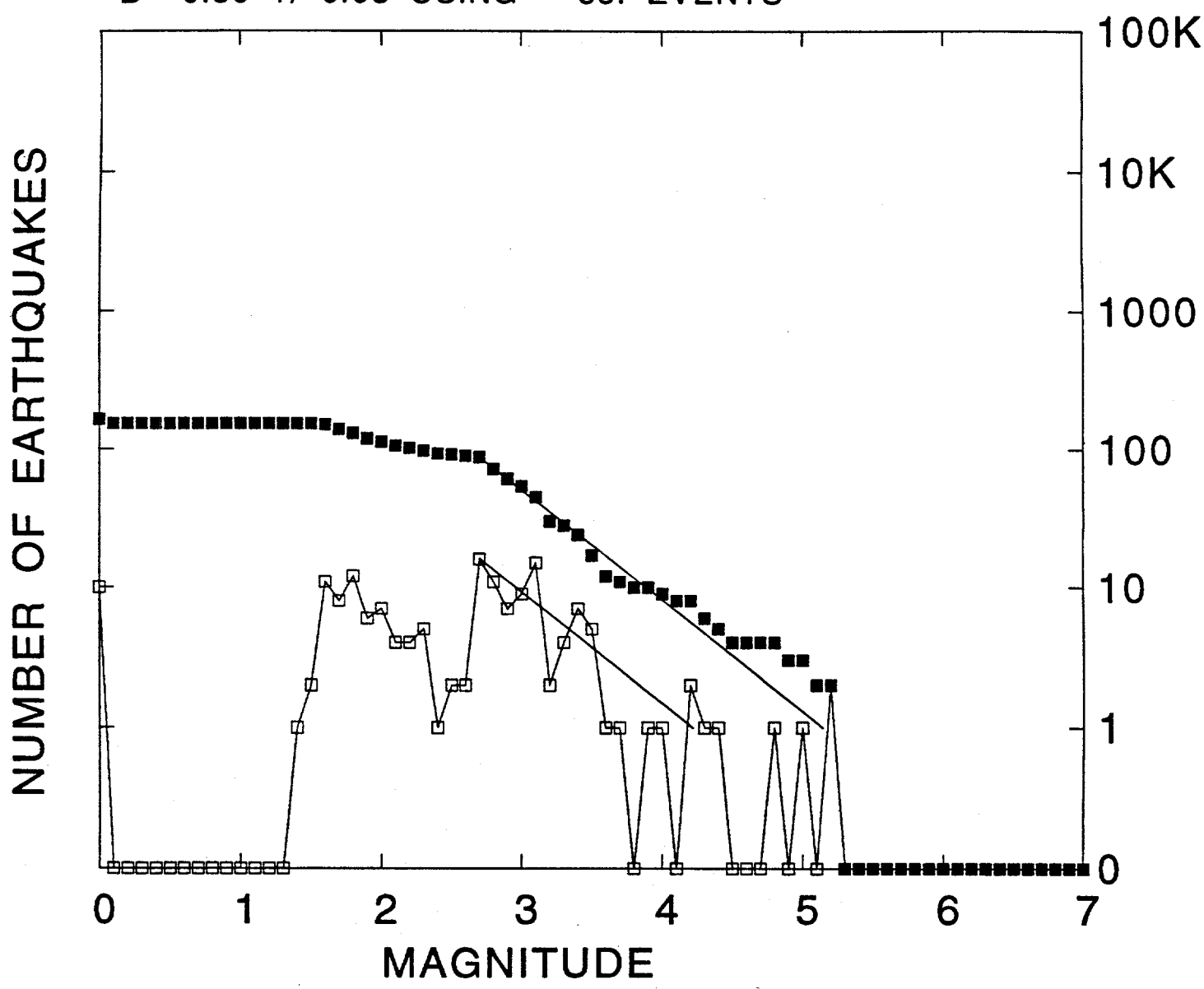
Region 9
B= 0.80 +/-0.08 USING 88. EVENTS
NUMBER OF EARTHQUAKES
100K
10K
1000
100
10
1
0
0
1
2
3
4
5
6
7
MAGNITUDE

Figure 4i.

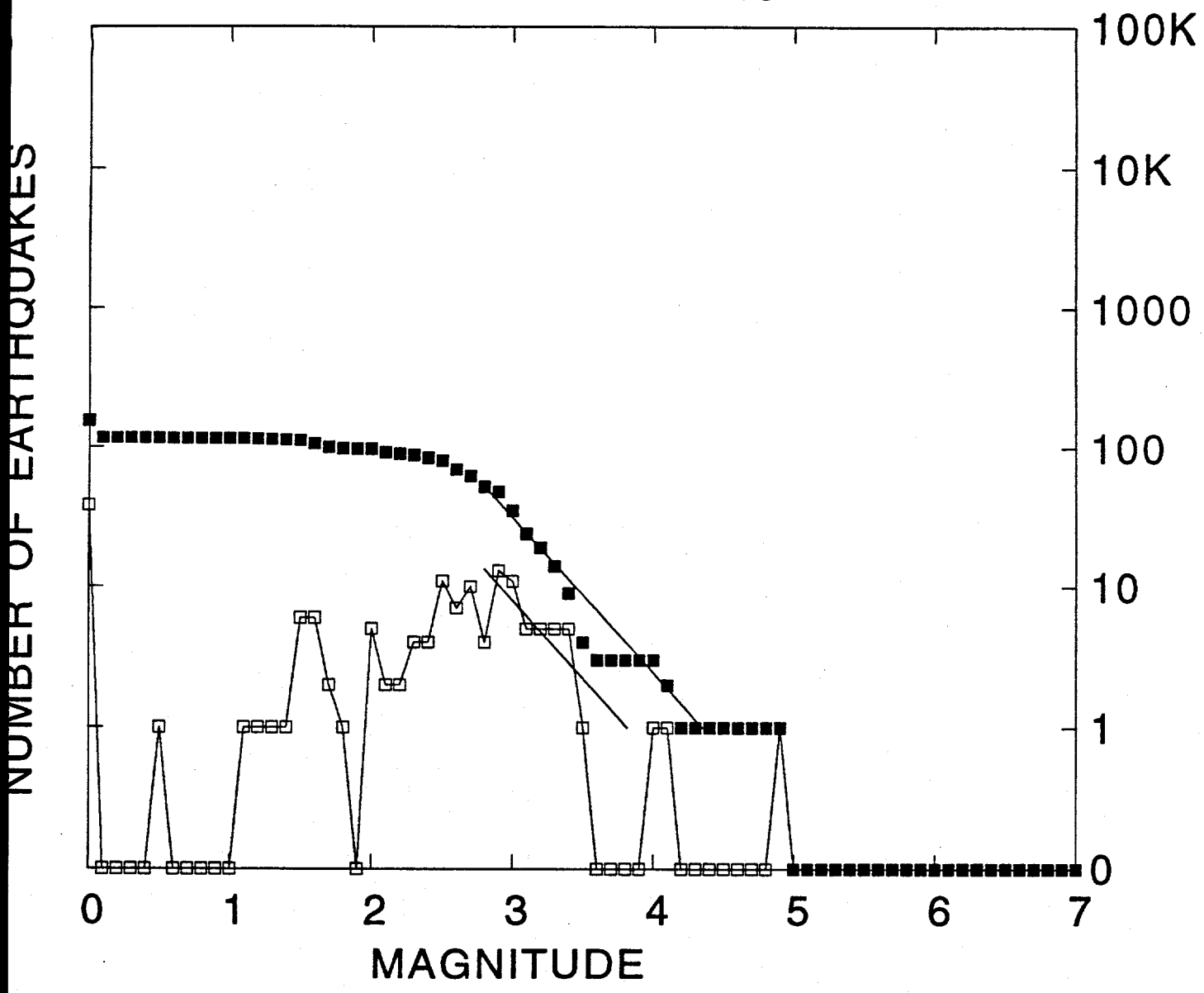
Region 10
B= 1.11 +/-0.15 USING 52. EVENTS
NUMBER OF EARTHQUAKES
100K
10K
1000
100
10
1
0
0
1
2
3
4
5
6
7
MAGNITUDE

Figure 4j.

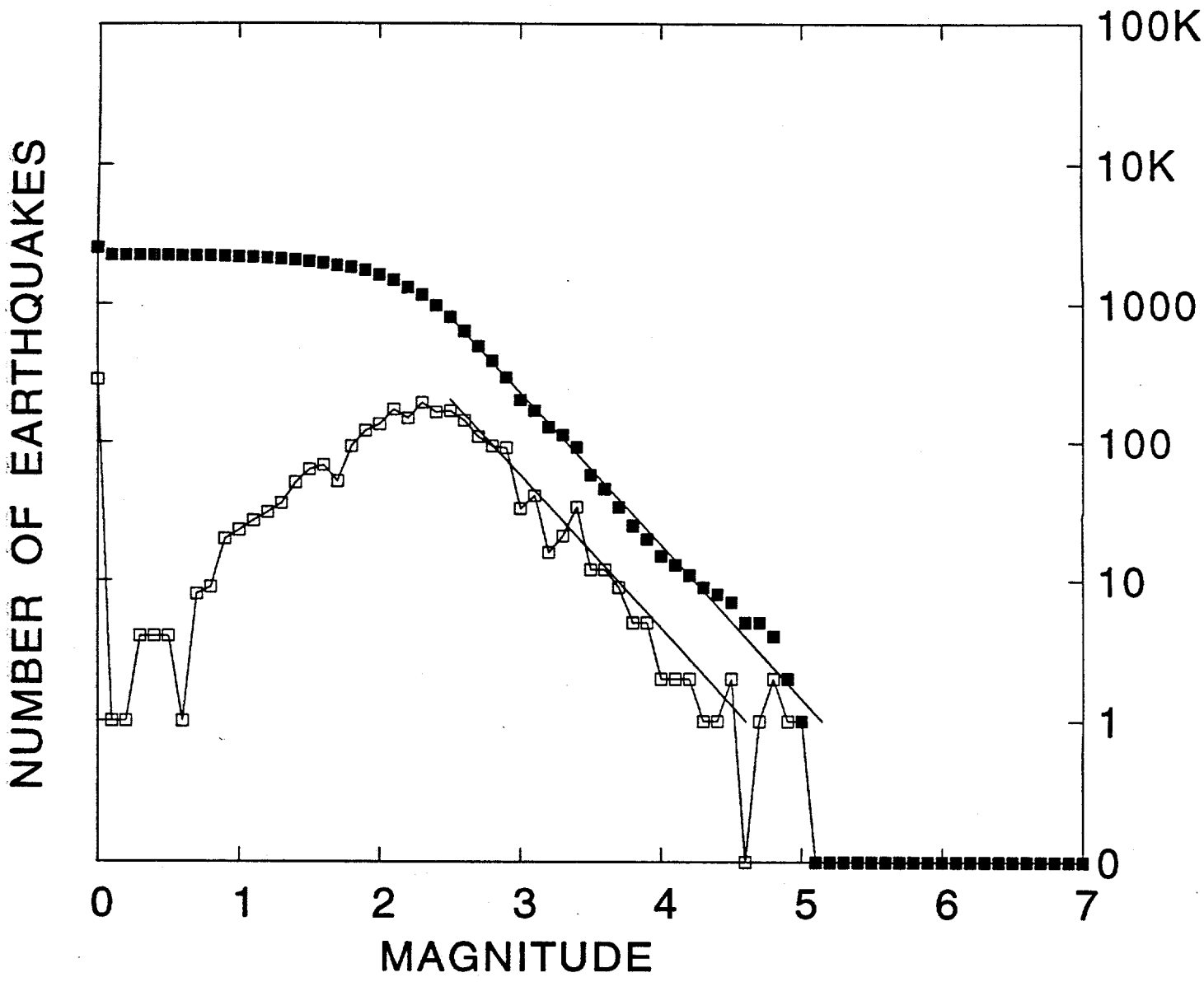
Region 11
B= 1.10 +/-0.04 USING 809. EVENTS
NUMBER OF EARTHQUAKES
100K
10K
1000
100
10
1
0
0
1
2
3
4
5
6
7
MAGNITUDE

Figure 4k.

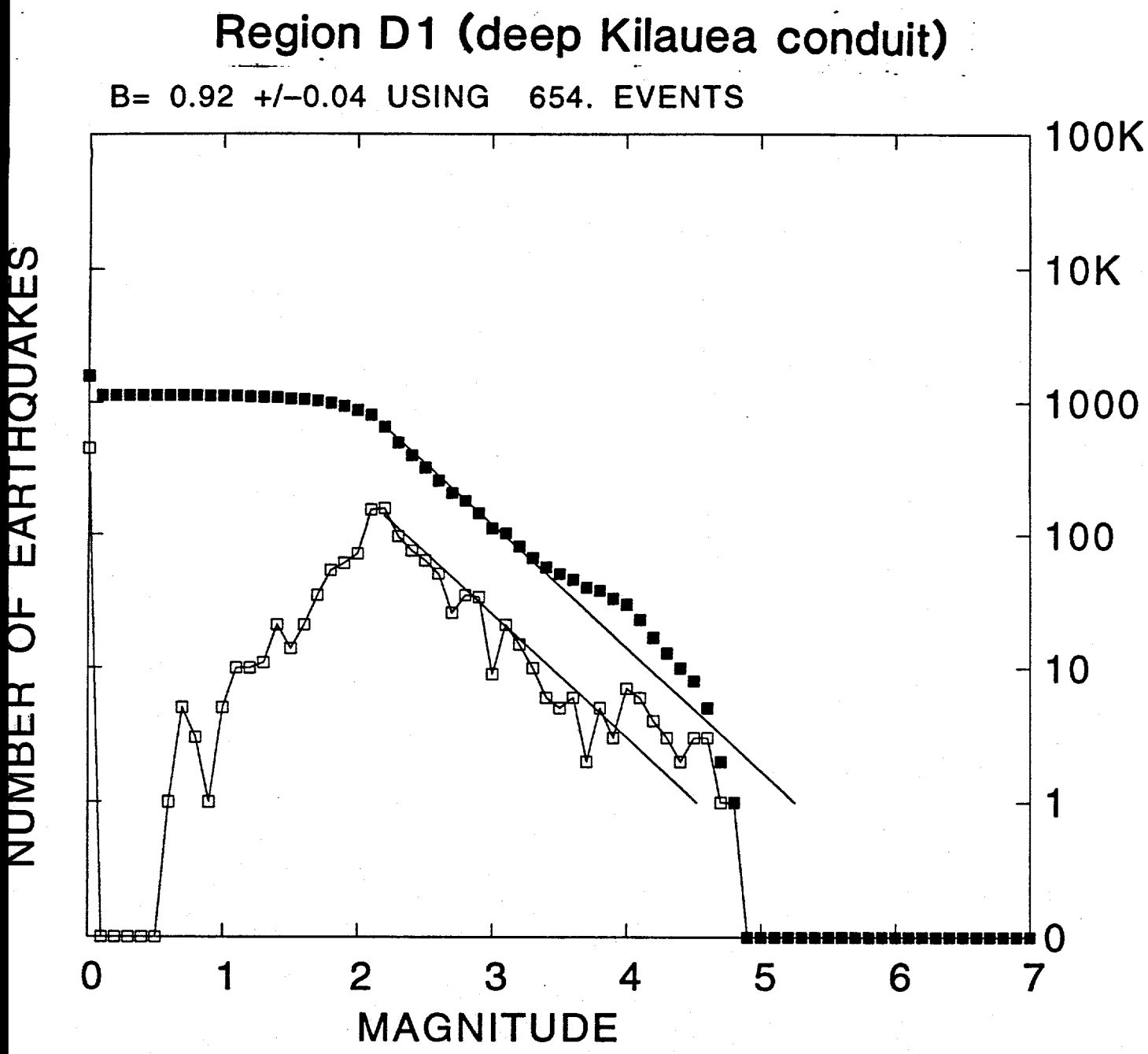
Region D1 (deep Kilauea conduit)
B= 0.92 +/-0.04 USING 654. EVENTS
NUMBER OF EARTHQUAKES
100K
10K
1000
100
10
1
0
0
1
2
3
4
5
6
7
MAGNITUDE

Figure 4L.

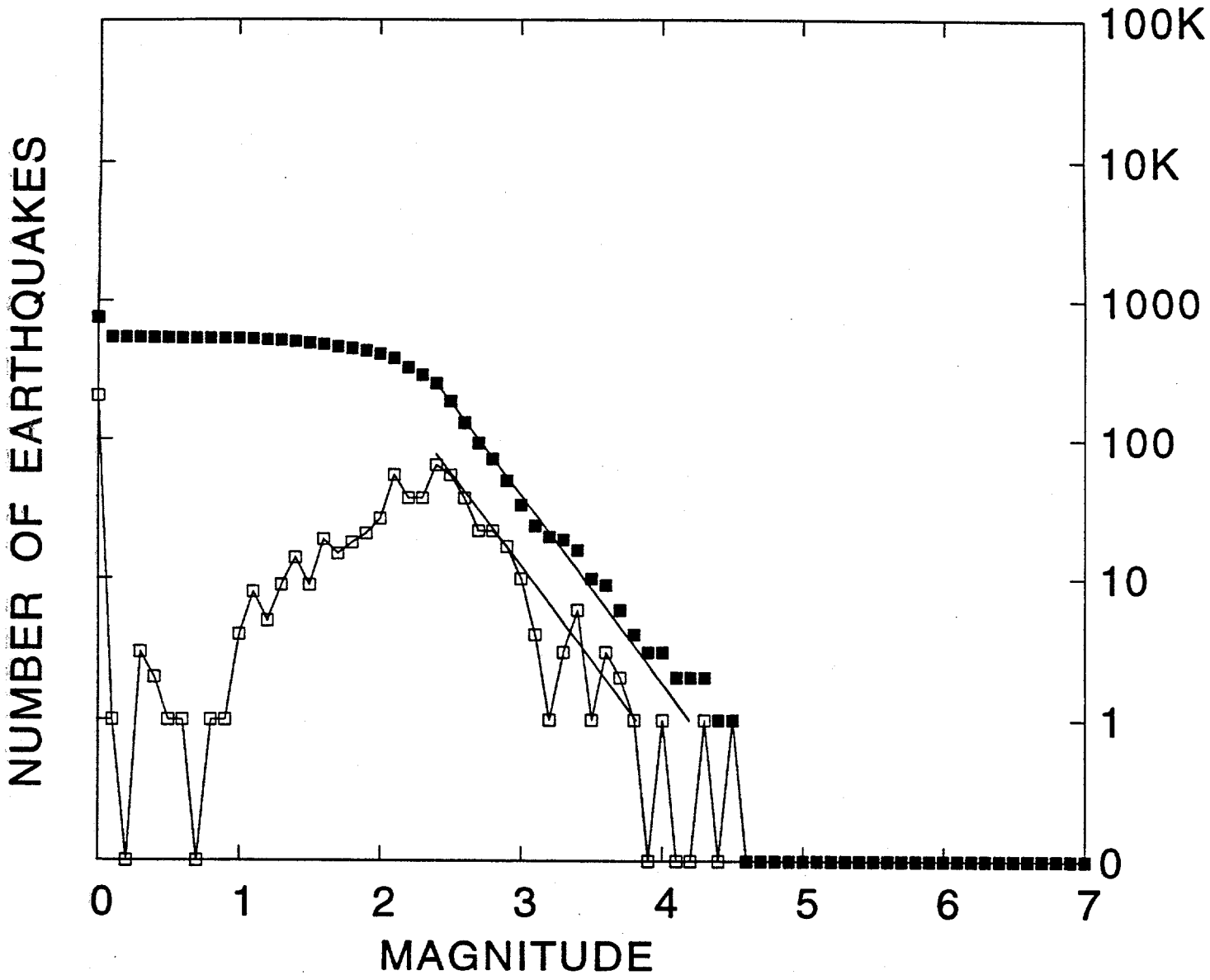
Region D2
B= 1.34 +/-0.08 USING 255. EVENTS
NUMBER OF EARTHQUAKES
100K
10K
1000
100
10
1
0
0
1
2
3
4
5
6
7
MAGNITUDE

Figure 4m.

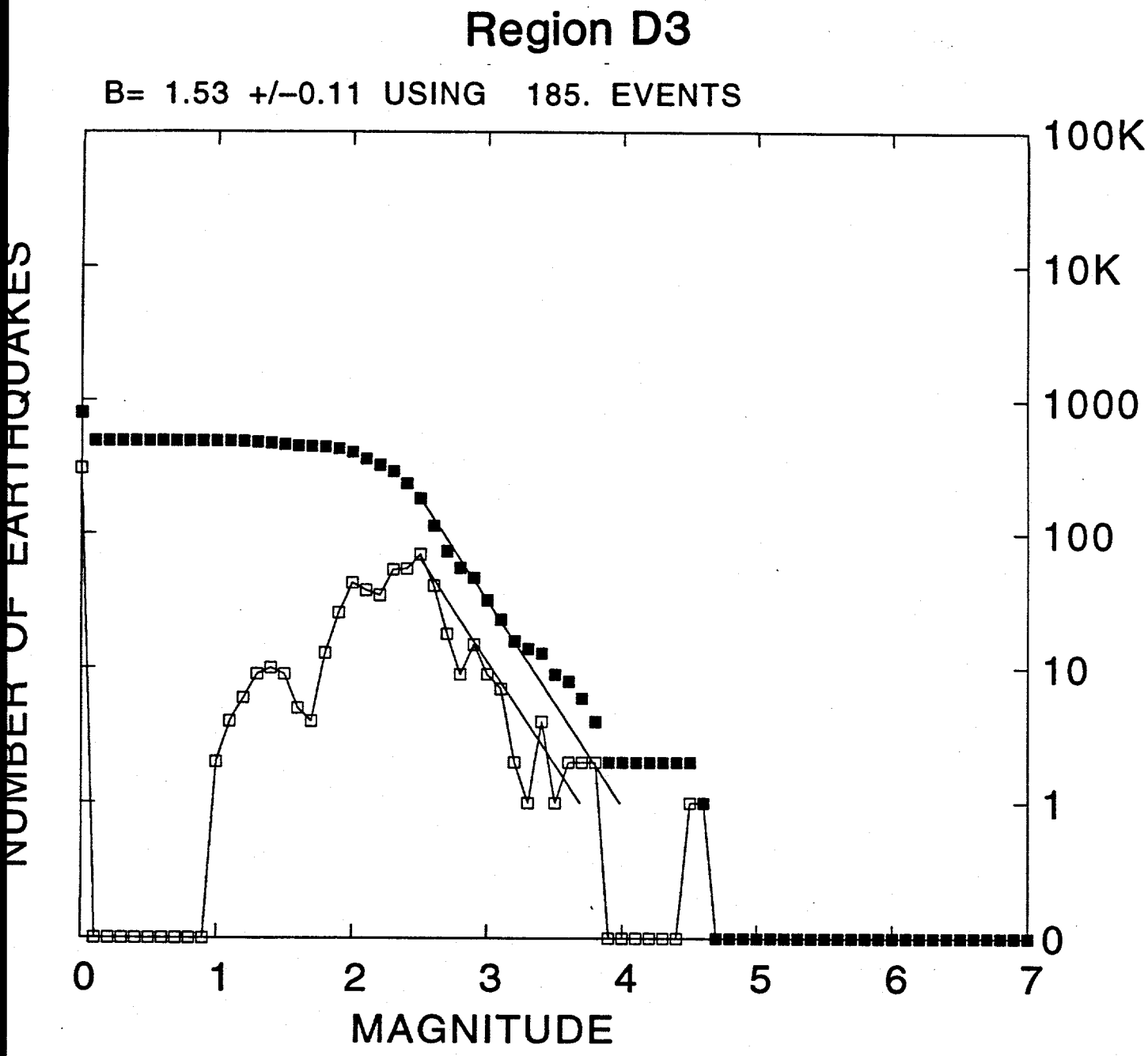
Region D3
B= 1.53 +/-0.11 USING 185. EVENTS
NUMBER OF EARTHQUAKES
100K
10K
1000
100
10
1
0
0
1
2
3
4
5
6
7
MAGNITUDE

Figure 4n.

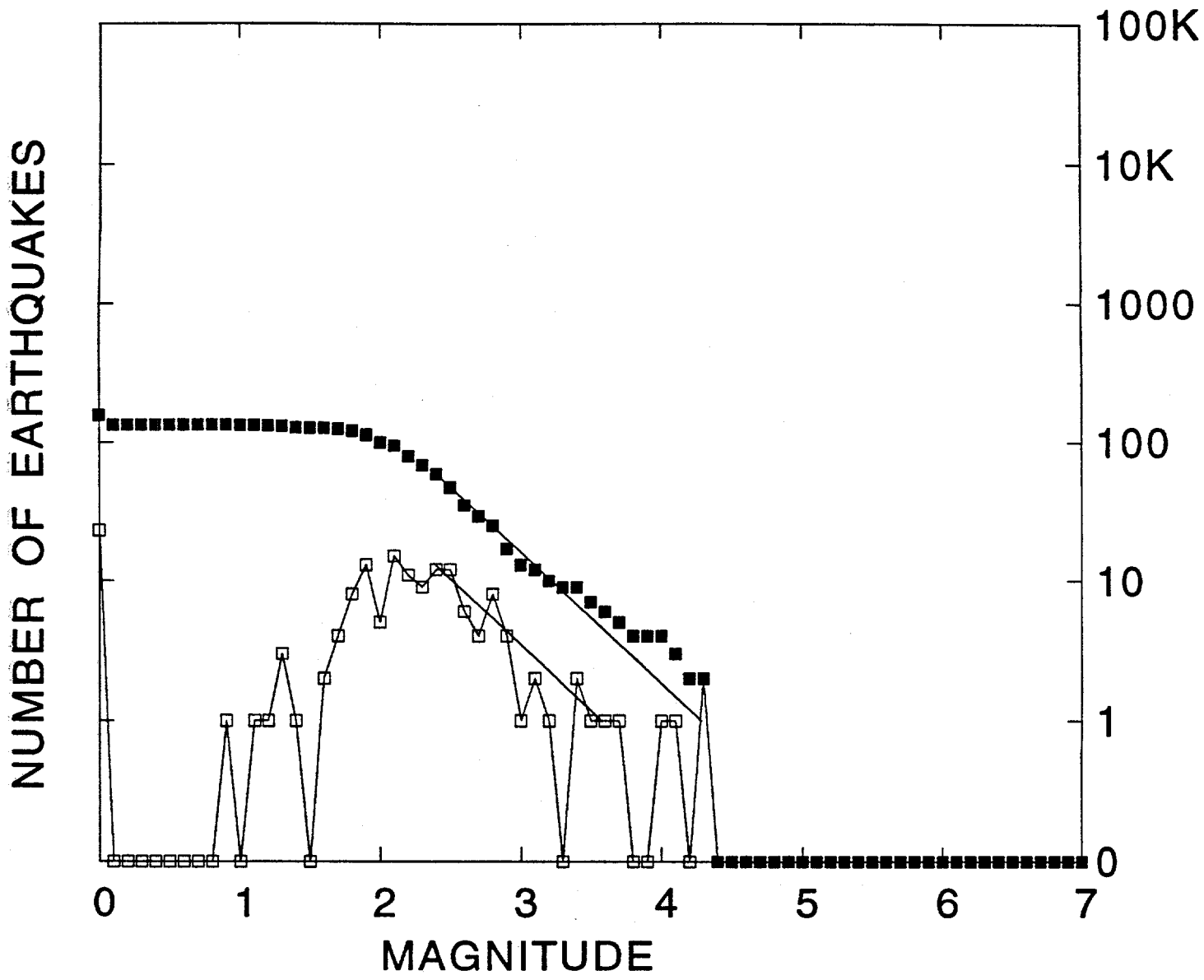
Region D4
B= 0.94 +/-0.12 USING 59. EVENTS
NUMBER OF EARTHQUAKES
100K
10K
1000
100
10
1
0
0
1
2
3
4
5
6
7
MAGNITUDE

Figure 4o.

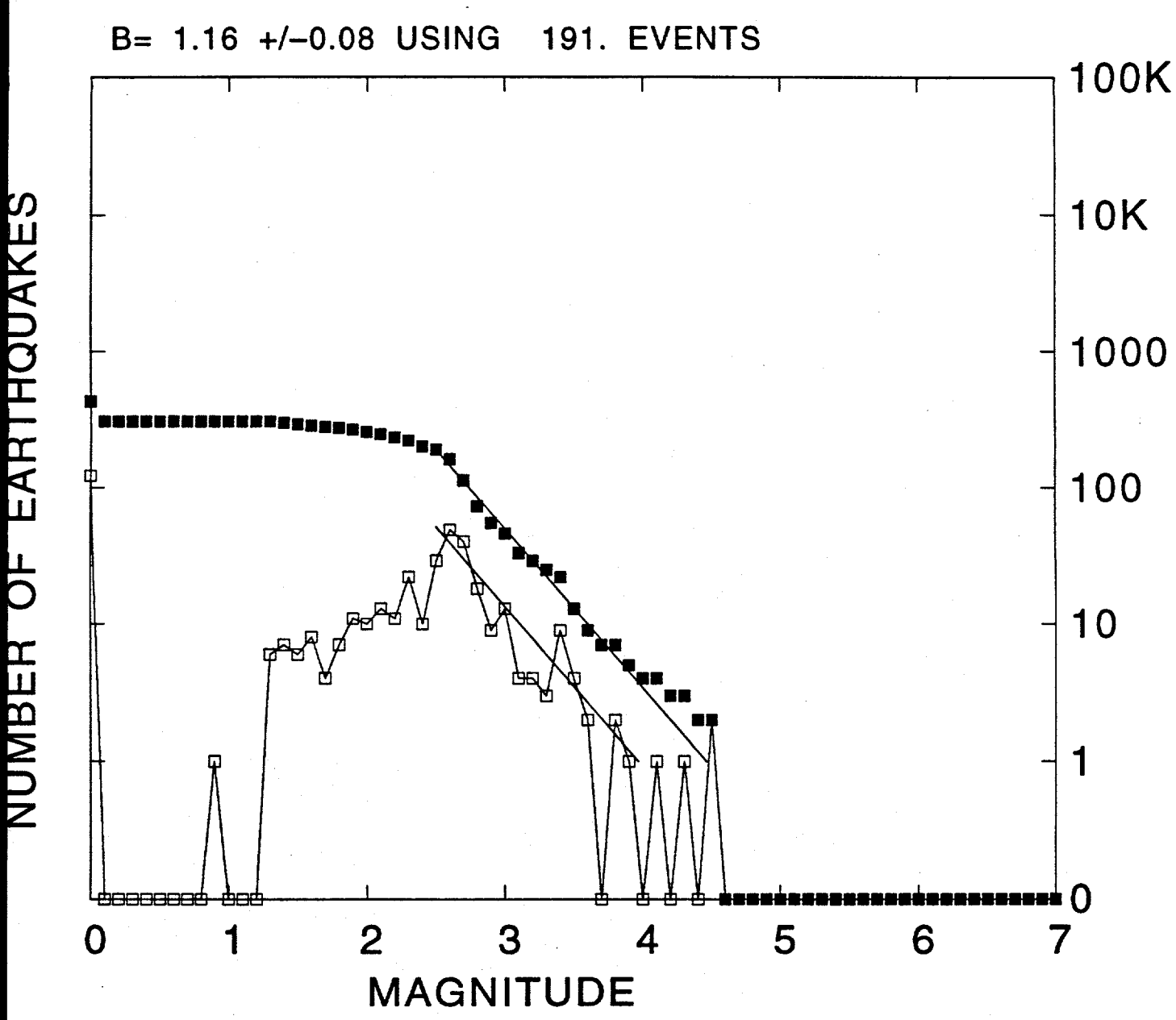
Region D5
B= 1.16 +/-0.08 USING 191. EVENTS
NUMBER OF EARTHQUAKES
100K
10K
1000
100
10
1
0
0
1
2
3
4
5
6
7
MAGNITUDE

Figure 4p.

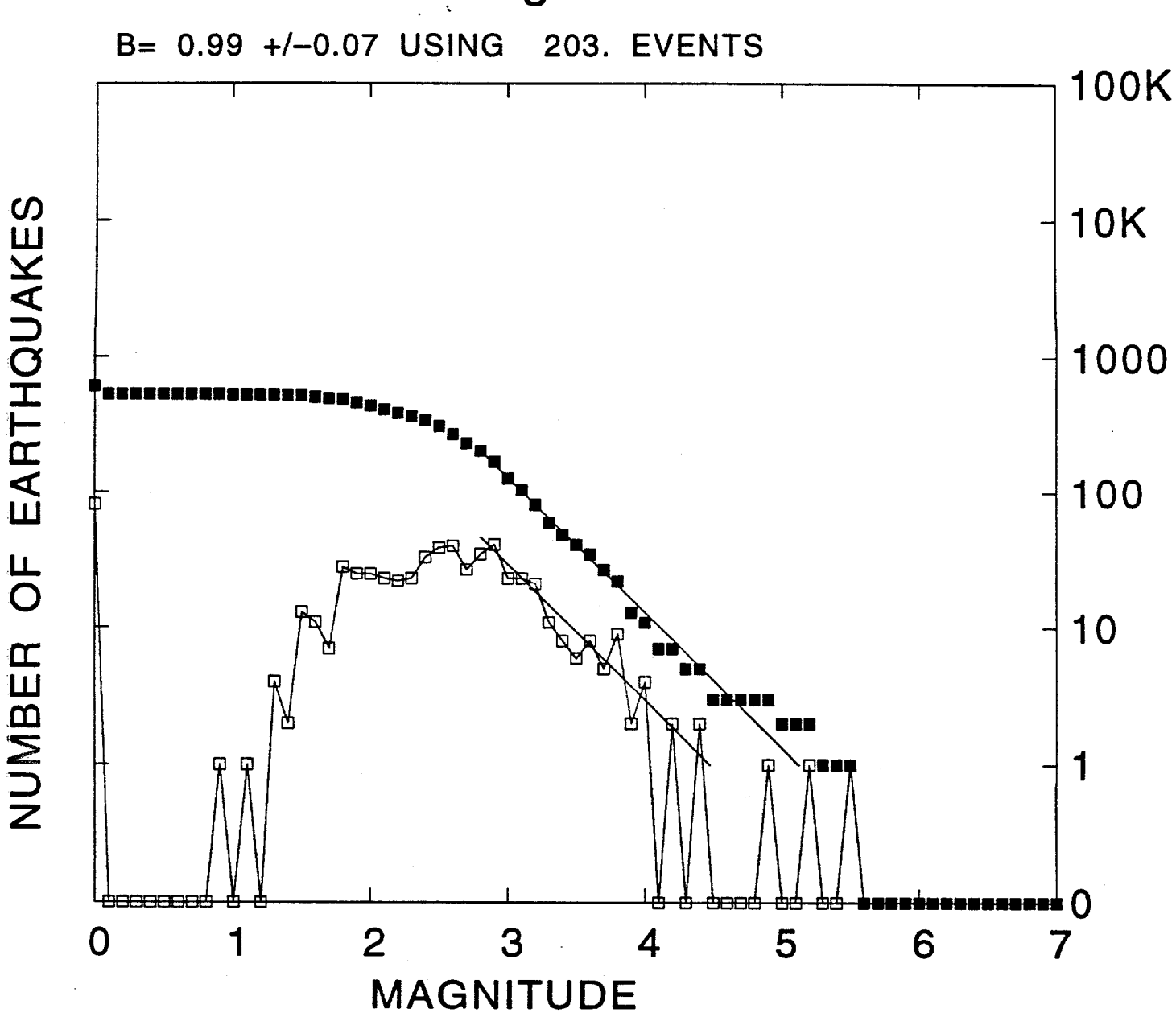
Region D6
B= 0.99 +/-0.07 USING 203. EVENTS
NUMBER OF EARTHQUAKES
100K
10K
1000
100
10
1
0
0
1
2
3
4
5
6
7
MAGNITUDE

Figure 4q.

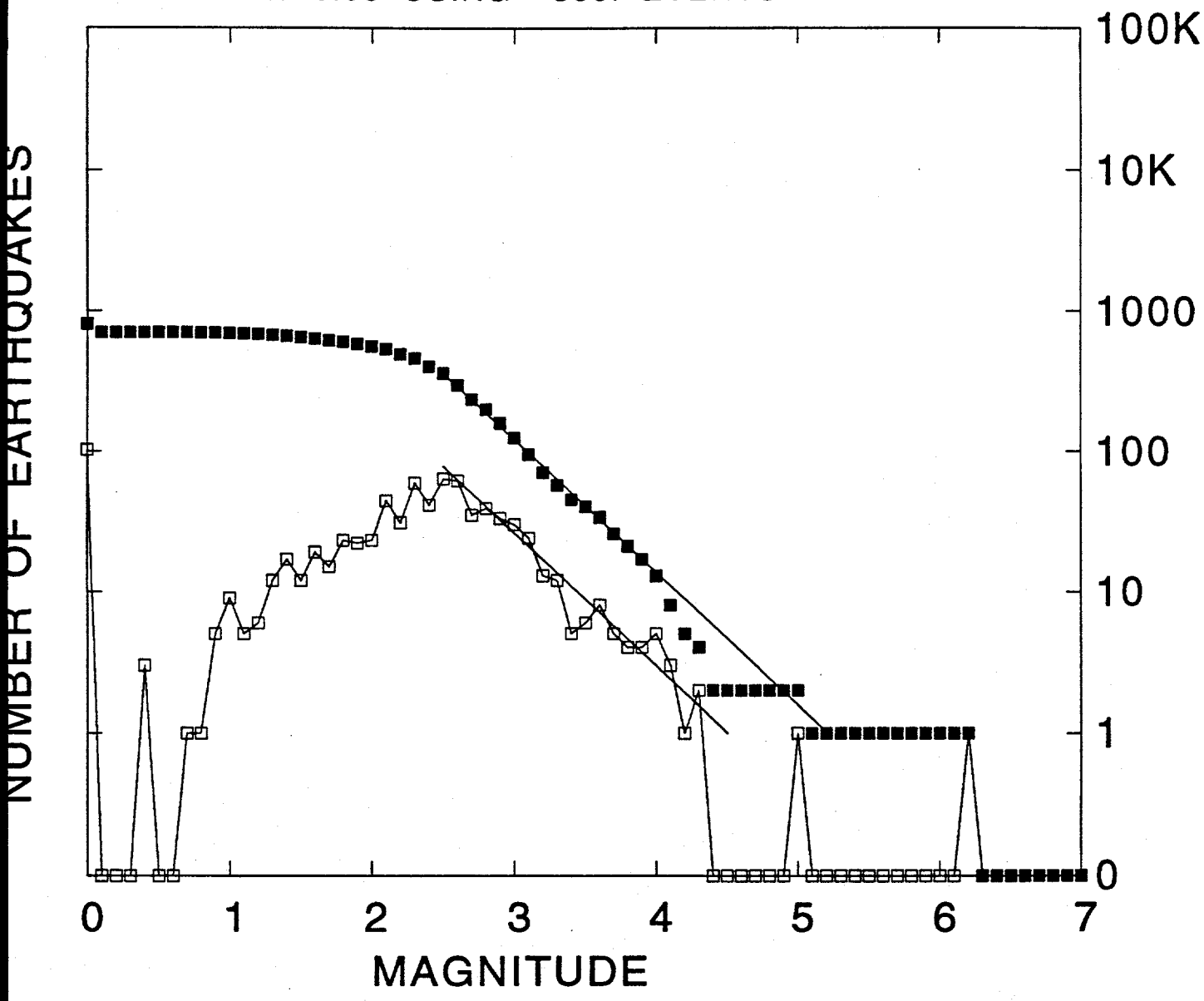
Region D7
B= 0.94 +/-0.05 USING 355. EVENTS
NUMBER OF EARTHQUAKES
100K
10K
1000
100
10
1
0
0
1
2
3
4
5
6
7
MAGNITUDE

Figure 4r.

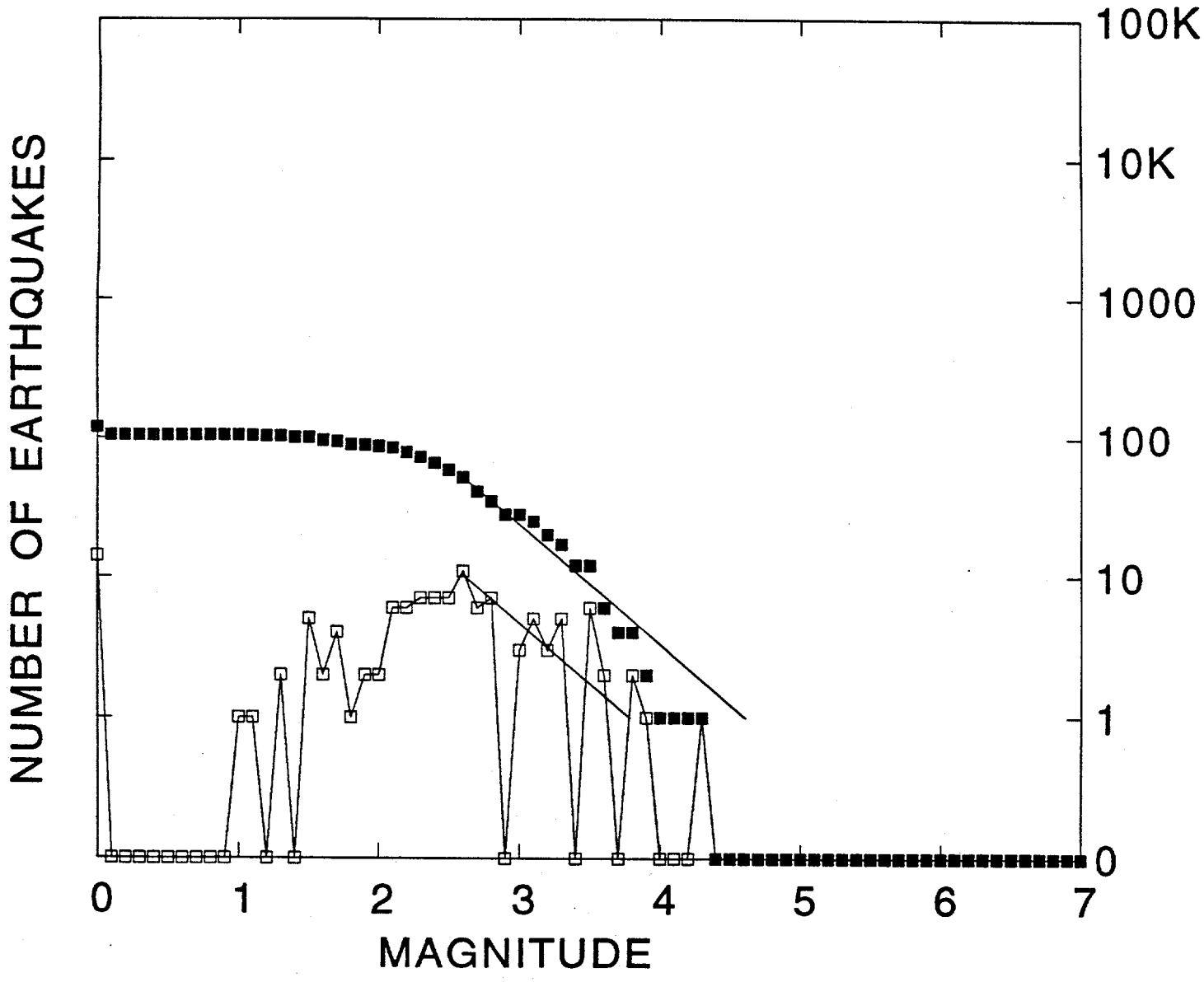
Region D8
B= 0.86 +/-0.12 USING 52. EVENTS
NUMBER OF EARTHQUAKES
100K
10K
1000
100
10
1
0
0
1
2
3
4
5
6
7
MAGNITUDE

Figure 4s.

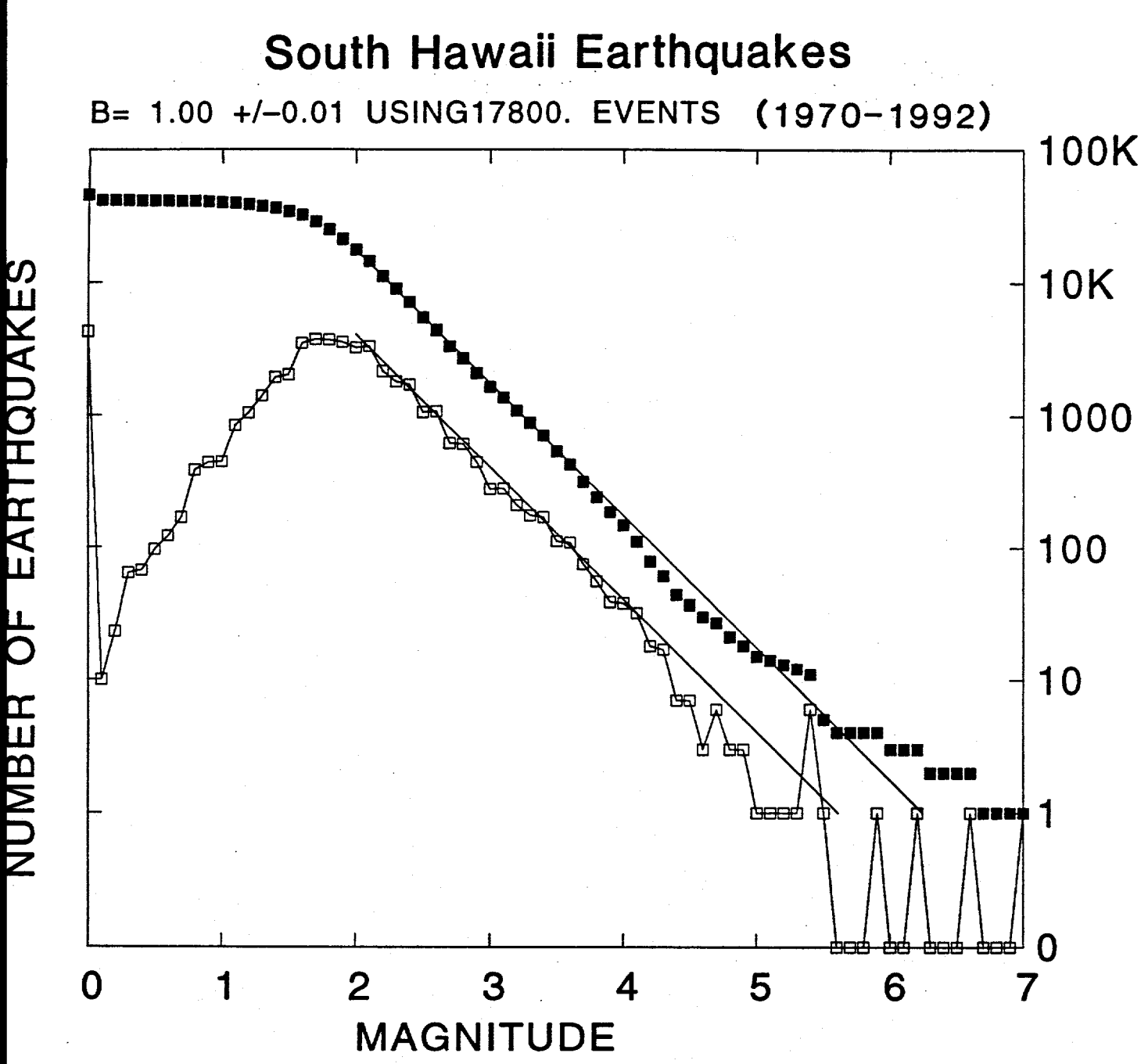

Figure 5. Log of combined earthquake frequency versus magnitude for seismic source zones 1-4 of south Hawaii in figure 3. Symbols and lines are the same as in figure 4.

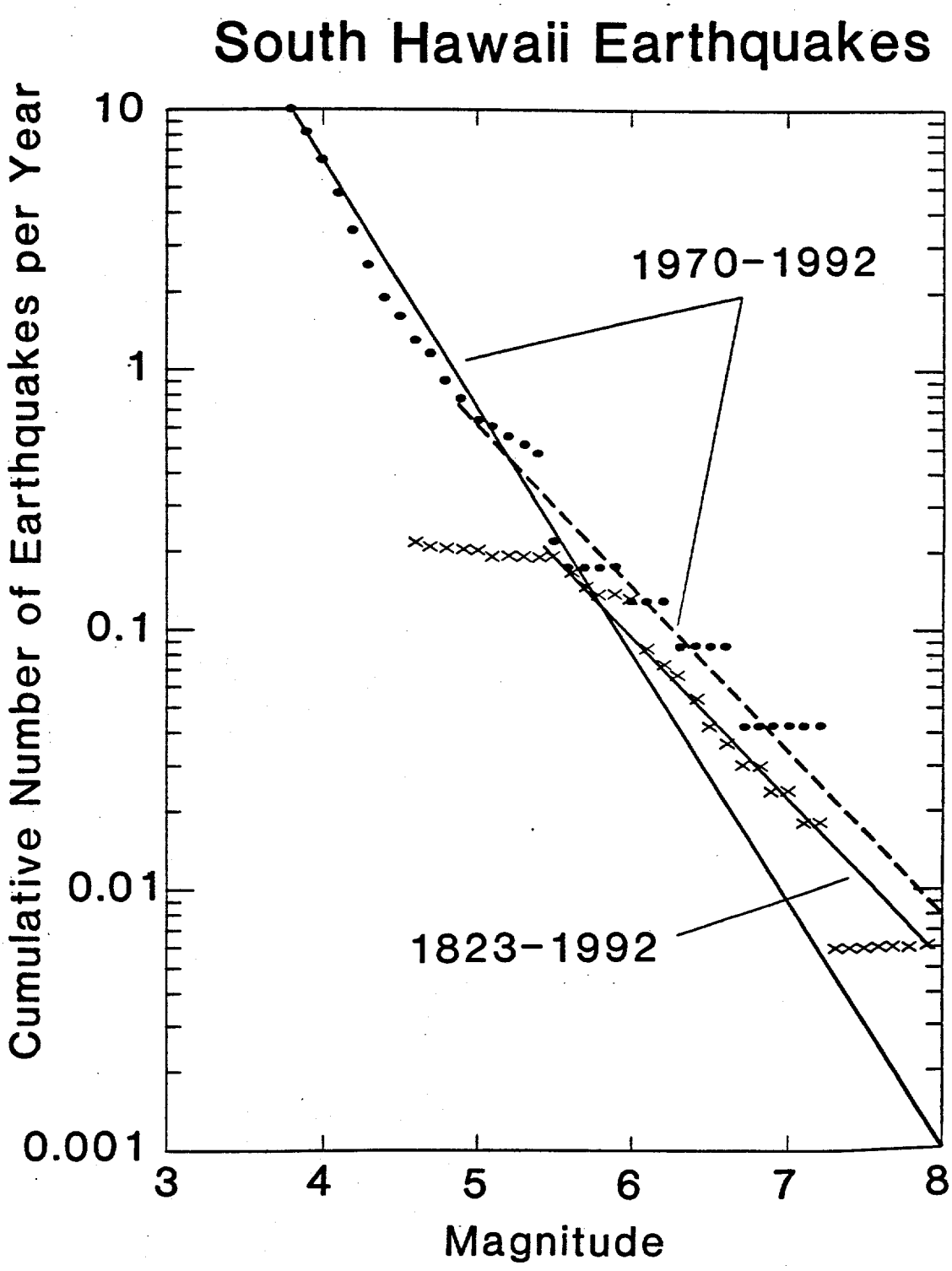

Figure 6. Log of cumulative number of earthquakes per year versus magnitude for south Hawaii. Solid dots are for earthquakes from the 1970-1992 HVO catalog in regions 1, 2, 3 and 4 (figure 3). The solid dots are the same as the solid squares of figure 5 normalized to one year. The thin solid line is the maximum liklihood fit to the M>2.0 HVO catalog earthquakes, and the dashed line fits the M>4.9 earthquakes. X symbols are the distribution of the 1823-1992 catalog of Wyss and Koyanagi (1992). Their catalog appears to be complete above M=5.5 and is fit by the heavy solid line of slope -0.63. The 1970-1992 earthquake rate is about 1.5 times the 1823-1992 rate. The average recurrence interval in years is the reciprocal of the cumulative number of earthquakes per year.

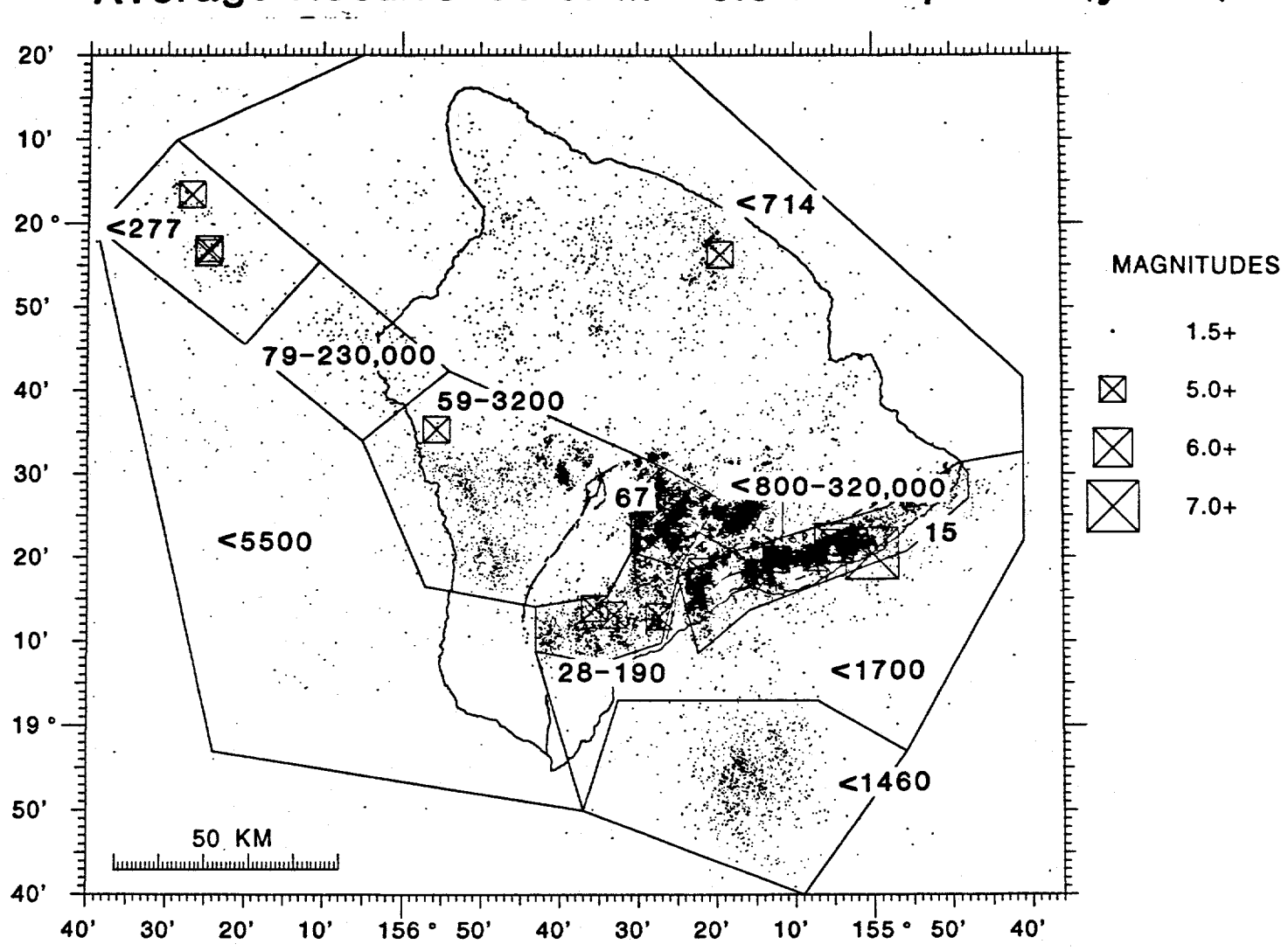

Figure 7. Average recurrence intervals in years for the crustal seismic source zones for M>6.5 earthquakes from table 2. If two numbers are given, the lower is derived from the historic earthquake catalog. The recurrence intervals are derived from the frequency-magnitude distribution, not from observed repetition of earthquakes. All intervals larger than 100 years are arbitrarily marked with a less than sign (<) because the earthquake catalog is much shorter than most recurrence intervals, and because large earthquakes may occur that are unanticipated by the catalog seismicity.

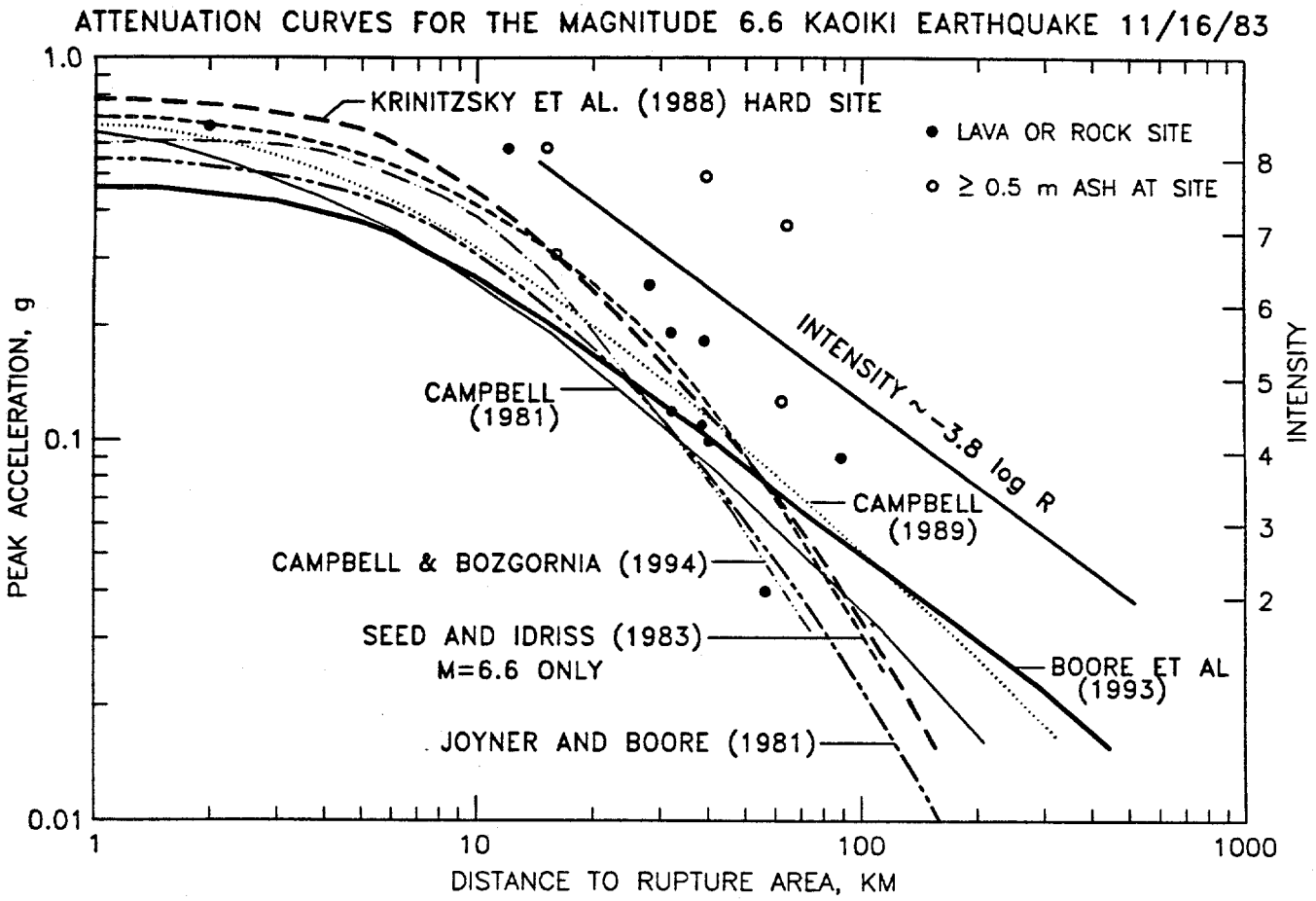

Figure 8. Peak ground acceleration (PGA) versus distance for the Nov. 16, 1983 M=6.6 Kaoiki earthquake. Solid dots are lava or rock sites and open dots are sites underlain by more than 0.5 m ash. The PGA values and ash thicknesses are from Buchanan-Banks (1987). Curves are for seven published attenuation relations for hard station sites. Campbell's curves are adjusted upward by 13% to compensate for our use of the maximum of the horizontal PGA components rather than the mean as assumed by Campbell (1989). This study uses the Boore et al. (1993, site class B) curve for the expected acceleration calculations after scaling it upward by a factor of 1.20. The intensity curve for this earthquake is scaled to PGA (Wyss and Koyanagi, 1992). The intensity curve decays as -3.8 log(R) and fits the larger PGAs of the ash sites better than the lava sites.

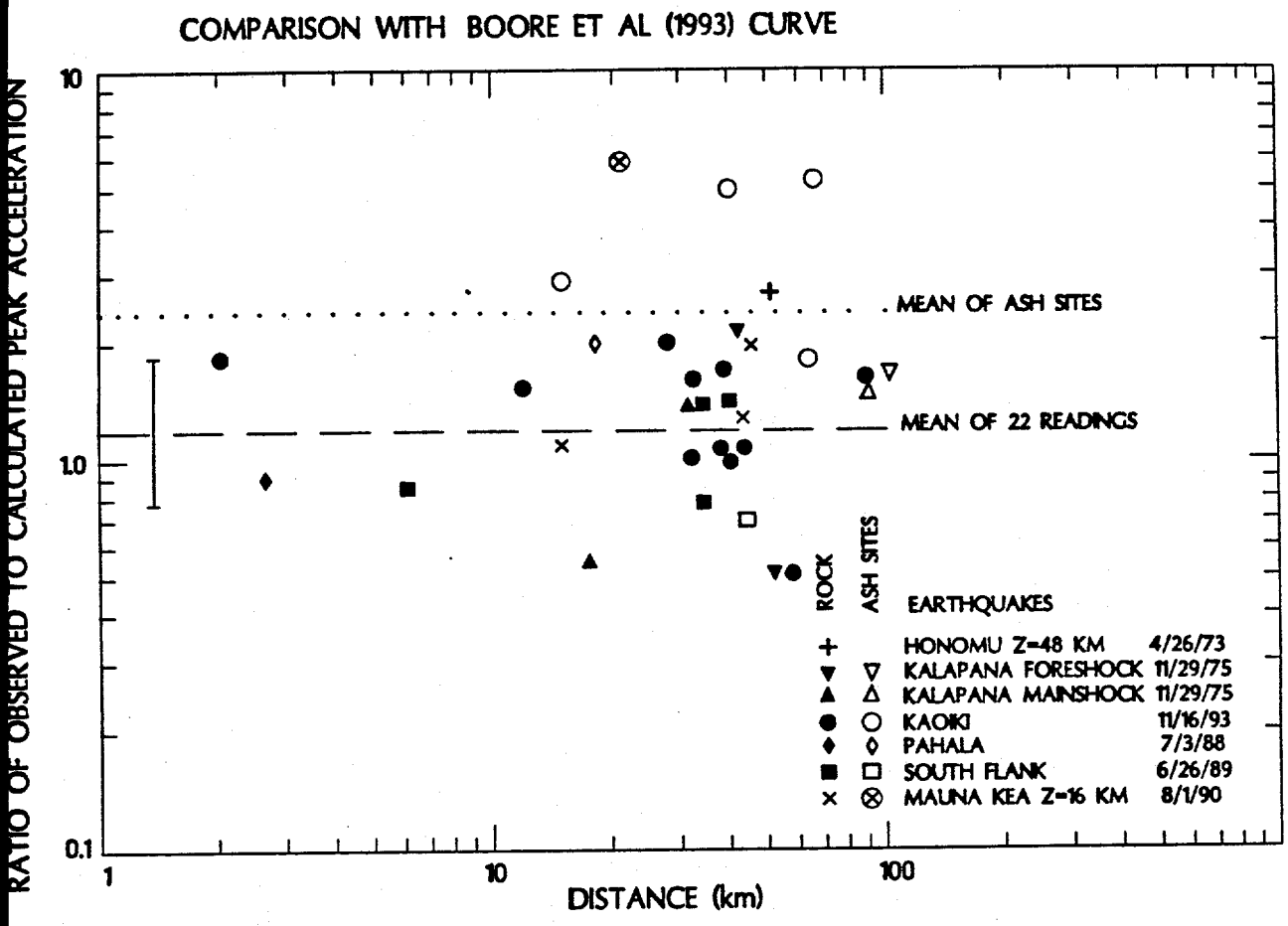

Figure 9a.

Figure 9. (a-f) Ratio of 33 observed peak ground accelerations (PGA) from 7 earthquakes to that calculated from six different attenuation relations. We seek the best fitting curve for lava or rock recording sites from crustal earthquake sources (solid and x symbols). This study uses the Boore et al. (1993, site class B) curve for the probabalistic PGA calculations for lava sites after scaling it upward by a factor of 1.20 (dashed line in figure a). The sites underlain by more than 0.5 m of ash (open symbols) are amplified by about 2.0 compared to lava sites (dotted line). The error bar indicates the mean and standard deviation of the log-ratios of the solid symbols. The standard deviation is 0.45 (natural log) or 57%. The distance dependence of other curves (b-f) do not fit the Hawaiian data, and the Campbell (1989) curve (e) does not apply to large magnitude earthquakes. (g) Ratio of PGAs to that calculated from the Boore et al. (1993) attenuation relation as a function of magnitude. The solid line is the mean of the rock sites from (a). The PGAs are from: Honomu earthquake: Nielsen et al. (1977); Kalapana foreshock and mainshock: Rojan and Morrill (1977); Kaoiki: Buchanan-Banks (1987); Pahala: Switzer and Porcella (1988); Kilauea south flank: Wyss and Koyanagi (1992) and Mauna Kea: Switzer and Porcella (1990).

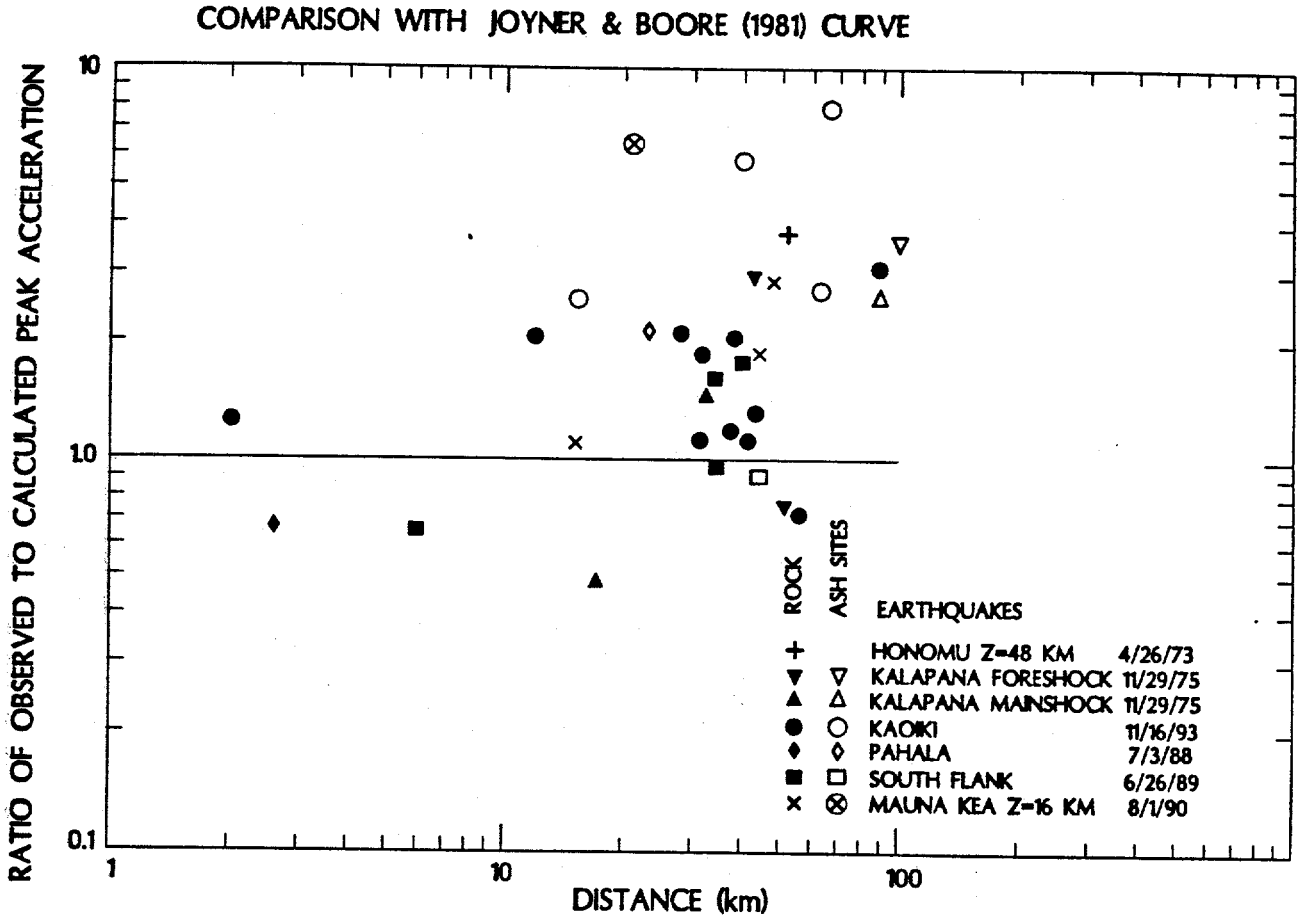
COMPARISON WITH JOYNER & BOORE (1981) CURVE
RATIO OF OBSERVED TO CALCULATED PEAK ACCELERATION
10
1.0
0.1
1
10
100
DISTANCE (km)
ROCK
ASH SITES
EARTHQUAKES
HONOMU Z=48 KM 4/26/73
KALAPANA FORESHOCK 11/29/75
KALAPANA MAINSHOCK 11/29/75
KAOIKI 11/16/93
PAHALA 7/3/88
SOUTH FLANK 6/26/89
MAUNA KEA Z=16 KM 8/1/90

Figure 9b.

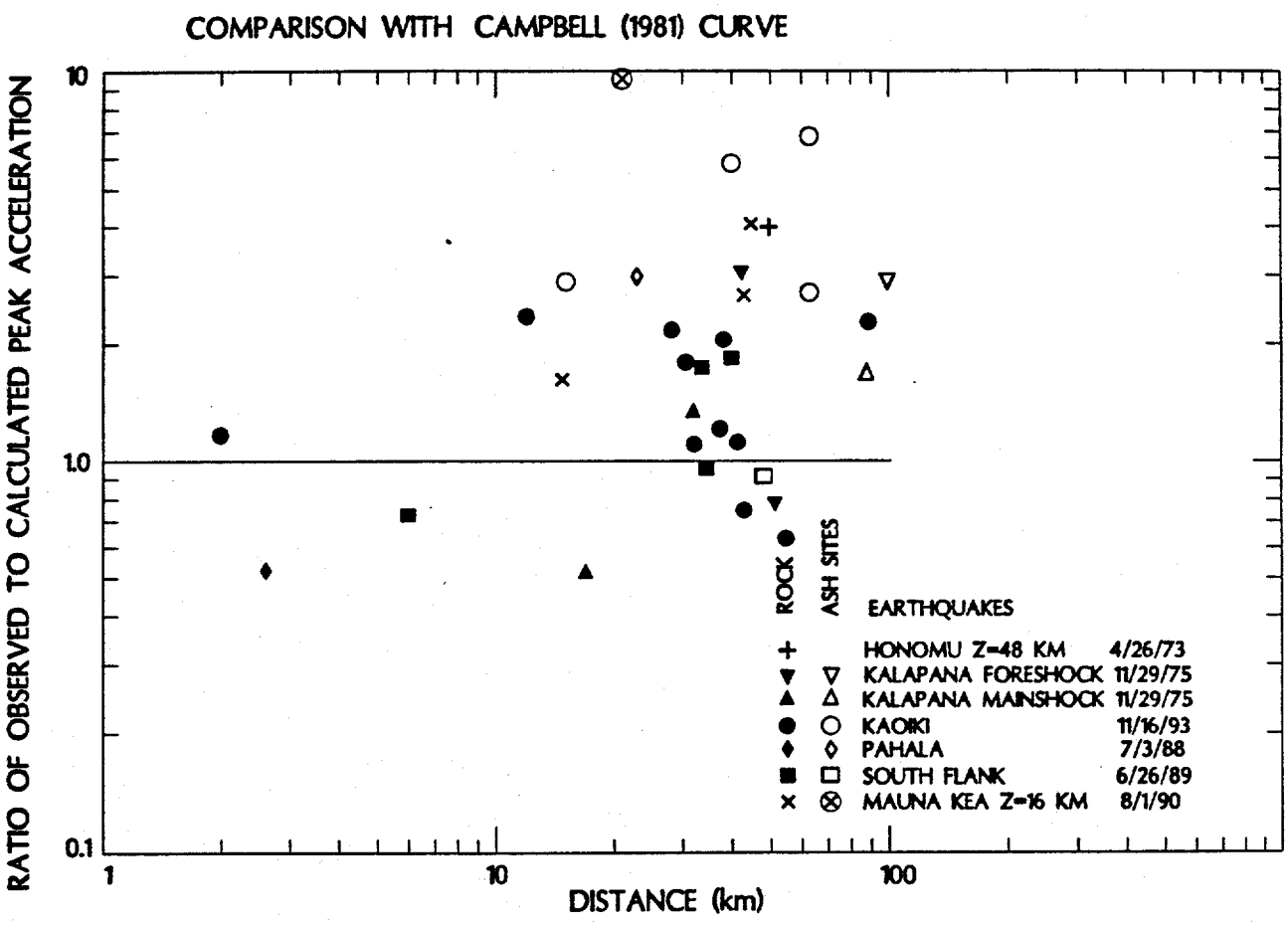
COMPARISON WITH CAMPBELL (1981) CURVE
RATIO OF OBSERVED TO CALCULATED PEAK ACCELERATION
10
1.0
0.1
1
10
100
DISTANCE (km)
ROCK
ASH SITES
EARTHQUAKES
HONOMU Z=48 KM 4/26/73
KALAPANA FORESHOCK 11/29/75
KALAPANA MAINSHOCK 11/29/75
KAOIKI 11/16/93
PAHALA 7/3/88
SOUTH FLANK 6/26/89
MAUNA KEA Z=16 KM 8/1/90

Figure 9c.

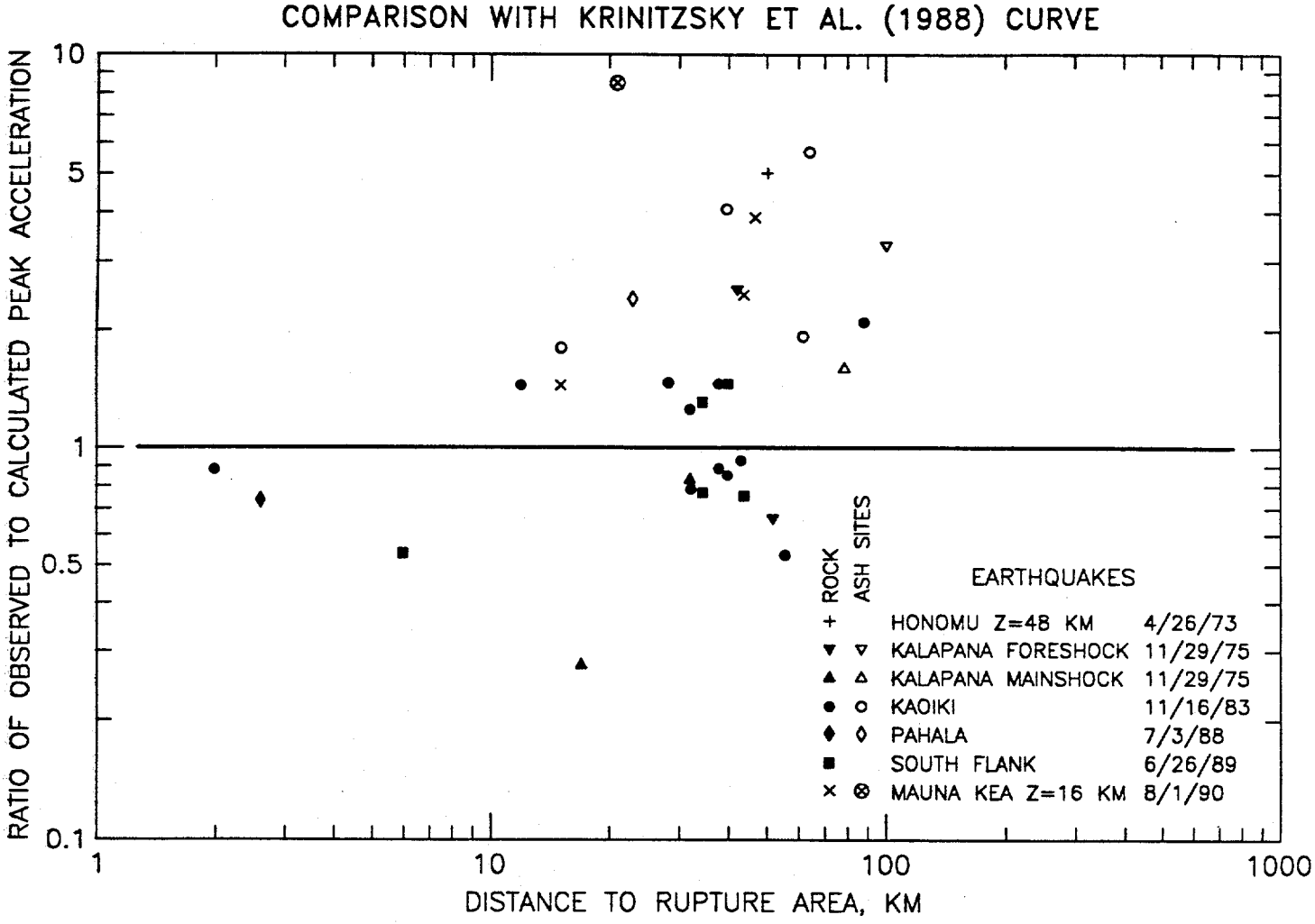
COMPARISON WITH KRINITZSKY ET AL. (1988) CURVE
RATIO OF OBSERVED TO CALCULATED PEAK ACCELERATION
10
5
1
0.5
0.1
1
10
100
1000
DISTANCE TO RUPTURE AREA, KM
+ ROCK
ASH SITES
EARTHQUAKES
+ HONOMU Z=48 KM 4/26/73
▼ ▽ KALAPANA FORESHOCK 11/29/75
▲ △ KALAPANA MAINSHOCK 11/29/75
● ○ KAOIKI 11/16/83
♦ ◇ PAHALA 7/3/88
■ SOUTH FLANK 6/26/89
× ⊗ MAUNA KEA Z=16 KM 8/1/90

Figure 9d.

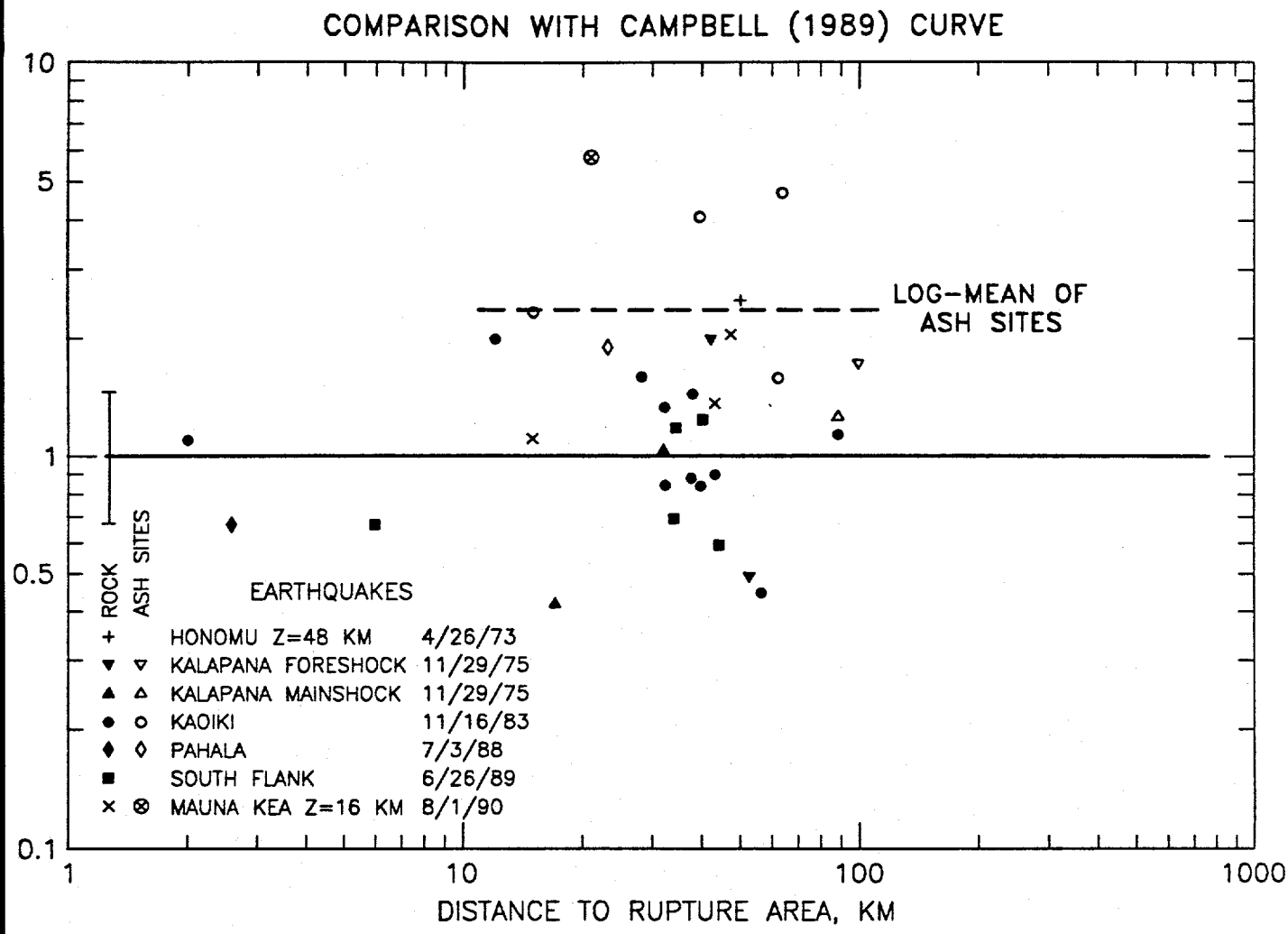
COMPARISON WITH CAMPBELL (1989) CURVE
10
5
1
0.5
0.1
1
10
100
1000
DISTANCE TO RUPTURE AREA, KM
LOG-MEAN OF ASH SITES
ROCK
ASH SITES
EARTHQUAKES
HONOMU Z=48 KM 4/26/73
KALAPANA FORESHOCK 11/29/75
KALAPANA MAINSHOCK 11/29/75
KAOIKI 11/16/83
PAHALA 7/3/88
SOUTH FLANK 6/26/89
MAUNA KEA Z=16 KM 8/1/90

Figure 9e.

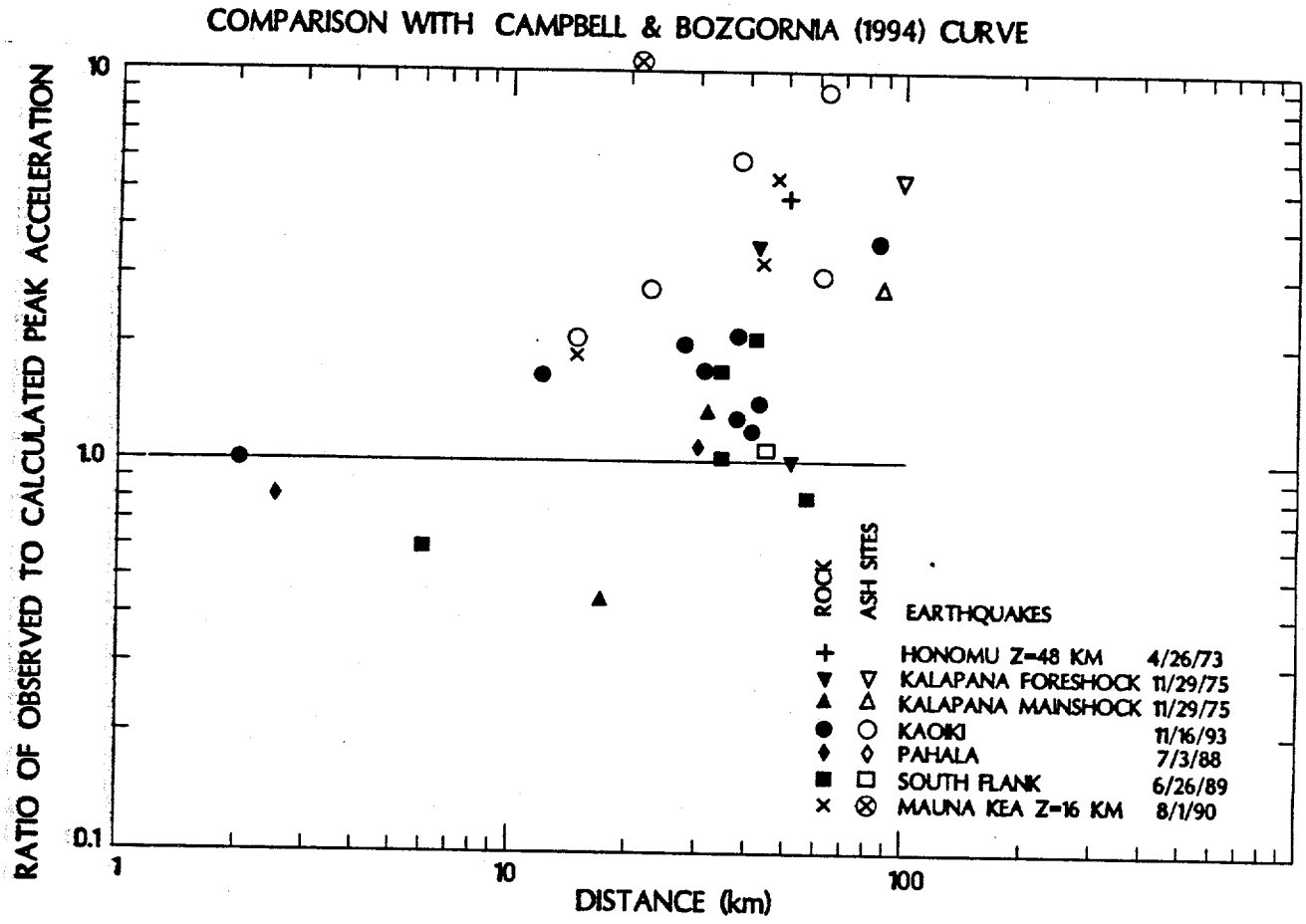
COMPARISON WITH CAMPBELL & BOZGORNIA (1994) CURVE
RATIO OF OBSERVED TO CALCULATED PEAK ACCELERATION
10
1.0
0.1
1
10
100
DISTANCE (km)
ROCK
ASH SITES
EARTHQUAKES
HONOMU Z=48 KM 4/26/73
KALAPANA FORESHOCK 11/29/75
KALAPANA MAINSHOCK 11/29/75
KAOIKI 11/16/93
PAHALA 7/3/88
SOUTH FLANK 6/26/89
MAUNA KEA Z=16 KM 8/1/90

Figure 9f.

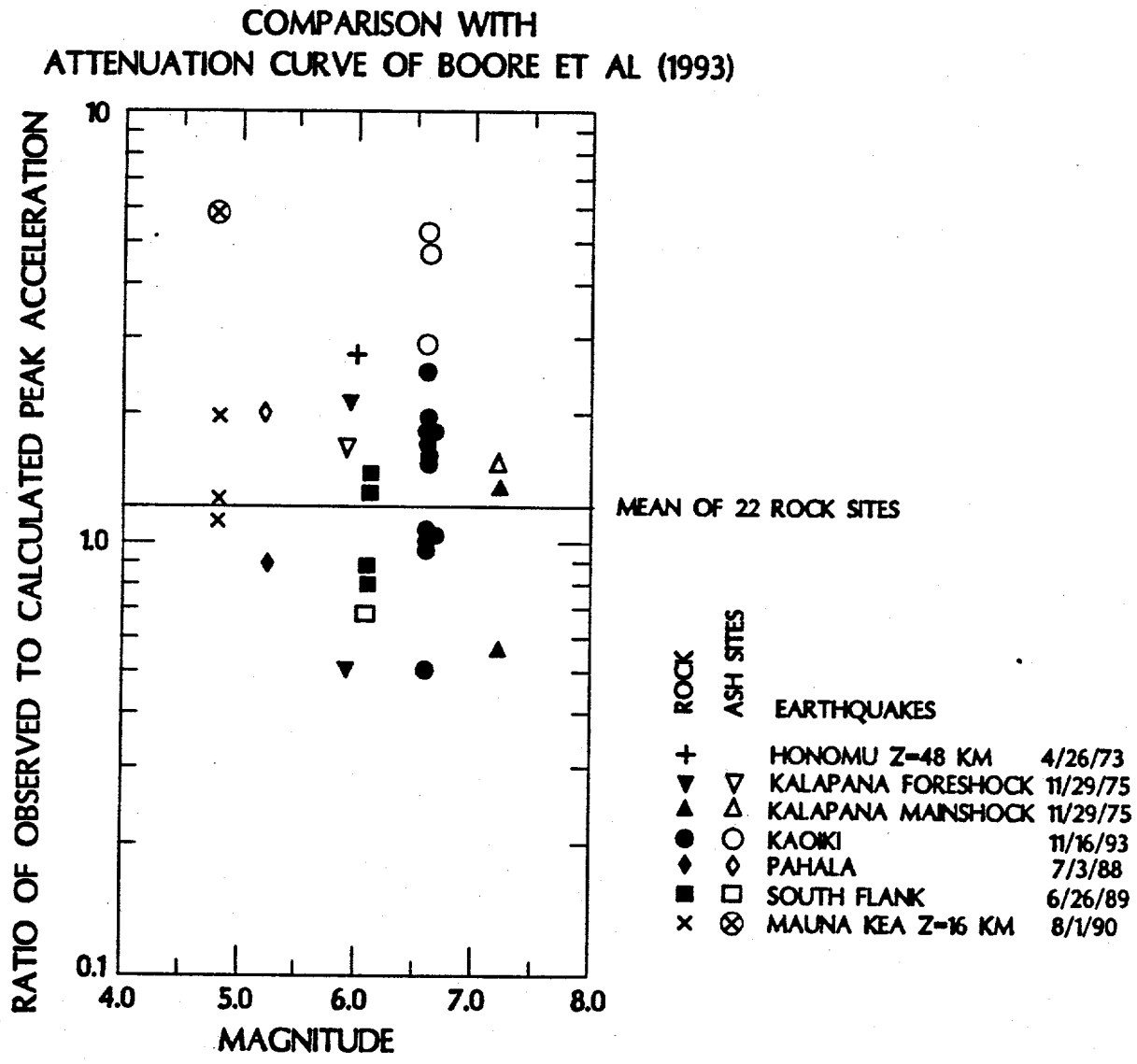

Figure 9g. Ratio of 33 observed peak ground accelerations (PGA) from 7 earthquakes to that calculated from the Boore et al. (1993) attenuation relation as a function of magnitude. The solid line is the mean of the rock sites from (9a). We seek the best fitting curve for lava or rock recording sites from crustal earthquake sources (solid and x symbols). This study uses the Boore et al. (1993, site class B) curve for the probabalistic PGA calculations for lava sites after scaling it upward by a factor of 1.20.

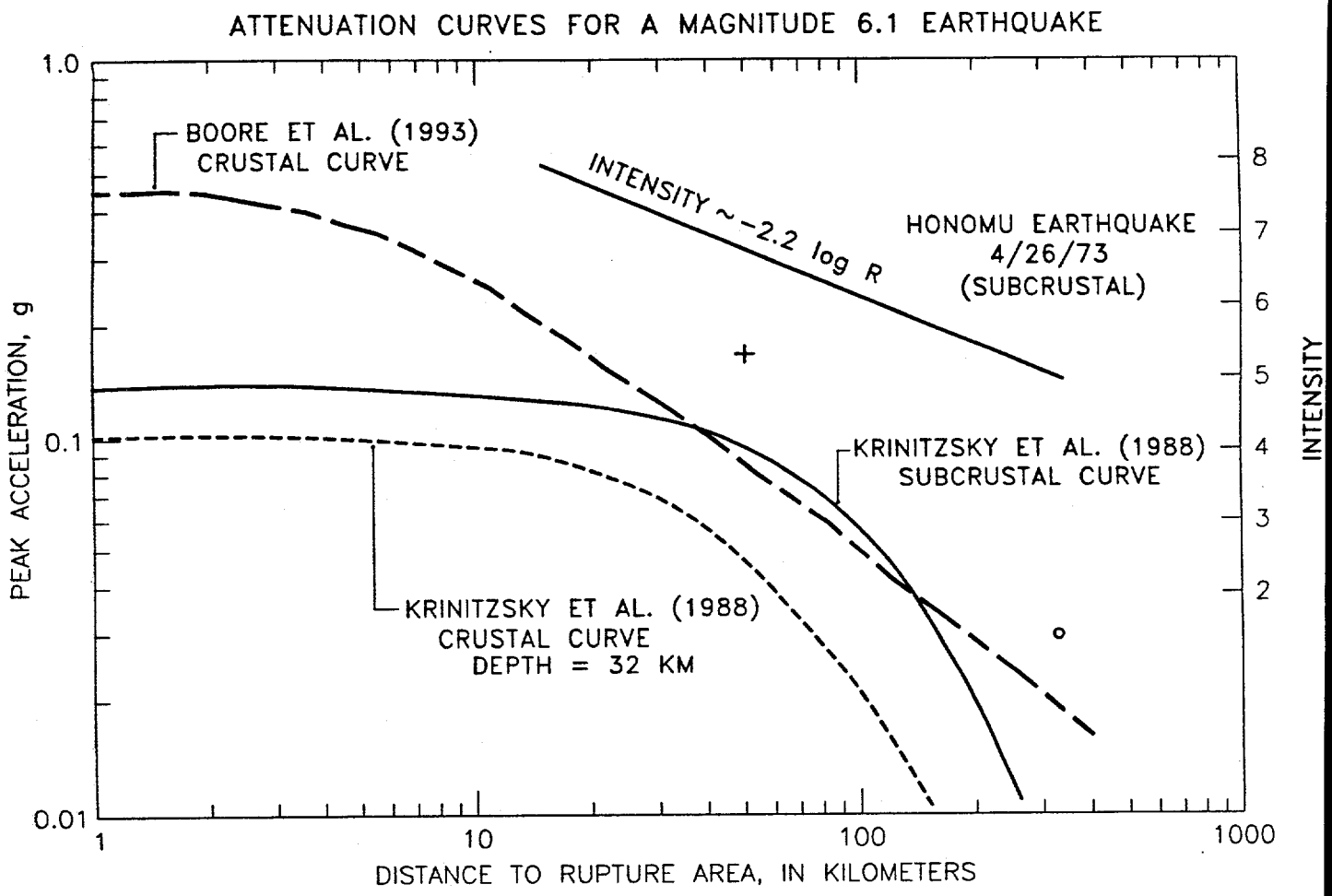

Figure 10. Peak ground acceleration (PGA) versus distance for the April 26, 1973 M=6.1 Honomu earthquake. The one observation from Hawaii island (+ plus symbol) is from the Namakani campground on Kilauea Volcano. The accelerogram recorded on Oahu (open circle) is too far away to be considered in the selection of an attenuation curve. The Krinitzsky et al. (1988) subcrustal curve (solid line) and crustal curve with a 32 km source depth (short dashes) are possible relations for upper mantle Hawaiian earthquakes. The Boore et al. (1993) crustal curve (long dashes) is shown for comparison. In this paper, the calculations of probabilistic PGA from deep earthquakes use the subcrustal curve (see text). The intensity curve is scaled to PGA (Wyss and Koyanagi, 1992). The intensity curve decays as -2.2 log(R) and falls off more slowly than the intensity of the crustal Kaoiki earthquake (figure 8).

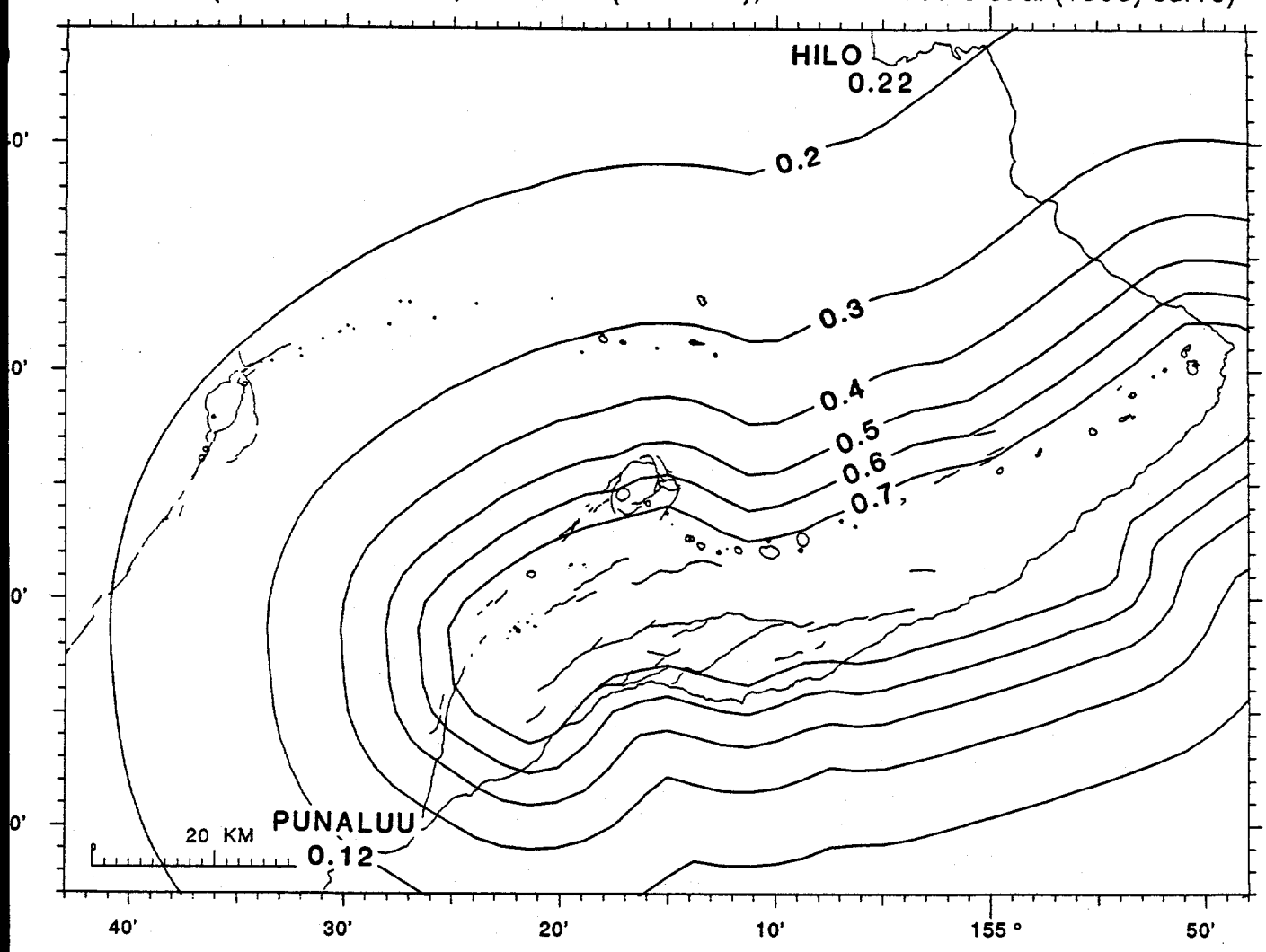

Figure 11a. Calculated peak ground accelerations (PGA) in g from the M=7.2 1975 Kalapana earthquake. Contour interval is 0.1 g (solid lines). Calculated PGAs are for lava or rock sites. The observed PGAs are also shown: the stations underlain by more than 0.5 m of ash are in parentheses and generally experience site amplification. PGAs are calculated from the Boore et al. (1993) attenuation curve. Sources for the crustal earthquakes are assumed uniform over the area of the aftershock zone.

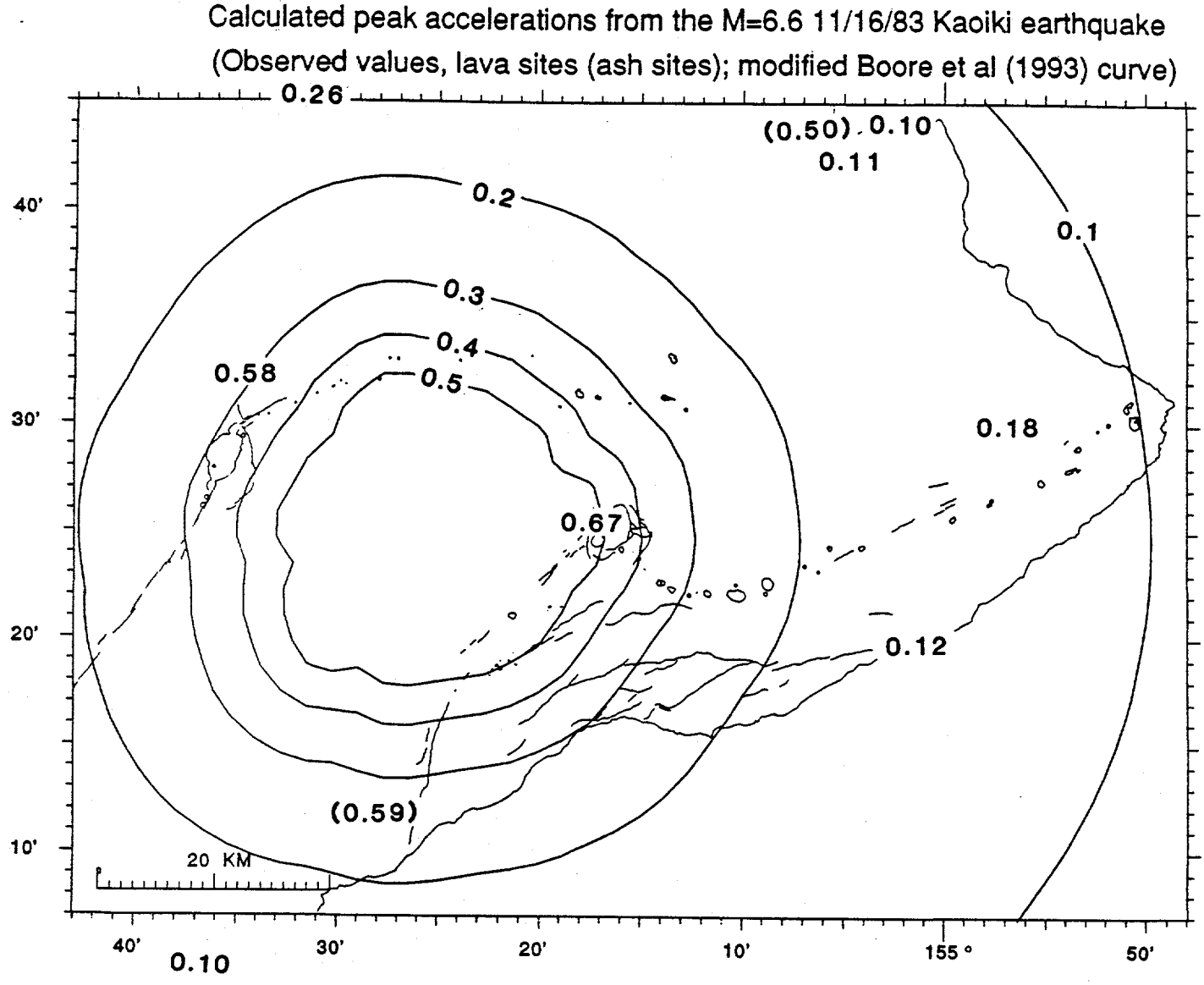

Figure 11b. Calculated peak ground accelerations (PGA) in g from the M=6.6 1983 Kaoiki earthquake. Contour interval is 0.1 g (solid lines). Calculated PGAs are for lava or rock sites. The observed PGAs are also shown: the stations underlain by more than 0.5 m of ash are in parentheses and generally experience site amplification. PGAs are calculated from the Boore et al. (1993) attenuation curve. Sources for the crustal earthquakes are assumed uniform over the area of the aftershock zone.

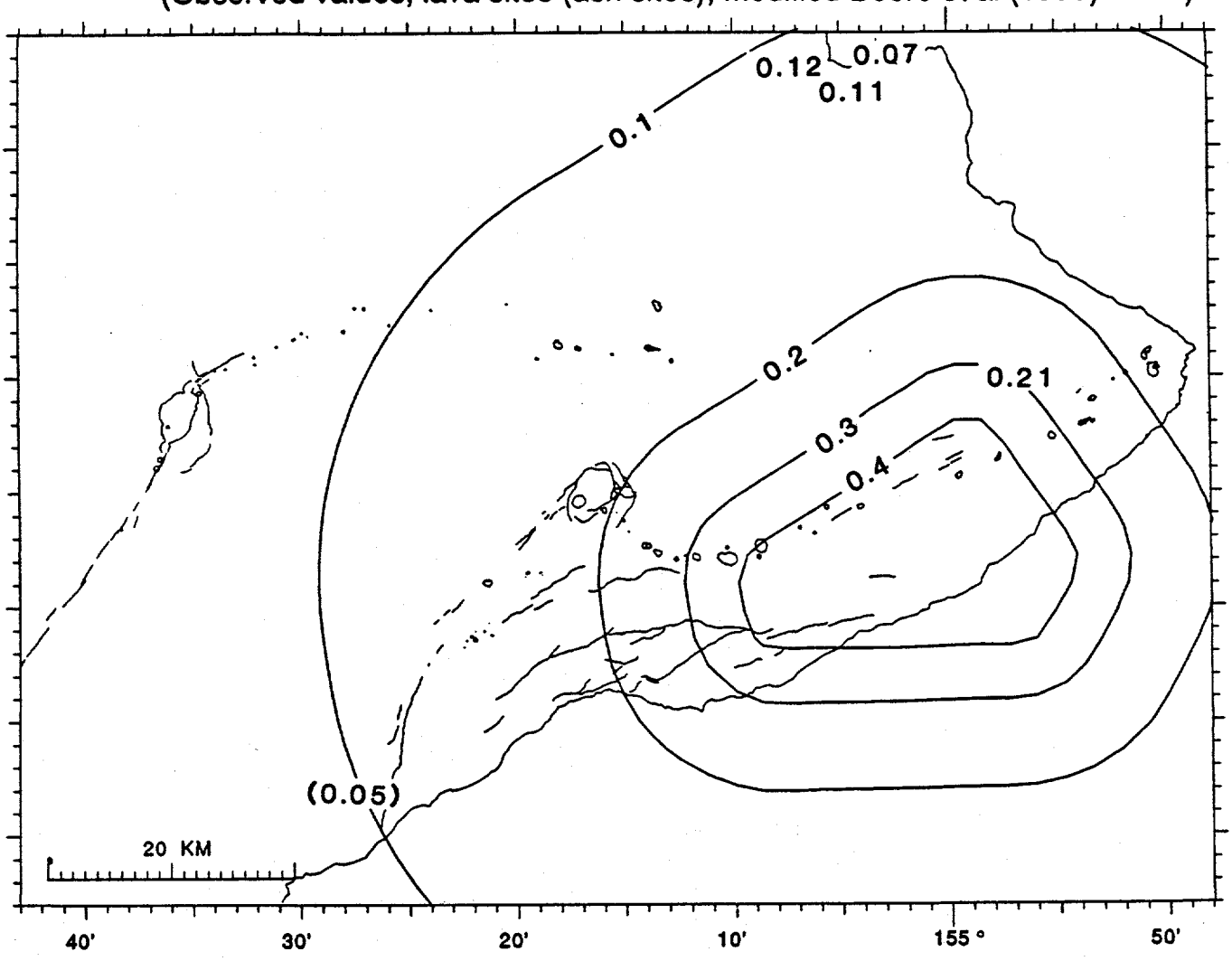

Figure 11c. Calculated peak ground accelerations (PGA) in g from the 1989 M=6.1 Kilauea south flank earthquake. Contour interval is 0.1 g (solid lines). Calculated PGAs are for lava or rock sites. The observed PGAs are also shown: the stations underlain by more than 0.5 m of ash are in parentheses and generally experience site amplification. PGAs are calculated from the Boore et al. (1993) attenuation curve. Sources for the crustal earthquakes are assumed uniform over the area of the aftershock zone.

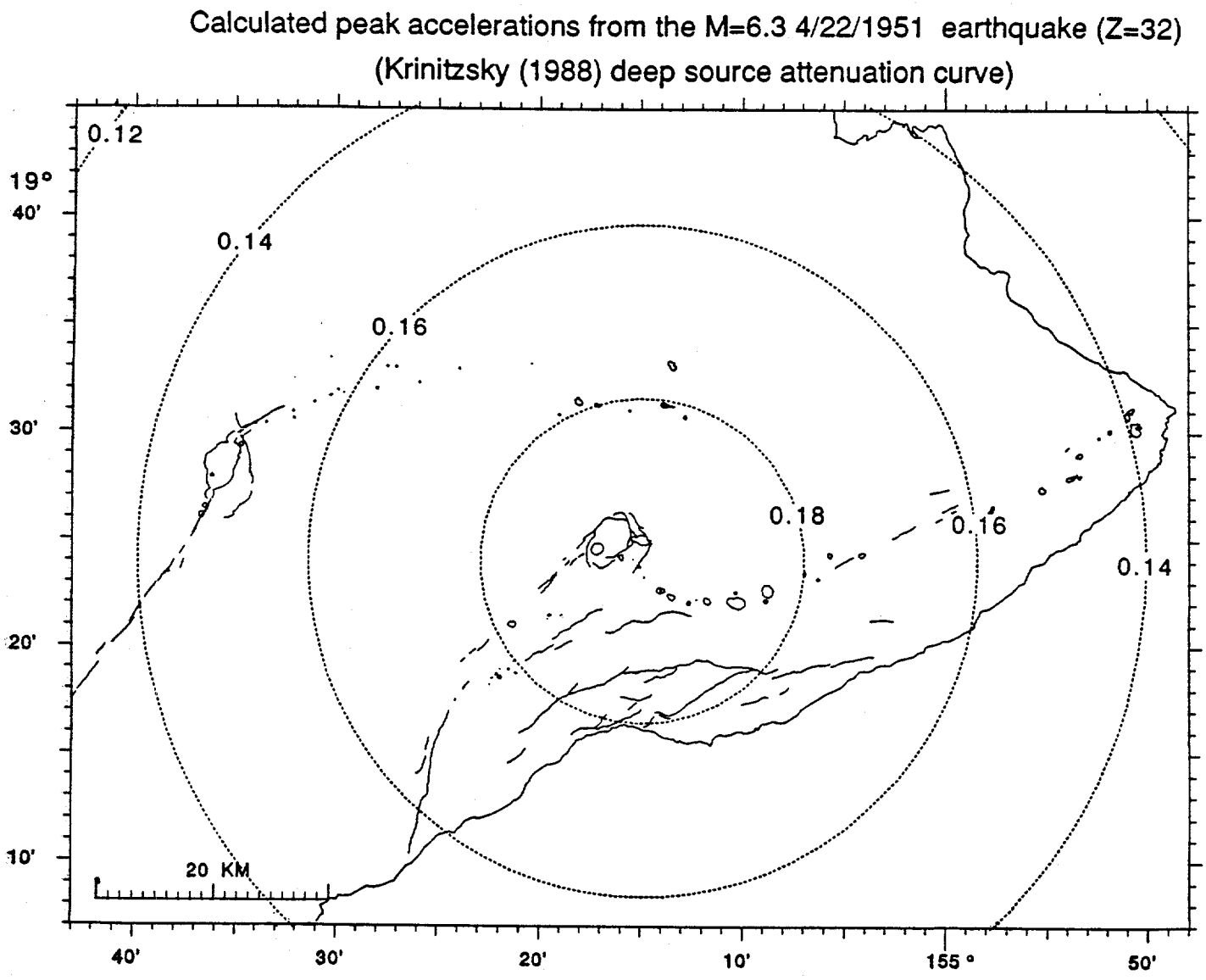

Figure 11d. Calculated peak ground accelerations (PGA) in g from the M=6.3 1951 deep (Z=32 km) Kilauea earthquake. Contour interval is 0.1 g (solid lines) or 0.02 g (dashed lines). Calculated PGAs are for lava or rock sites. The observed PGAs are also shown: the stations underlain by more than 0.5 m of ash are in parentheses and generally experience site amplification. PGAs are calculated from the Krinitzsky et al. (1988) subcrustal curve. PGAs assume a point source for the earthquake.

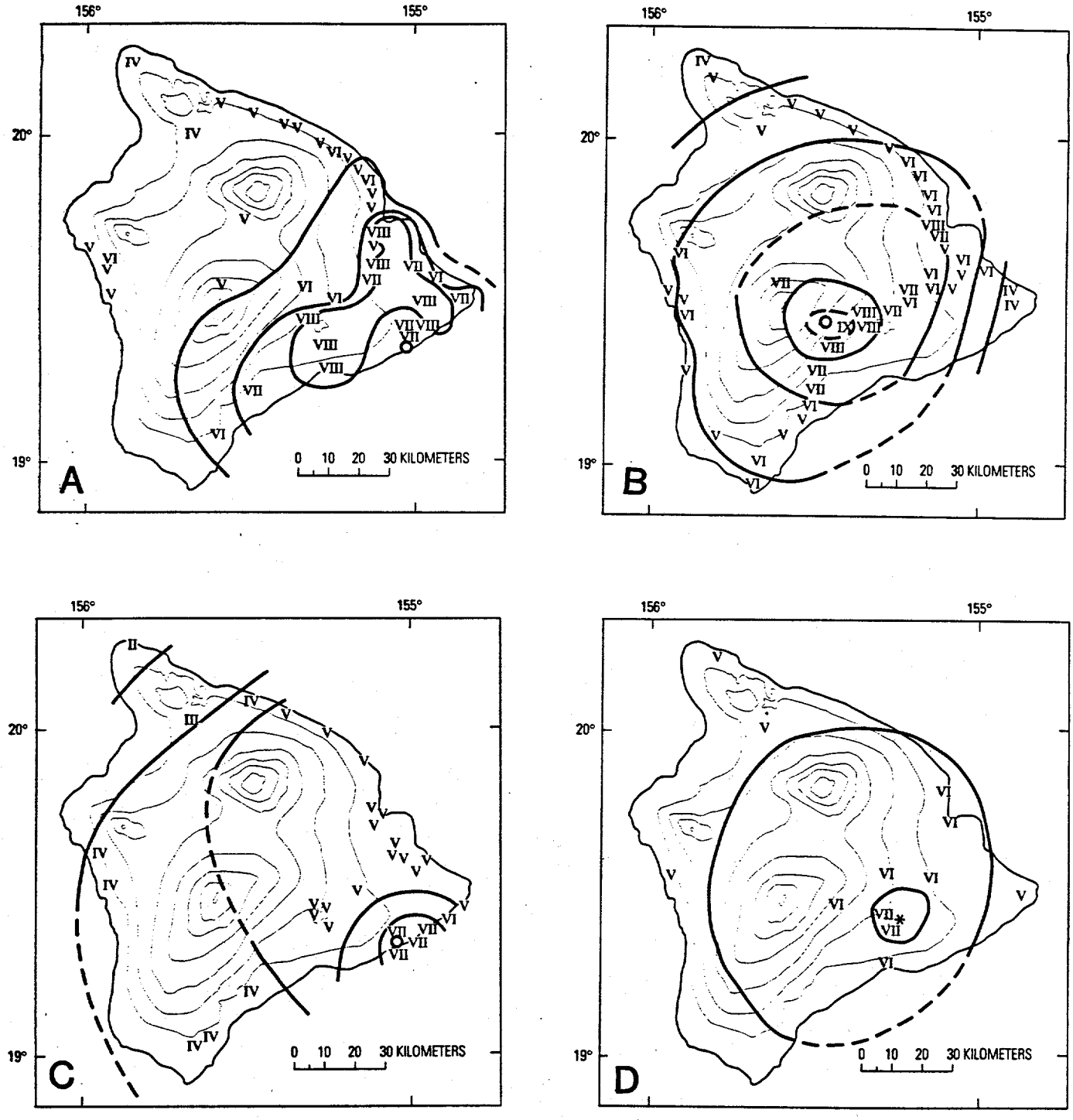

Figure 12. Isoseismal maps of intensities from the four earthquakes of figure 11. (a) M=7.2 1975 Kalapana earthquake, (b) M=6.6 1983 Kaoiki earthquake, (c) M=6.1 Kilauea south flank earthquake, and (d) M=6.3 1951 deep (Z=32 km) Kilauea earthquake. From Wyss and Koyanagi (1992).

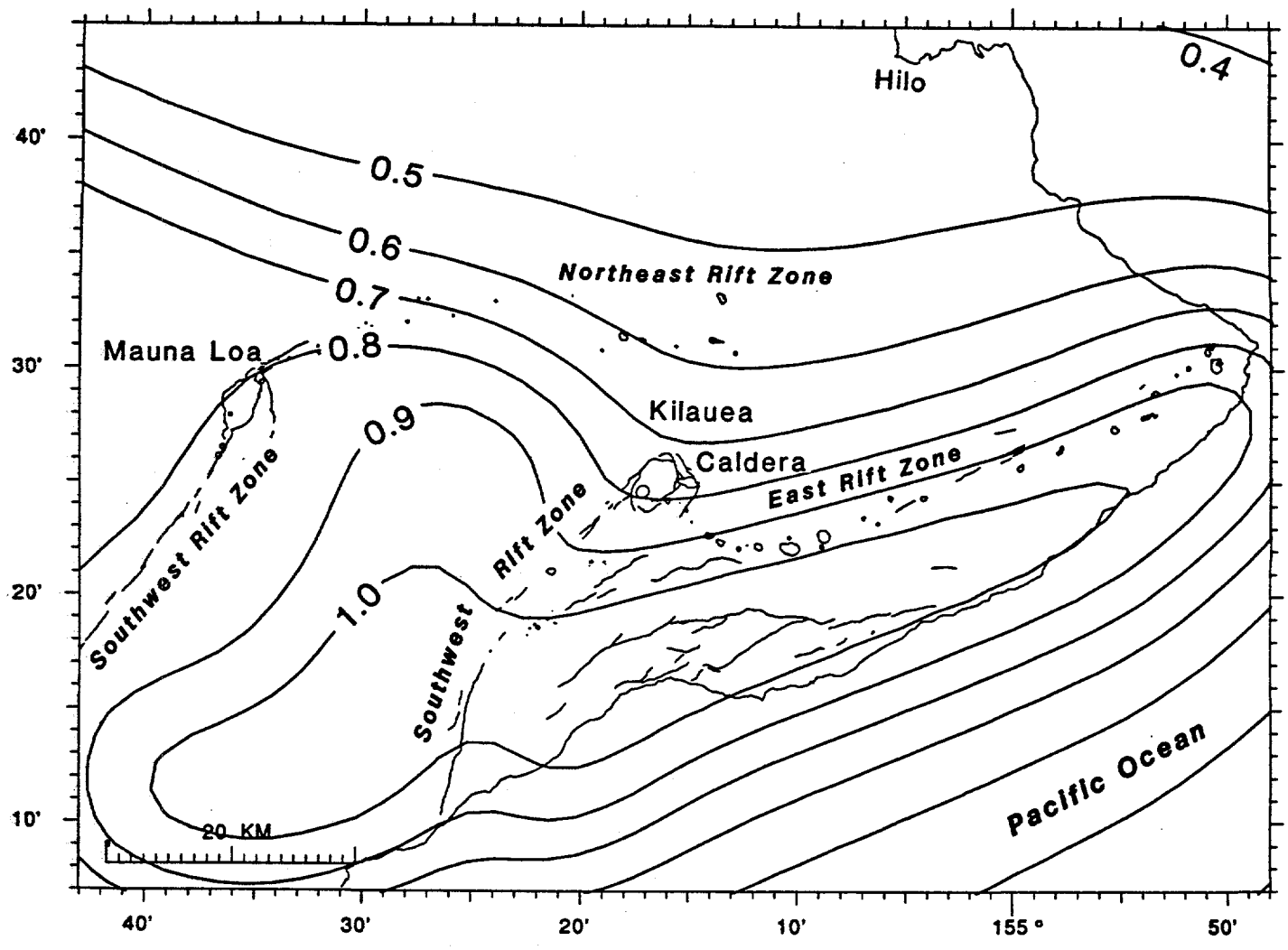

Figure 13. Peak ground acceleration (PGA) in g that has a 90% probability of not being exceeded during an exposure time of 50 years. Values are based on the earthquake frequency-magnitude parameters and maximum magnitudes listed in tables 2 and 3 for each seismic source zone. PGAs were calculated by the SeisriskIII program using the Boore et al. (1993) attenuation curve and 0.45 for the standard deviation of the natural log of PGA residuals. The expected PGAs are for lava or rock sites. Locations with more than 0.5 m of ash should expect roughly twice these PGAs.

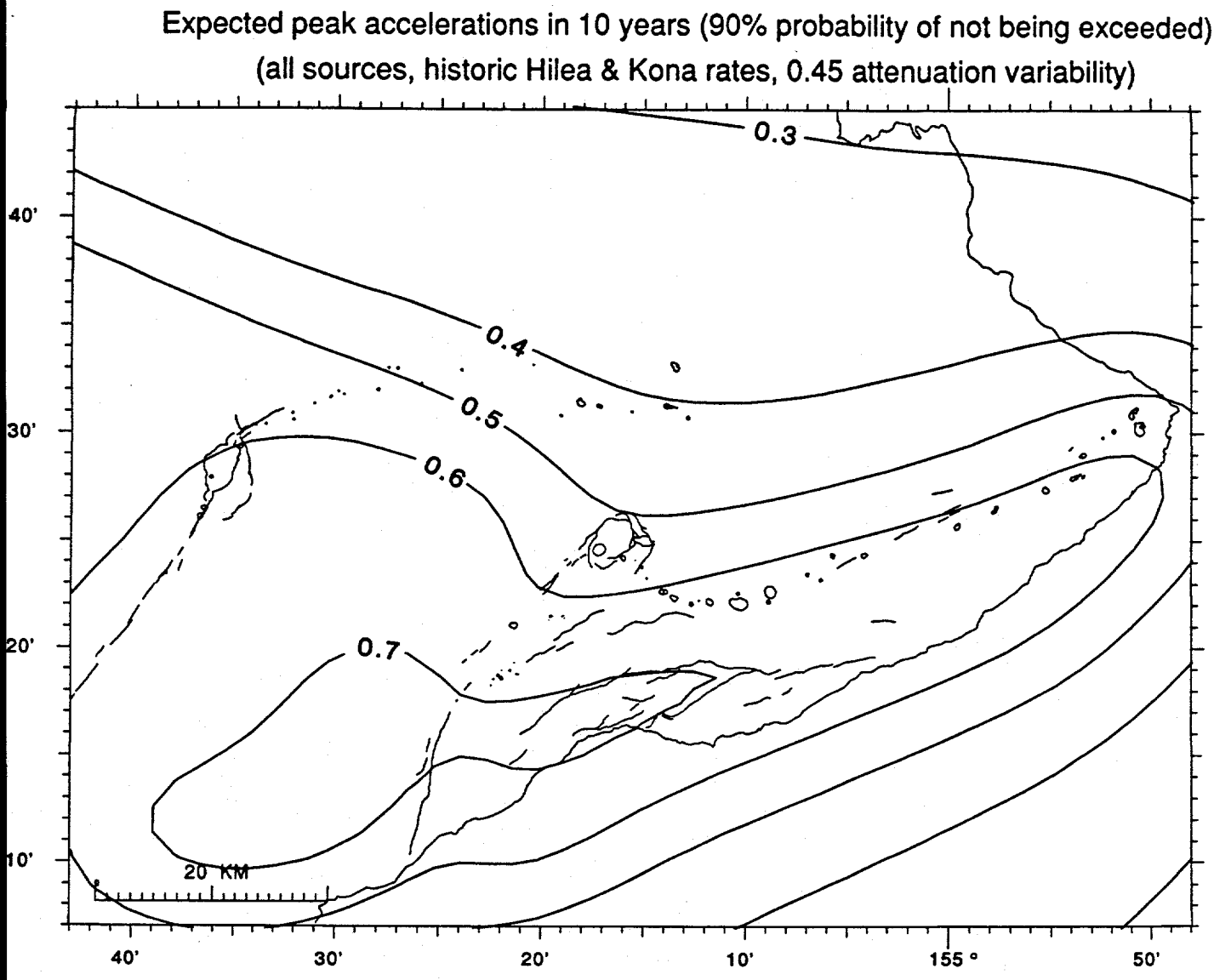

Figure 14a. Peak ground acceleration that has a 90% probability of not being exceeded during a 10 year exposure time. All other assumptions are the same as figure 13.

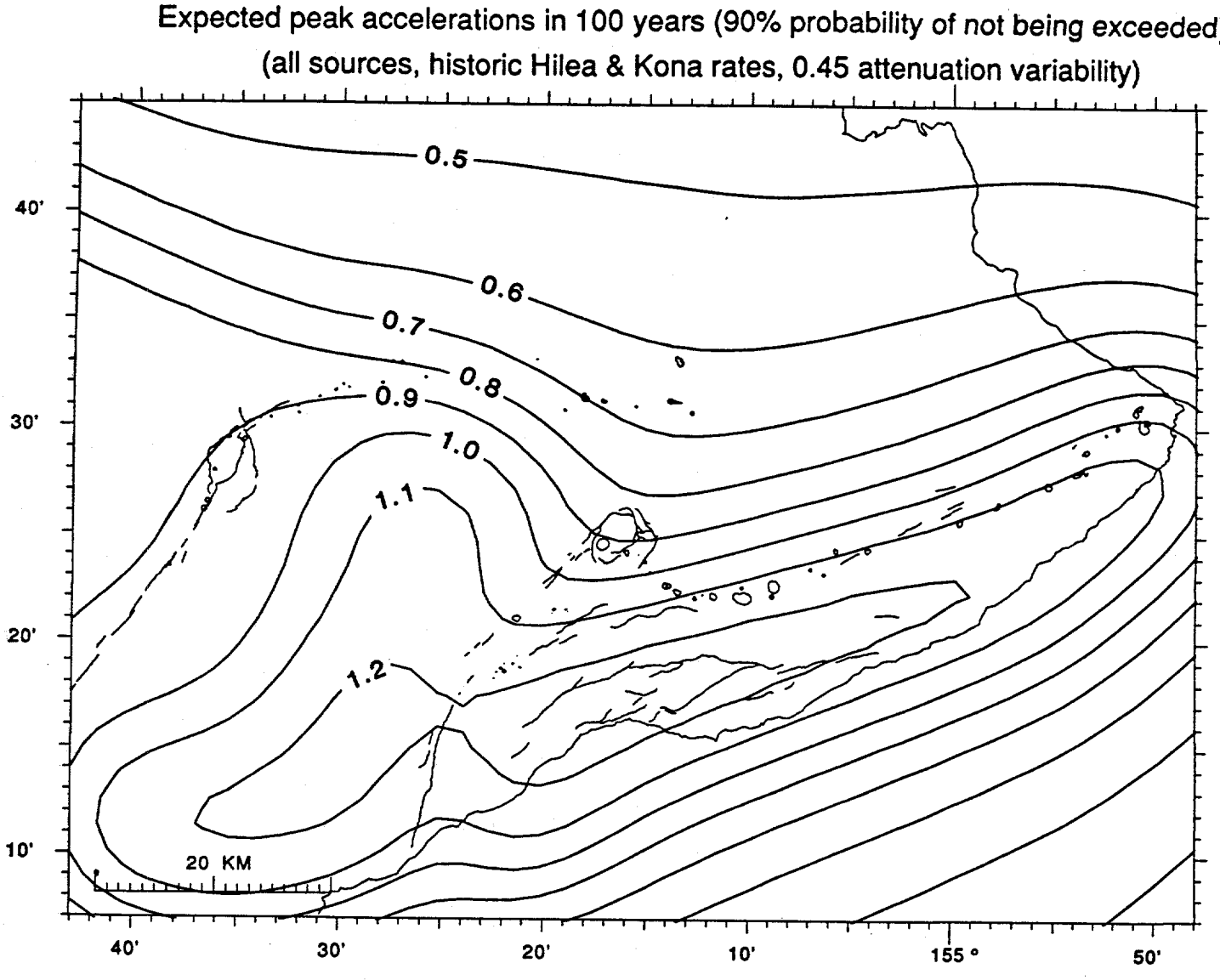

Figure 14b. Peak ground acceleration that has a 90% probability of not being exceeded during a 100 year exposure time. All other assumptions are the same as figure 13.

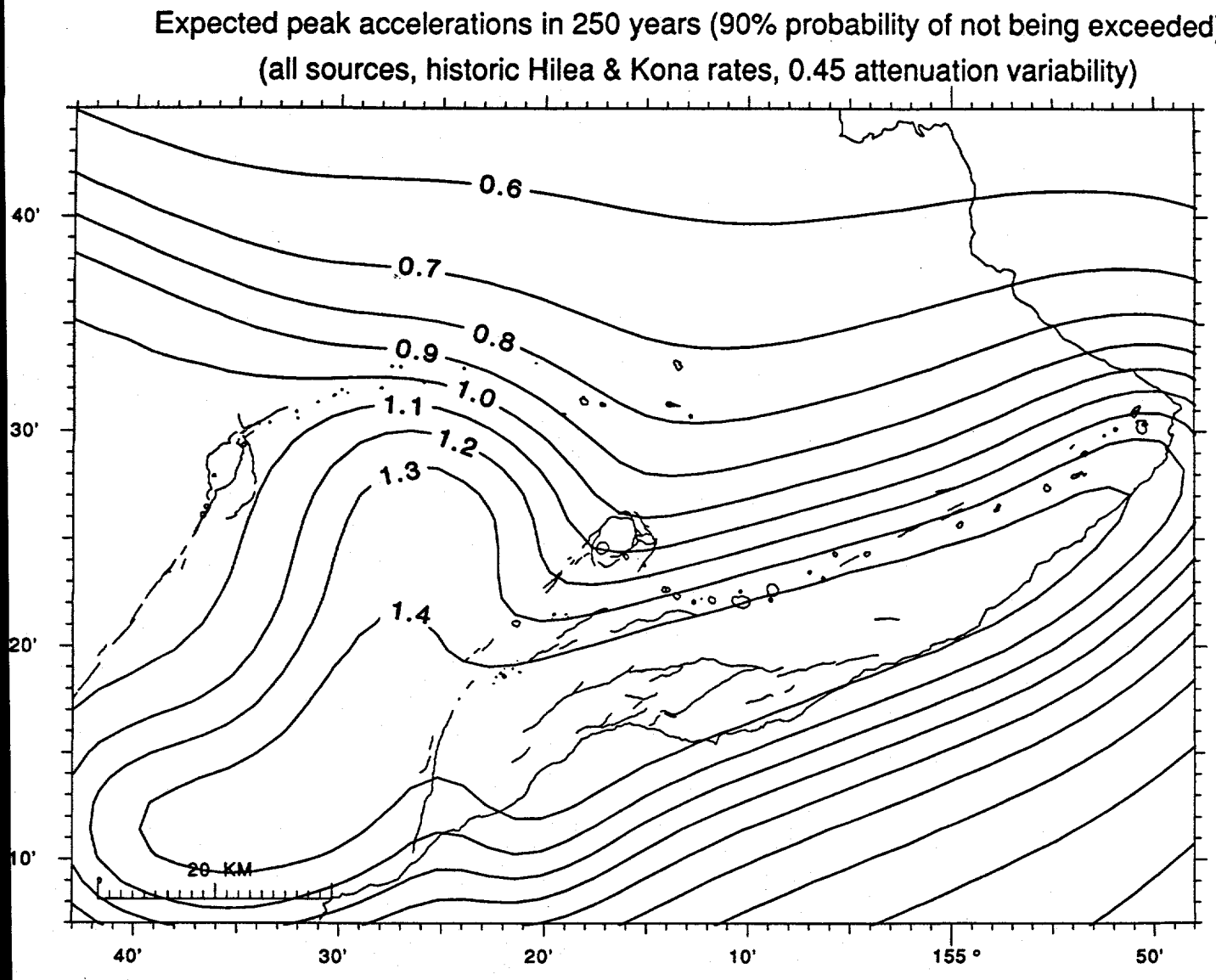

Figure 14c. Peak ground acceleration that has a 90% probability of not being exceeded during a 250 year exposure time. All other assumptions are the same as figure 13.

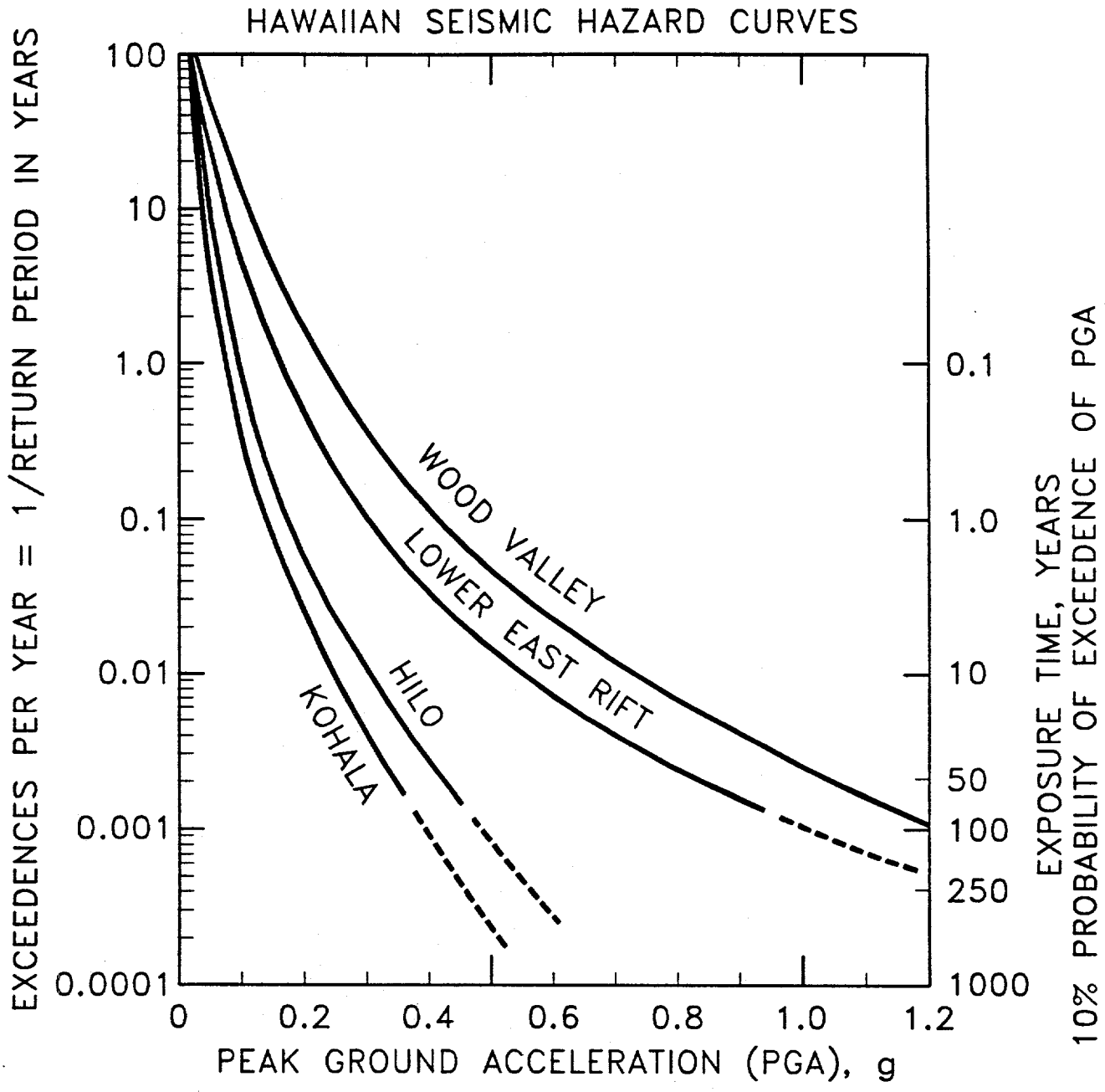

Figure 15. Seismic hazard curves for four locations on the island of Hawaii. These curves estimate the probable peak ground acceleration (PGA) for exposure times other than those mapped in figures 13 and 14. The exceedences per year is the probable number of times a given level of PGA or larger will occur. The return period is the reciprocal of the exceedences per year. The exposure time is proportional to the return period, but depends on the level of probability at which the PGA is not to be exceeded. The exposure times indicated assume a 90% probability of the PGA level not being exceeded. The exposure time is the natural log of the non-exceedence probability [-ln(0.9) = 0.1054] times the return period. The exposure time equals the return period when the probability of the PGA not being exceeded is 37%. The locations of the four sites are: Wood Valley in the center of the Hilea Seismic Zone at 19° 16' N, 155° 30' W; Lower East Rift at Kaniuhiku Village at 19° 30', 154° 55'; Hilo at 19° 43', 155° 5'; and Kohala at the north tip of the island at 20° 14', 155° 52'. For an exposure time of 50 years, the entire island of Hawaii has a probable PGA of greater than 0.3 g.

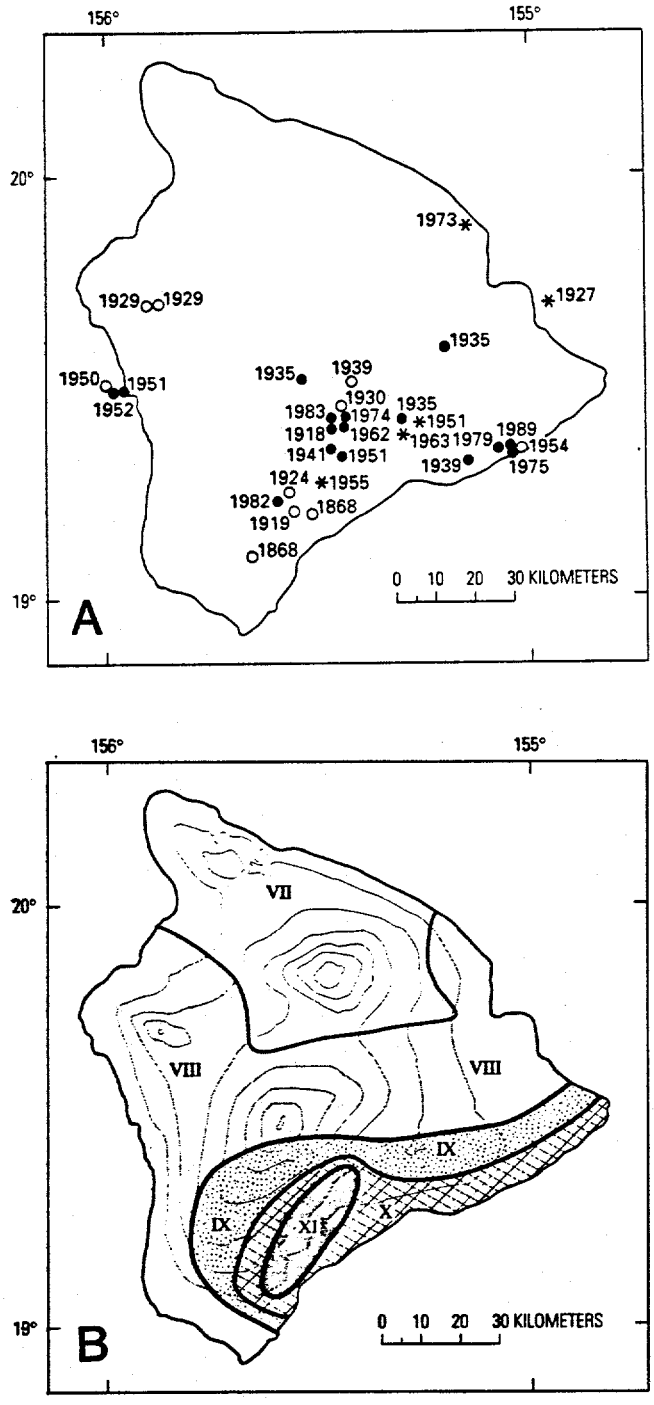

Figure 16. Historic earthquake data pertaining to seismic hazard. (A) epicenters of larger events for which isoseismal maps are available. (B) Maximum historic intensity from all earthquakes with isoseismal maps. The intensity pattern is mostly controlled by the M=7.9 great Kau earthquake of April 2, 1868. From Wyss and Koyanagi (1992).

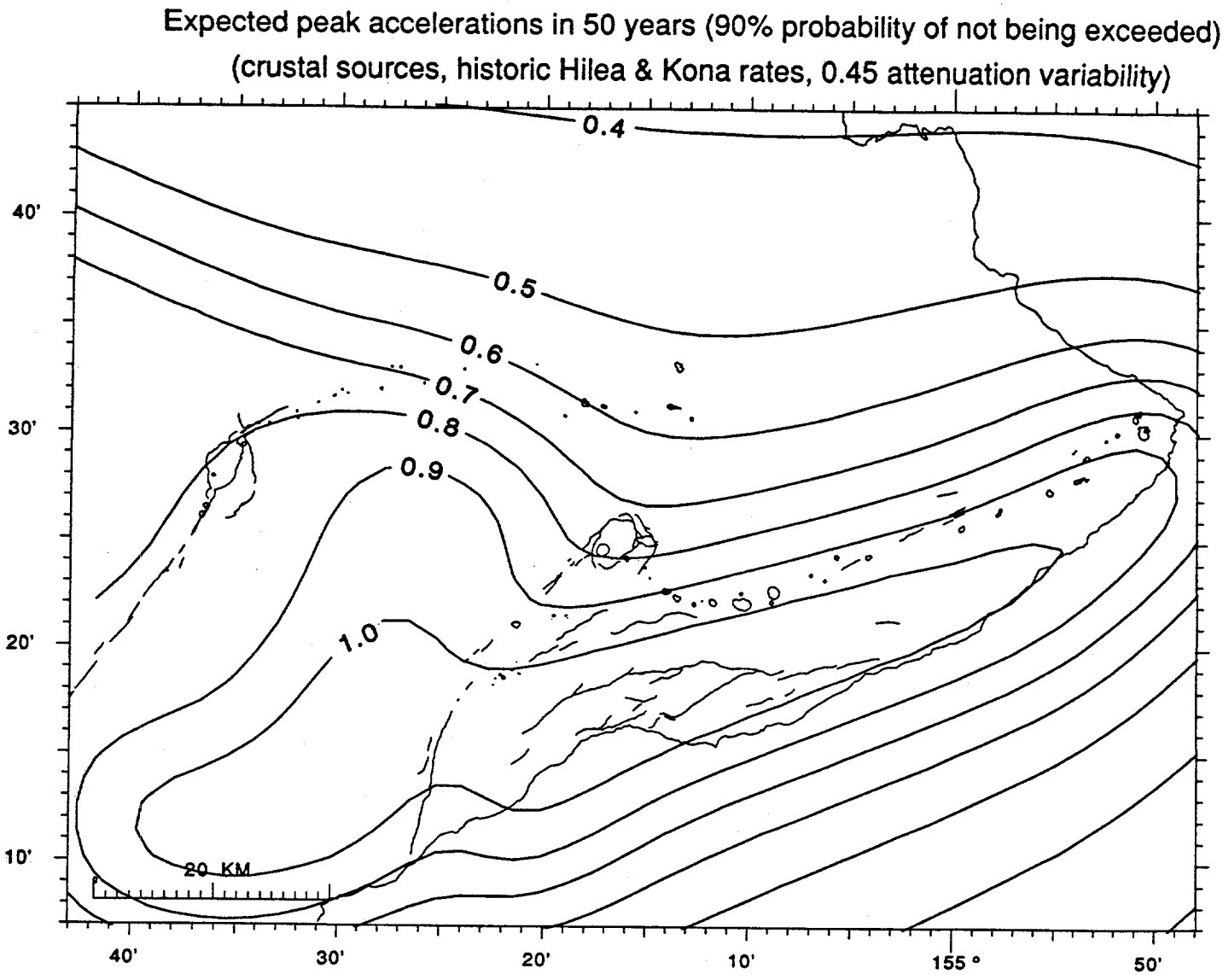

Figure A1a. Contributions from all crustal seismic source regions 1-11 to the probablistic peak ground accelerations (PGA) of figure 13. All figures in appendix 1 show PGAs with a 90% probability of not being exceeded in a 50 year exposure time. The earthquake rates for regions 1 and 2 are from 1970-1992 adjusted for the higher rate of M>5.5 events, and the rates for regions 3, 7 and 8 are derived from historic earthquakes (table 3, bottom part). All figures have contour intervals of 0.1 (solid lines) and 0.02 (dashed lines). Figures A2-A8 make different rate and parameter assumptions and should be compared with figure A1a.

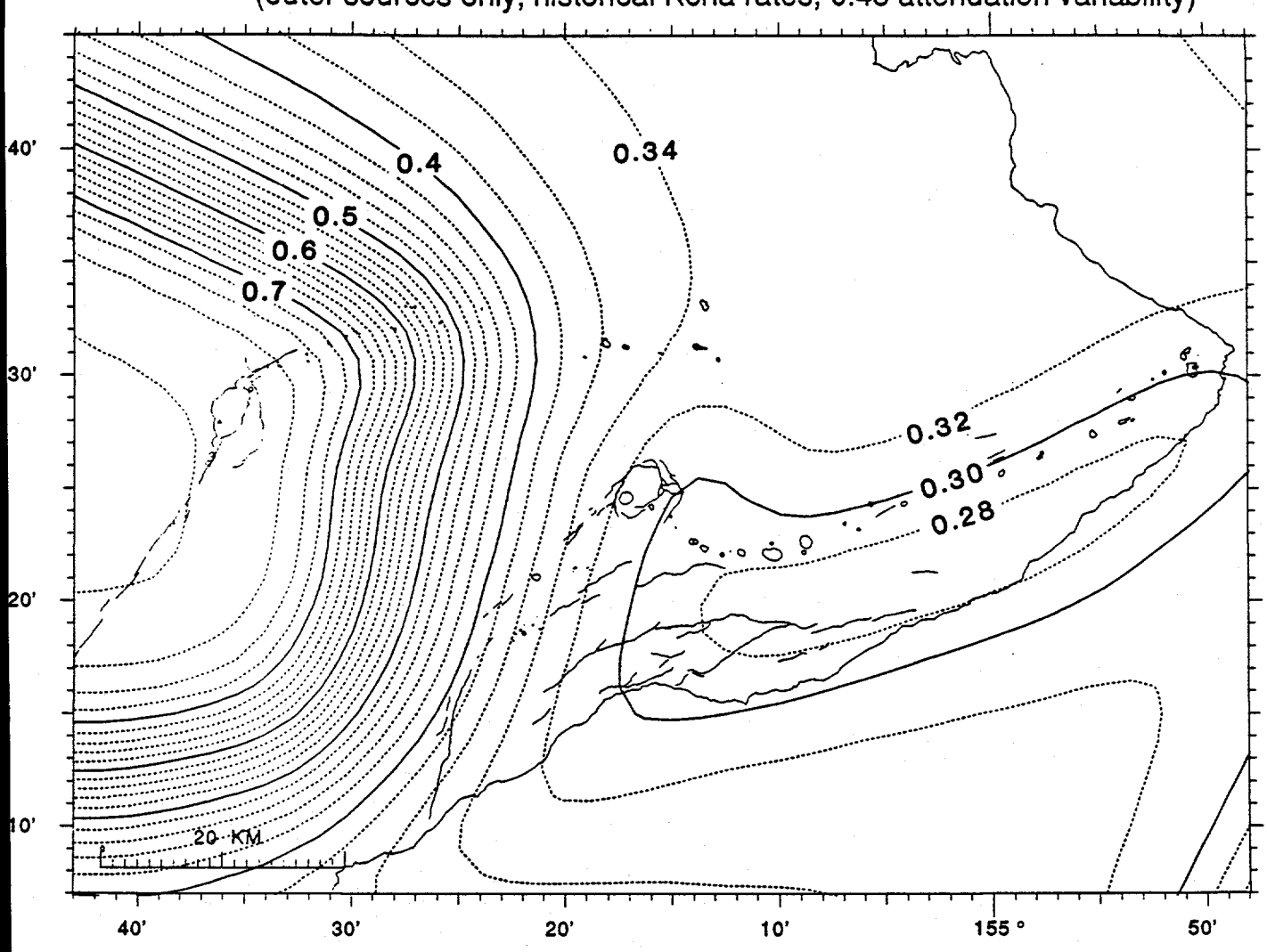

Figure A1b. Contributions from regions 5-11 (which exclude Kilauea) to the probablistic peak ground accelerations (PGA) of figure 13. All figures in appendix 1 show PGAs with a 90% probability of not being exceeded in a 50 year exposure time. The earthquake rates for regions 1 and 2 are from 1970-1992 adjusted for the higher rate of M>5.5 events, and the rates for regions 3, 7 and 8 are derived from historic earthquakes (table 3, bottom part). All figures have contour intervals of 0.1 (solid lines) and 0.02 (dashed lines).

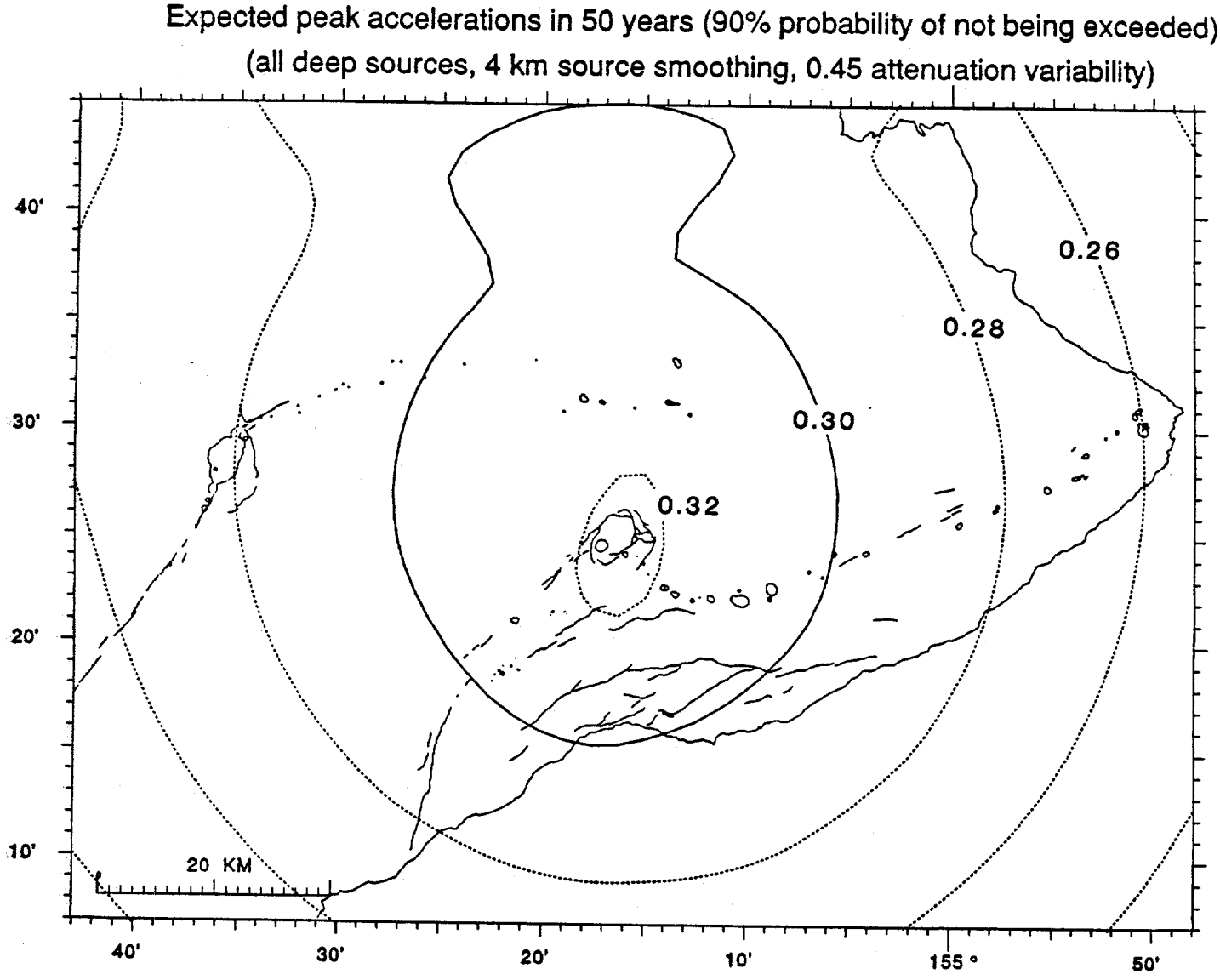

Figure A1c. Contributions from all mantle seismic zones D1-D8 to the probablistic peak ground accelerations (PGA) of figure 13. All figures in appendix 1 show PGAs with a 90% probability of not being exceeded in a 50 year exposure time. The earthquake rates for regions 1 and 2 are from 1970-1992 adjusted for the higher rate of M>5.5 events, and the rates for regions 3, 7 and 8 are derived from historic earthquakes (table 3, bottom part). All figures have contour intervals of 0.1 (solid lines) and 0.02 (dashed lines).

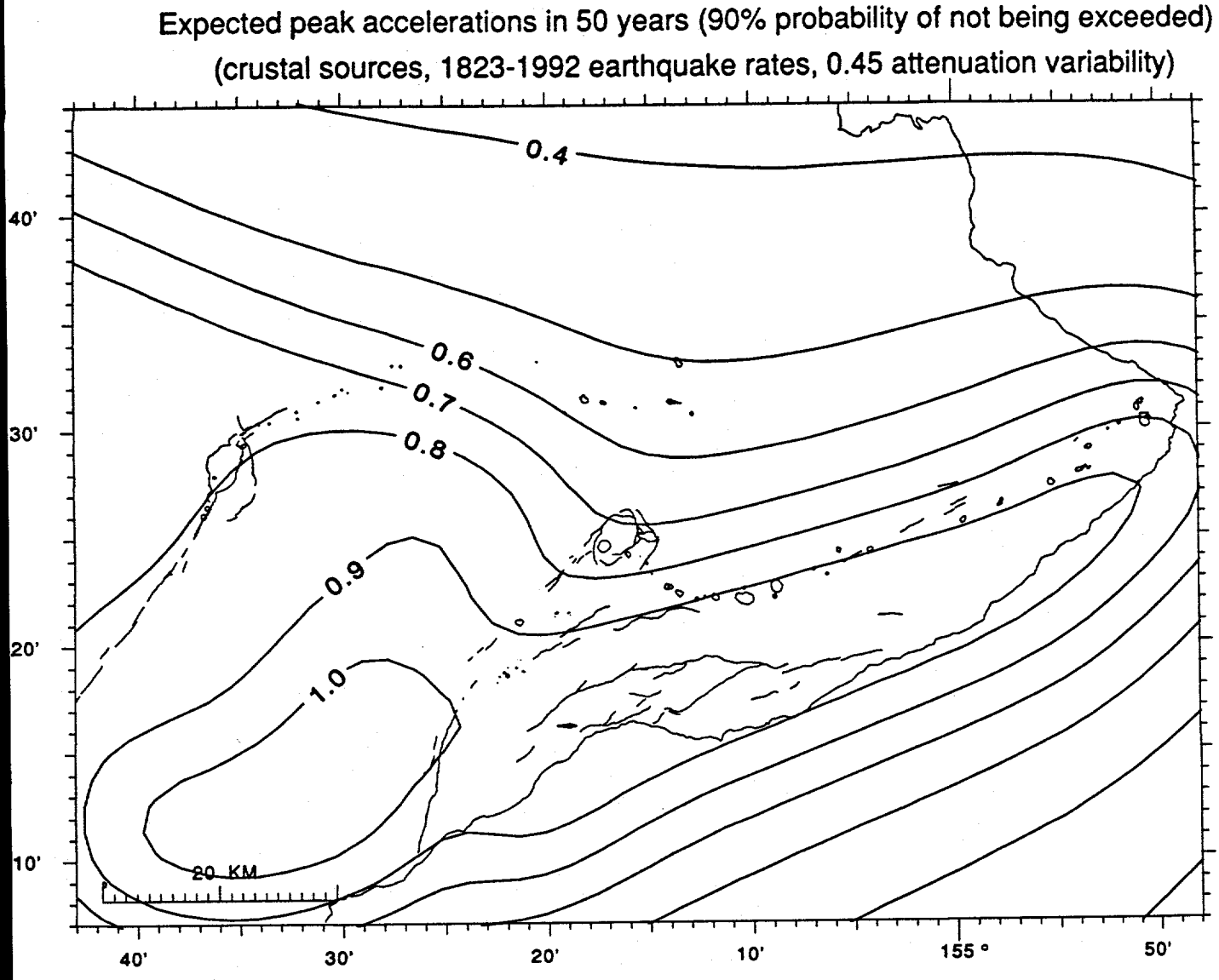

Figure A2. Probable peak ground accelerations (PGA) assuming the rate of M 5.5 to 8.0 earthquakes is from the 1823-1992 Wyss and Koyanagi (1992) catalog. The rates for regions 1 and 2 are as in figure A1a but are reduced by a factor of 0.67 (figure 6). Figures A2-A8 show PGAs with a 90% probability of not being exceeded in a 50 year exposure time from all crustal sources.

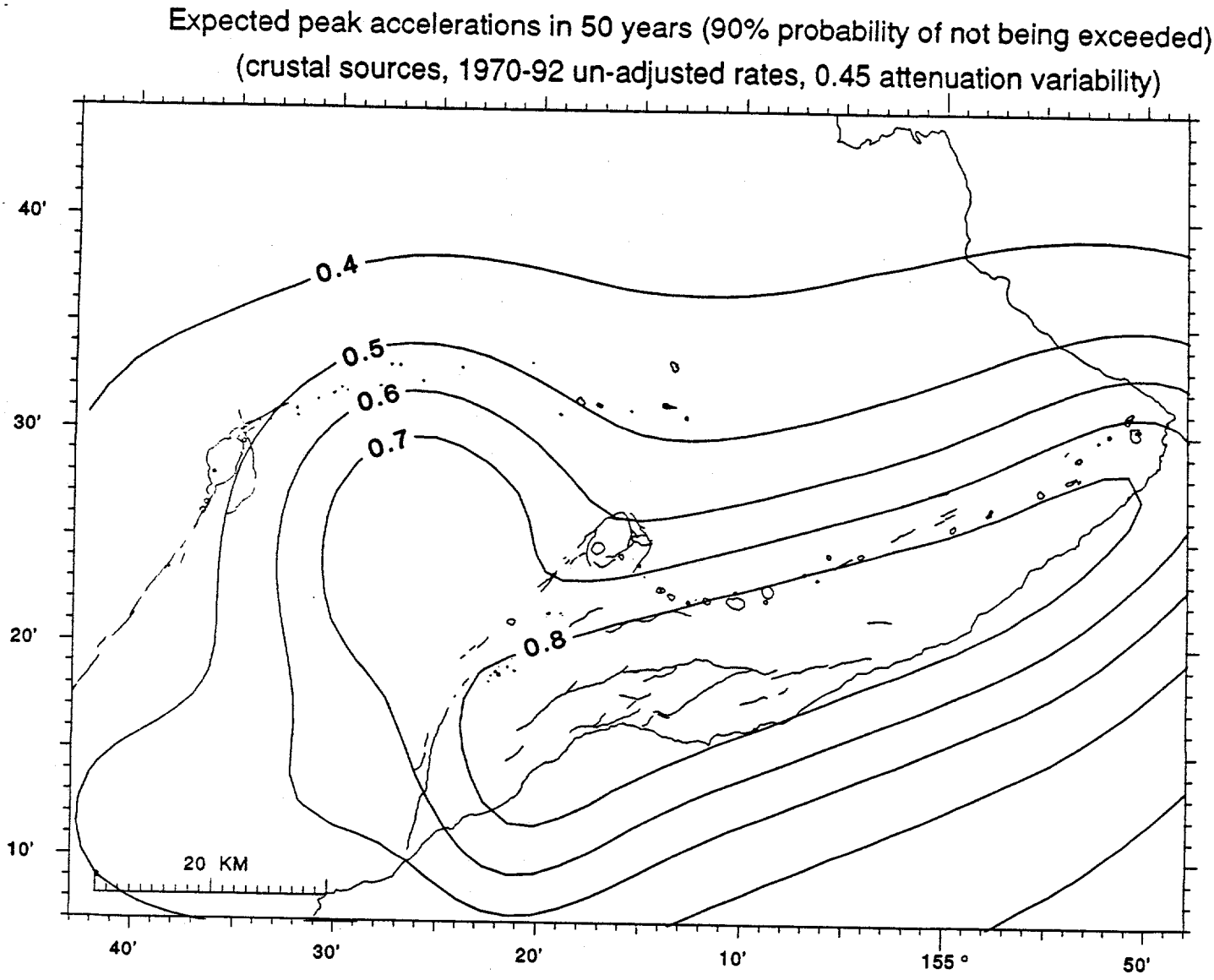

Figure A3. Probable peak ground accelerations assuming earthquake rates are derived from the 1970-1992 frequency-magnitude distributions (table 2) without adjustment for the observed higher rate of M>5.5 events. Contrast this figure with the adjusted and historic rates used in figure A1a.

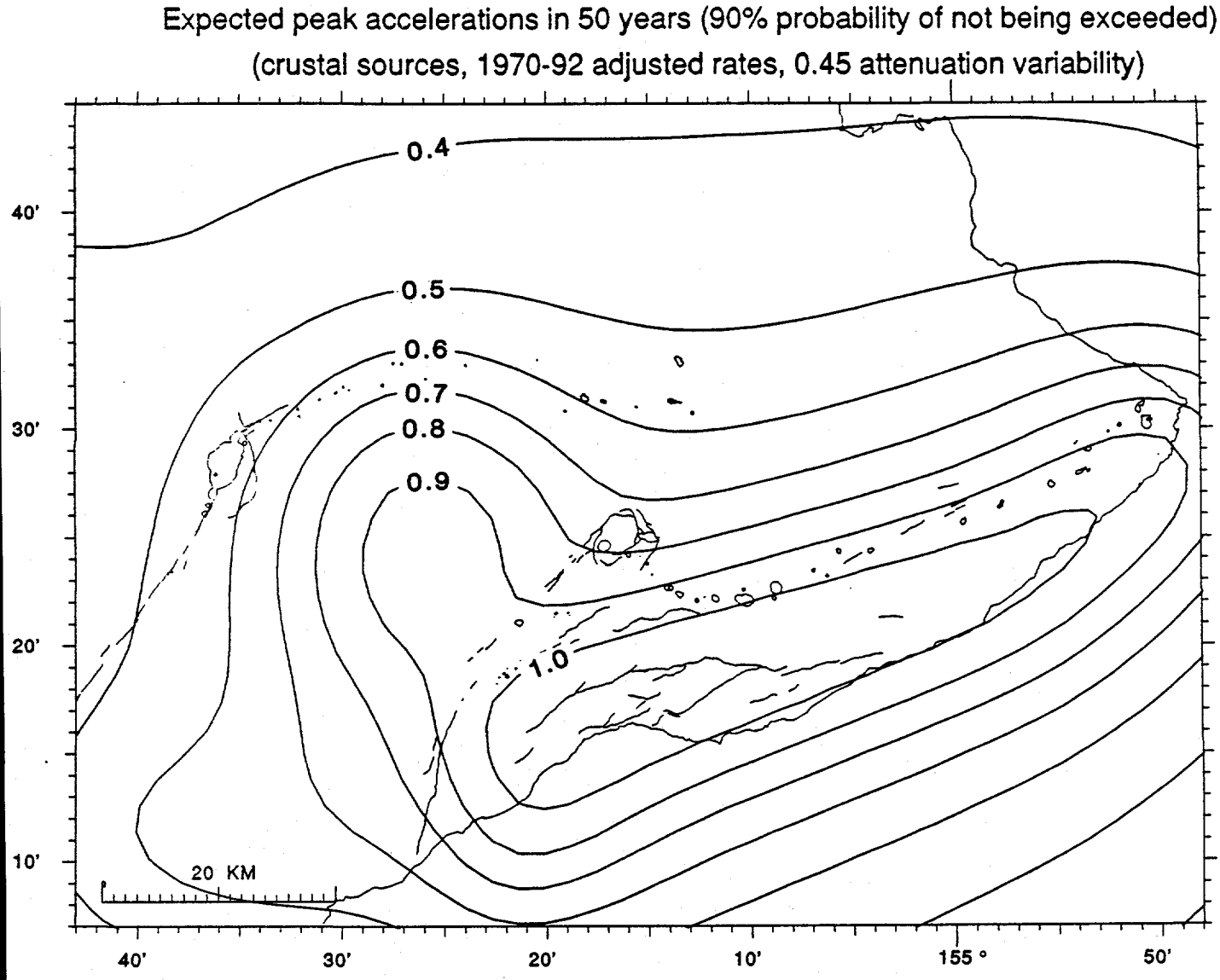

Figure A4. Probable peak ground accelerations assuming earthquake rates for regions 1 and 2 are derived from the 1970-1992 frequency-magnitude distributions adjusted for the observed higher rate of M>5.5 events (table 3). The rates for regions 3, 7 and 8 are from 1970-1992 (table 2) and ignore the historic activity in those regions. Contrast this figure with the historic rates used in figure A1a.

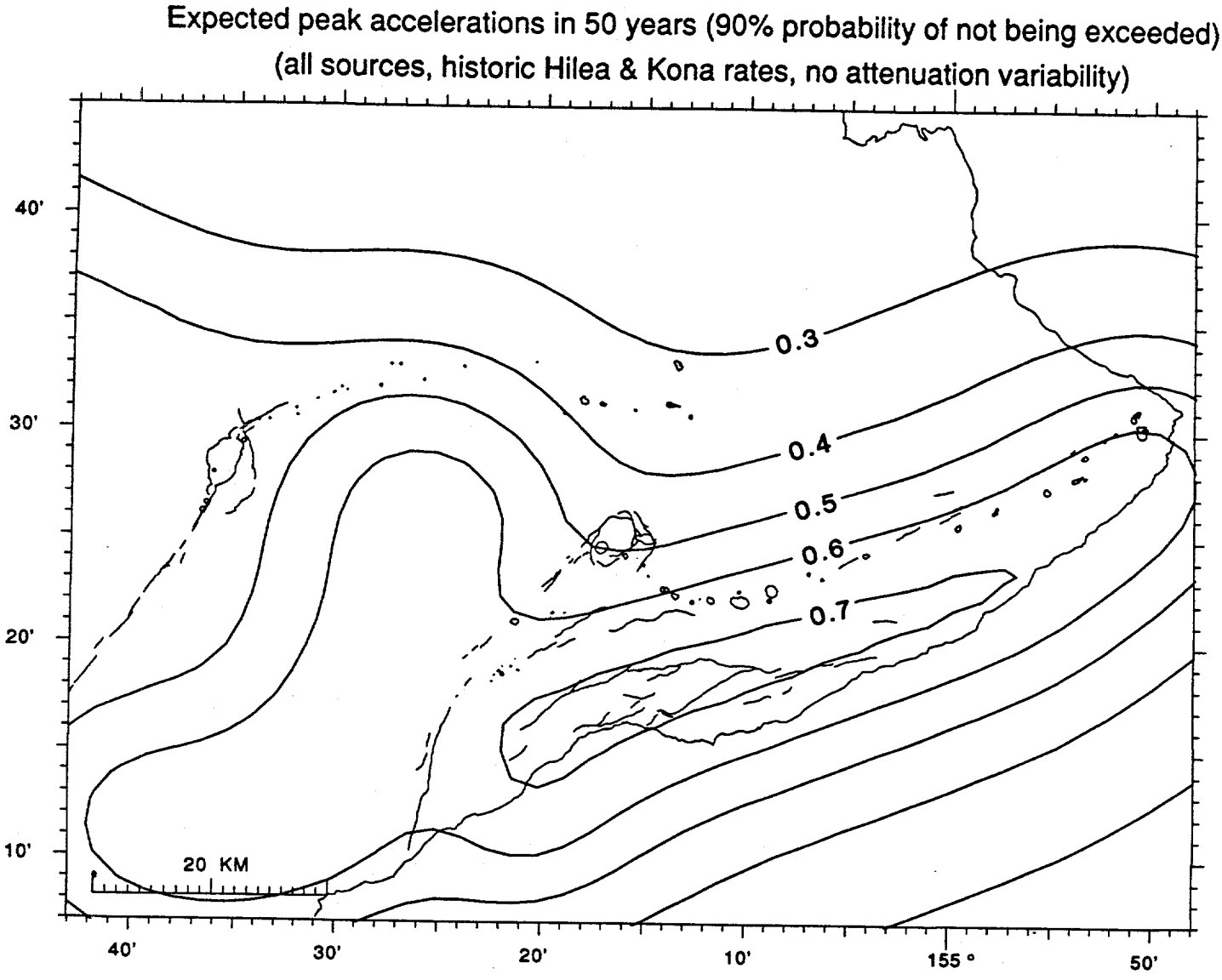

Figure A5. Probable peak ground accelerations (PGA) assuming no variation of PGA from the Boore et al. (1993) curve. Allowing for site variation increases the maximum PGA that will be seen with a 90% non-exceedence probability. Contrast this figure with the 57% variation used in figure A1a.

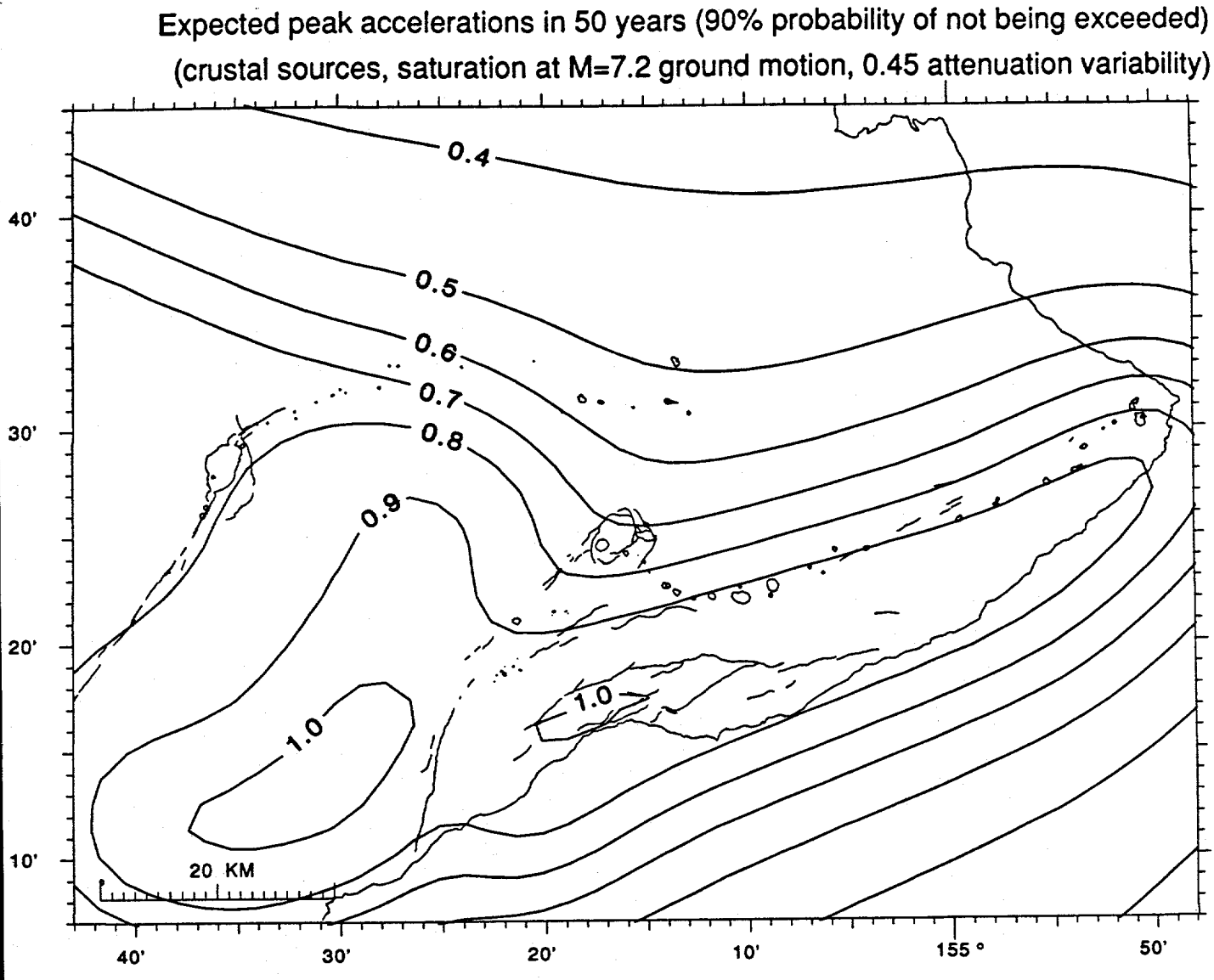

Figure A6. Probable peak ground accelerations (PGA) assuming that PGAs from M>7.2 earthquakes are saturated and produce the same PGAs as a M=7.2 earthquake. Contrast this figure with figure A1a.

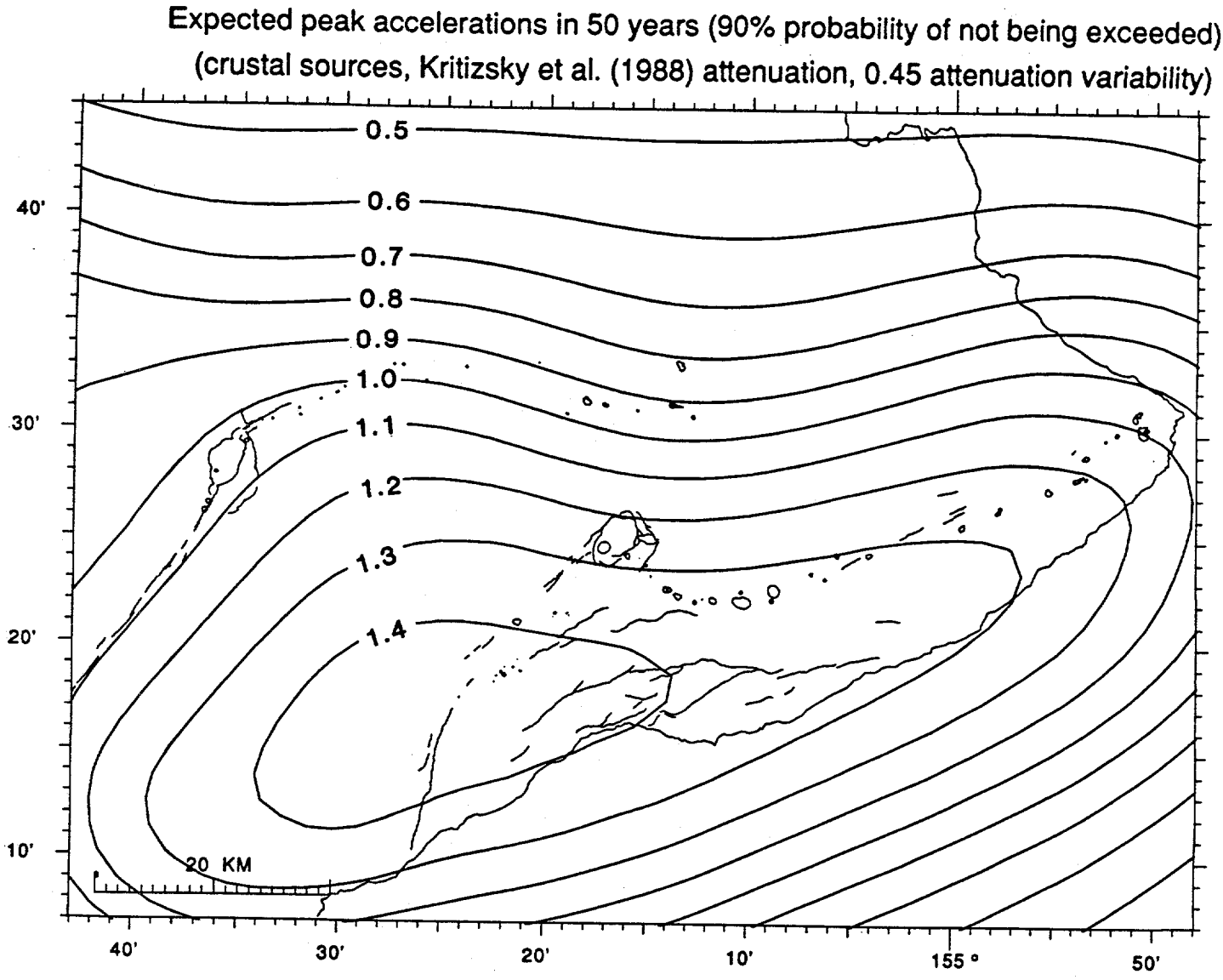

Figure A7. Probable peak ground accelerations using Krinitzsky et al.'s (1988) attenuation curve and all crustal seismic source regions. Contrast this figure with Boore et al.'s (1993) attenuation curve used in figure A1a.

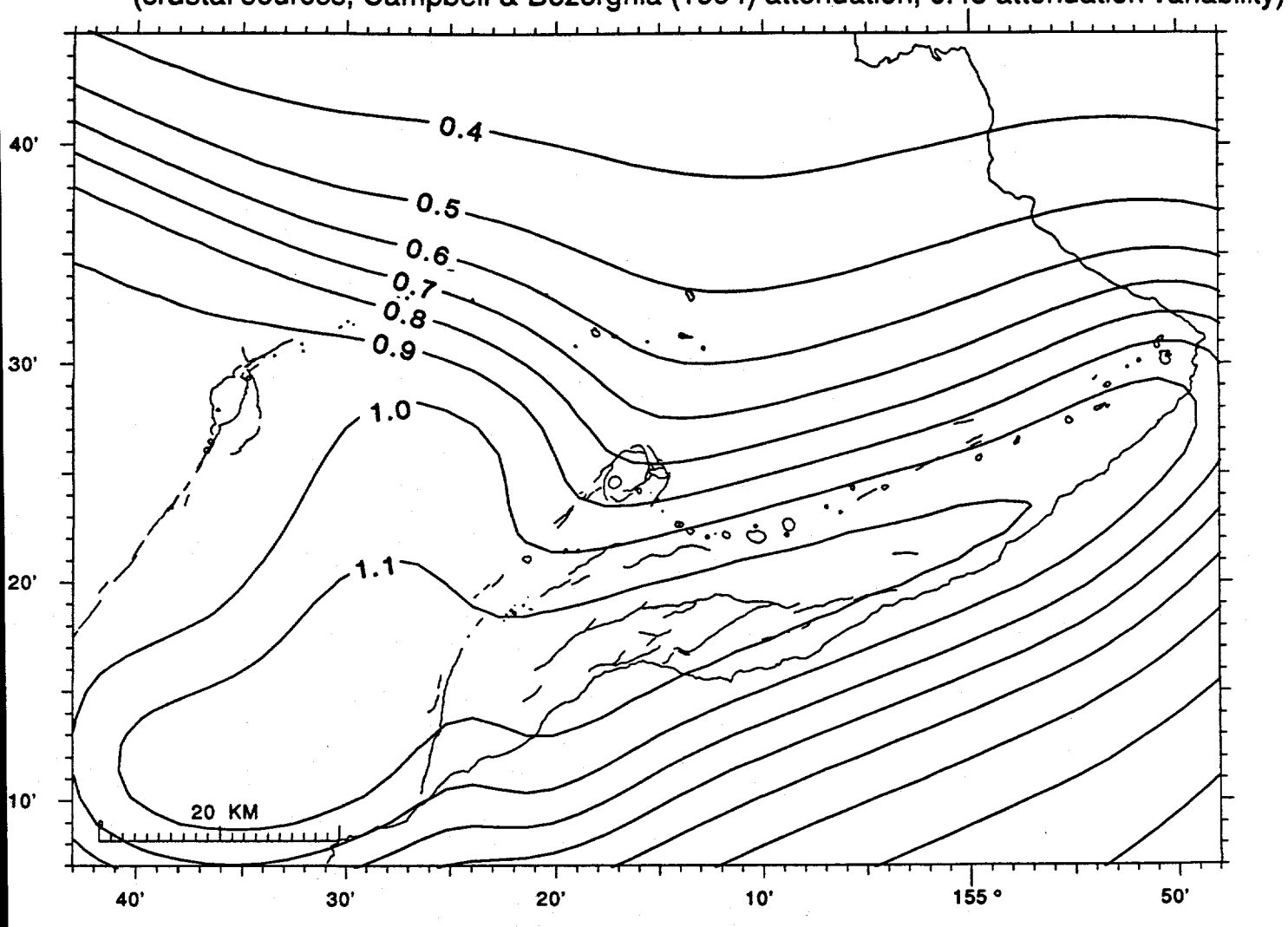

Figure A8. Probable peak ground accelerations using Campbell and Bozorgnia's (1994) attenuation curve and all crustal seismic source regions. Contrast this figure with Boore et al.'s (1993) attenuation curve used in figure A1a.

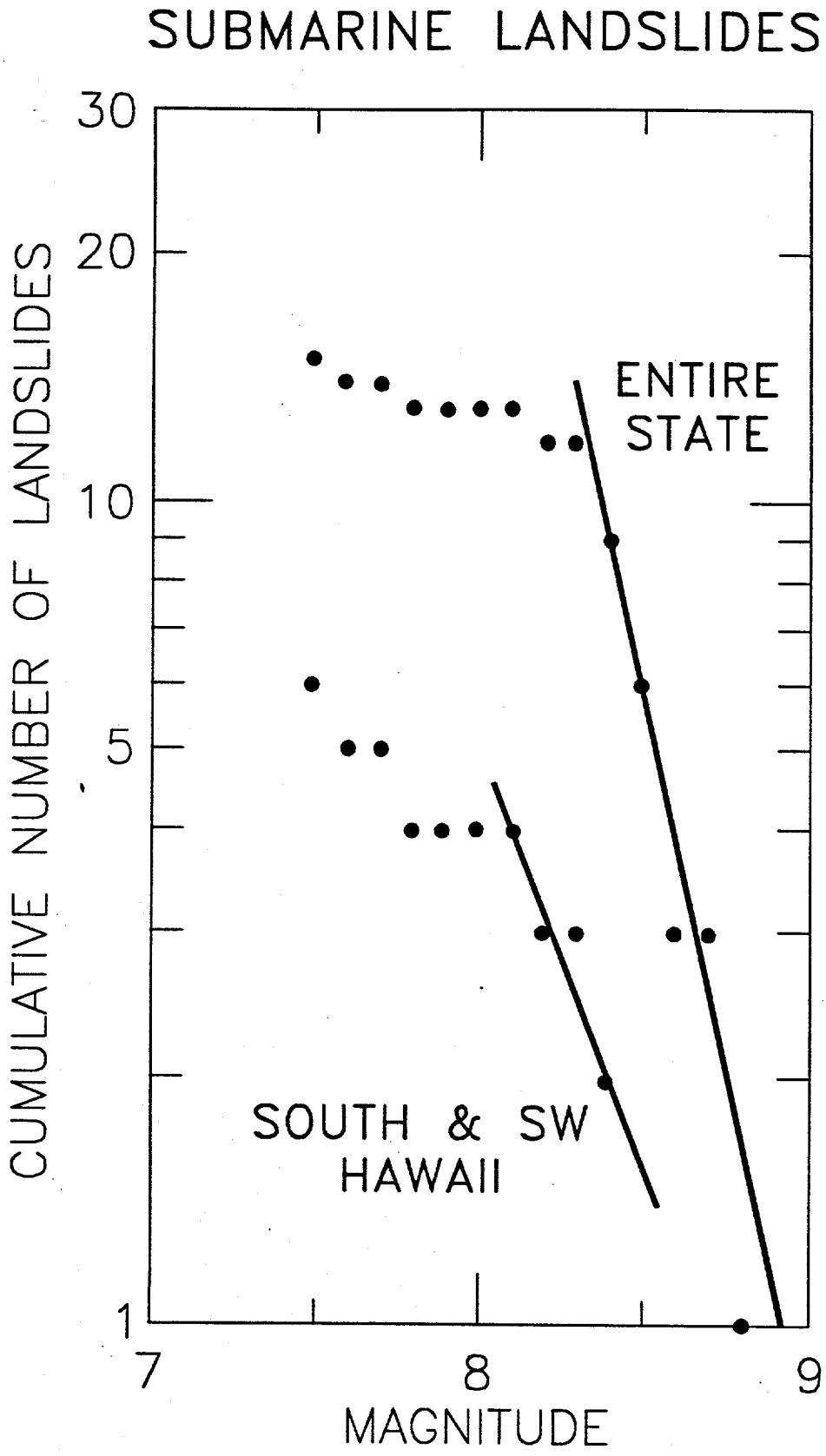

Figure A9. Cumulative frequency-magnitude distributions of submarine landslides (Moore et al., 1989) adjacent to the state of Hawaii, and near south and southwest Hawaii. The lines are eyeball fits to the linear part of the distributions.

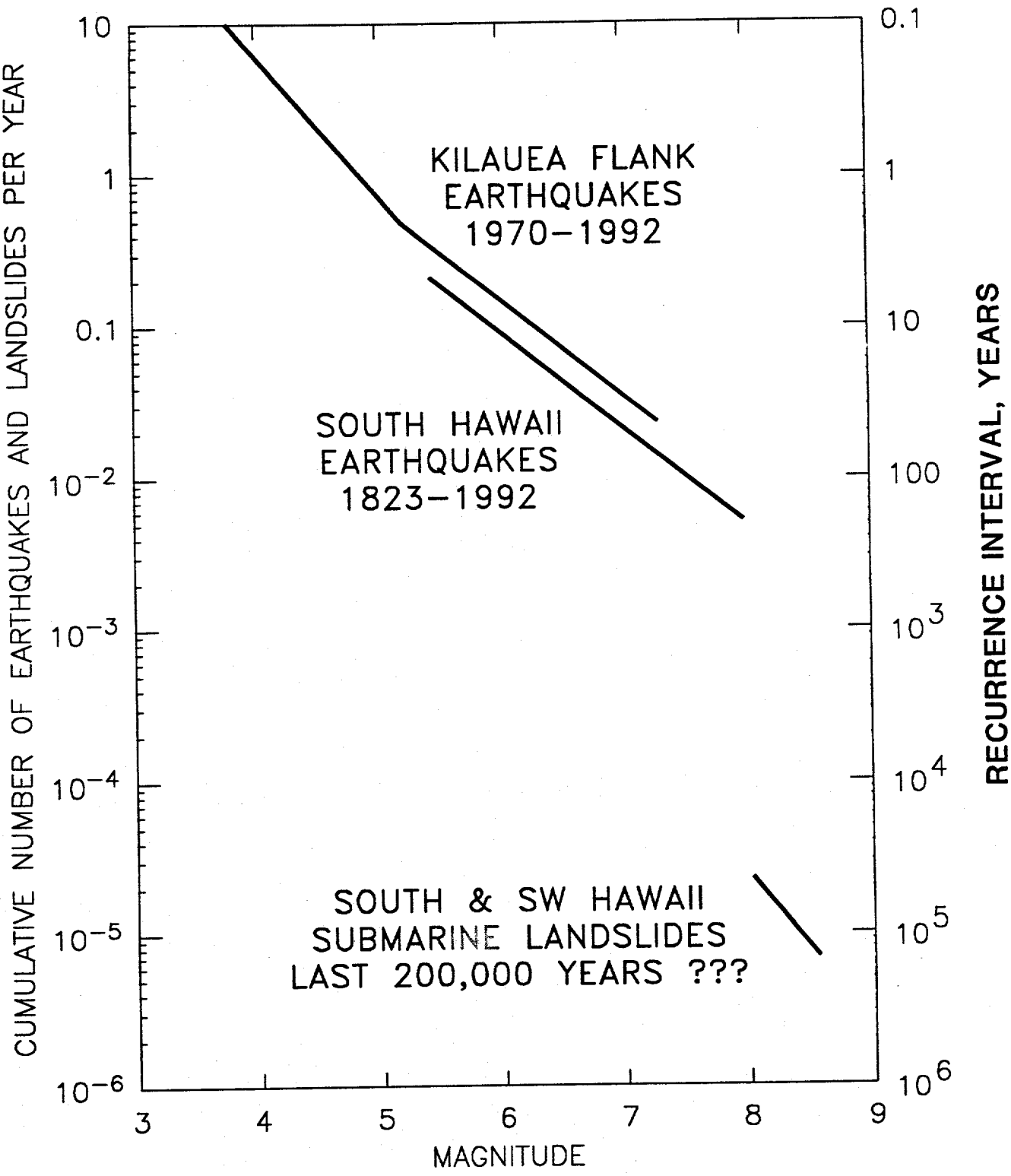

Figure A10. Annualized frequency-magnitude distributions (rates) of south Hawaii earthquakes and submarine landslides. The 1970-1992 distribution is from the HVO catalog and the 1823-1992 distribution is from Wyss and Koyanagi (1992) (their figure 6). The submarine landslide distribution is from figure A9 assuming that the slides were formed in the last 200,000 years.